CODEN:LUTEDX/(TEAT-5039)/1-109/(2001)

Wave Propagation through Vegetation at 3.1 GHz and 5.8 GHz

Peter Johannesson

Department of Electroscience
Electromagnetic Theory
Lund Institute of Technology
Sweden

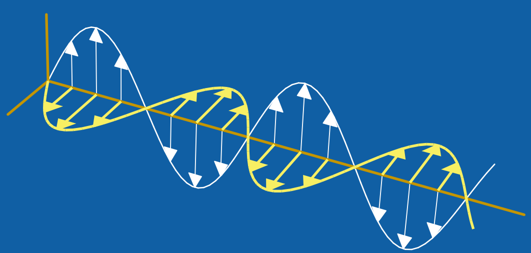

Handledare: Anders Karlsson
Christian Bergljung, Telia Research

Editor: Gerhard Kristensson

Abstract

A model for vegetation attenuation, based on the total cross section for leaves and branches, has been developed. The model is valid for microwave propagation in general but the analysis has been made with the emphasize on the frequencies 3.1 GHz and 5.8 GHz with application to Fixed Wireless Access. Since the scattering bodies, i.e. the leaves and the branches, are of the same size as the wavelength, resonance effects will occur. To calculate the scattered electric field in the far zone, under these circumstances, the T-matrix method has been applied. This method is applicable to arbitrarily shaped particles and can thus be applied to axisymmetric particles, i.e. bodies-of-revolution. Leaves have been modeled as thin lossy dielectric oblate spheroids and the branches as finitely-long lossy circular dielectric cylinders. A detailed analysis of different models in different frequency regions has been performed together with a survey of commonly used microwave models. These existing models are foremost used when short wave approximations, i.e. physical optics, or long wave approximations, Rayleigh scattering, can be done. In the short and long wave approximations the branches are modeled in the same way as in the T-matrix method. The leaves are, on the contrary, modeled as flat-circular lossy dielectric discs. In the analysis has multiple scattering effects been neglected. The results from the simulations are compared to measurements that were made on a large test beech.

Table of contents

Abstract 1
Table of contents 3
1 Introduction 5
2 Basic relationships 7
2.1 Maxwell s field equations 7
2.2 Poynting vector 11
3 Existing models 13
3.1 Leaf model 13
3.2 Canopy opacity model 13
3.3 Attenuation of a tree 15
3.4 Microwave transmissivity of a forest canopy 20
4 Tree modeling 24
4.1 Dielectric model of Leaves 24
4.2 Dielectric Model of branches 29
4.3 Crown structure 30
5 Propagation and attenuation of the electromagnetic field 32
5.1 Attenuation by leaves and branches 32
5.2 The total cross section 38
5.2.1 Long wave approximation 40
5.2.2 Resonance region 43
5.2.3 Short wave approximation 43
5.2.4 Expectation value of the total cross section 48
6 Measurements 53
7 Results 56
8 Discussion and conclusions 67
8.1 Future work 67
9 Acknowledgements 68
10 References 69
A Wave propagation in multiple dimensions 70
A.1 Basic derivations 70
A.2 Reflection and transmission at a plane dielectric boundary 76
A.2.1 Field solutions 76
A.3 Reflection and transmission at multiple dielectric interfaces 79
A.3.1 Field solutions 80
B Scattered electric field from a body with arbitrary volume 86
B.1 Scattered field 86
B.2 Far field 91
C The T-matrix method 96
C.1 General formulations 96
C.2 Plane wave 100
C.3 Far field 101
C.4 Scattering from a dielectric oblate spheroid 103
D Calculation of two integrals 106

1 Introduction

In communication systems where antennas are used to transfer information the environment between (and around) the transmitter and receiver has a major influence on the quality of the transferred signal. Buildings are the main source of attenuation but vegetation elements such as trees and large bushes can also have some reducing effects, on the propagated radio signal. In the case of attenuation by trees and bushes the incident electromagnetic field is mainly interacting with the leaves and the branches. The trunk does of course also have some influence on the attenuation but since the volume occupied by the trunk is much smaller than the total volume of a tree, for example, these effects can be considered as negligible. In the case of wave propagation between antennas that are located on heights — i.e. on rooftops — it will in principal only be the upper part of the tree crown that affects the attenuation. Since one of the fundamental assumptions, in this thesis, is communication between fixed antennas on heights, the attenuation effects, from the trunks, will thus be neglected in the vegetation models.

The attenuation due to vegetation is also very sensitive to the wavelength. Since the interaction between the tree and the electromagnetic field mainly is due to leaves and branches, the size and shape of these are important. For low frequencies — when the wavelength is much larger than the scattering body — leaves and branches have only a small interaction to the electromagnetic field, which means that surface irregularities have no — or minor — influence on the attenuation. The incident field will approximately have the same magnitude over the whole body, which leads to that the body experiences the incident field as uniform. Since the vegetation element is exposed by an electric field, an internal electric field is induced. This give rice to secondary radiation and since the wavelength is much larger than the scattering body, the emitted radiation is spread out and forms a radiation pattern close to that formed by a dipole antenna. When the wavelength is decreased, the losses increase due to a larger interaction between the incident field and the vegetation elements. This proceeds until the wavelength approach the same size as the scattering body and thus enters the resonance region. Here will the absorption and scattering values fluctuate strongly and the attenuation becomes irregular and very frequency dependent. The size and shape of the body is the main reason why this happens. The incident electric field induces an internal electric field that takes different values at different parts of the scattering body (these values are of course time dependent) since the wavelength no longer is much larger than the size of the body. These different parts work as scatterers and will thus emit secondary radiation. The radiation from the different emitters interferes, which leads to that specific directions are predominated and radiation lobes are formed. When the frequency is increased further, the effects of the resonance gradually decay, which leads to a more predictable behavior. The attenuation of the leaves and branches increases with increasing frequency. When the wavelength is much less than the scattering body no resonance effects occur and the attenuation will be purely exponential. The number of scatterers — in the scattering body — will of course increase, which leads to an increase in the number of radiation lobes. For very high frequencies the width of the maximum lobes is thin and thus forms radiation beams. This means that the intensity in the lobes, whose direction corresponds to the beam directions, is much higher and differs by many orders of magnitude compared to the other lobes.

The fundamental principles behind the interaction between the incident field and the scattering elements are very complicated and will therefore not be discussed here. It should be mentioned though that some factors that contribute to the losses are the fact that the incident field changes the permanent dipole moment in the liquid and induces currents in the medium. The induced currents can be created due to the charges in the saline water that the organic components contain.

We have so far discussed the interaction in general between the incident electromagnetic field and the vegetation elements at different frequencies. From the discussion we find that three types of interacting exist from which approximations can be done. In the case of low frequencies we are dealing with Rayleigh scattering (long wave approximations) and in the case of high frequencies, physical optics or geometric optics (short wave approximations) are considered. In the resonance region there is no simple way to do any approximations which leads to that the electromagnetic problems are difficult to solve. If the electric properties of the scattering body can be considered as weak, Born or Rytov approximations can be used to simplify the calculations. In this case the internal fields inside the scattering body is approximated by the incident field which makes it possible to treat cases when resonance occurs.
In the common microwave propagation models that are used today, assumptions of small or large wavelength in comparison to the scatterers are often done. Thus is Rayleigh scattering or physical optics considered. But when the wavelength of the transmitted field approach the size of the leaves and branches, resonance effects occur which leads to that these models generates incorrect results.
The purpose of this work is to study the vegetation attenuation and scattering at 3.1 GHz and 5.8 GHz. Since the wavelengths of the transmitted fields are about the same size as the leaves and branches ($\lambda = 9.7\ \mathrm{cm}$ and $\lambda = 5.2\ \mathrm{cm}$) resonance effects occur. Since the common models can not be used the wave propagation through the canopy must be analyzed in detail which leads to an improved model for the attenuation. The attenuation model is based on the total cross section of a leaf and a branch. A computer program, based on the T-matrix theory, makes the computations of the total cross section. The results from the simulations of the improved attenuation model will finally be compared with measurements that have been made on a large test beech.

2 Basic relationships

This section gives a brief introduction to the theory of microwave propagation. We will start with the fundamental equations, i.e. Maxwell s equations, and from these derive the vector differential equation called the Helmholtz equation. This equation can be used to explain and predict how the fields propagate. Furthermore will also concepts like attenuation and average power density be treated.

2.1 Maxwell s field equations

For a medium characterized by a source density ρ the electromagnetic fields satisfies Maxwell s equations

$$\begin{cases} \nabla \times \boldsymbol{E}(\boldsymbol{r},t) = -\dfrac{\partial \boldsymbol{B}(\boldsymbol{r},t)}{\partial t} \\ \nabla \times \boldsymbol{H}(\boldsymbol{r},t) = \boldsymbol{J}(\boldsymbol{r},t) + \dfrac{\partial \boldsymbol{D}(\boldsymbol{r},t)}{\partial t} \\ \nabla \cdot \boldsymbol{B}(\boldsymbol{r},t) = 0 \\ \nabla \cdot \boldsymbol{D}(\boldsymbol{r},t) = \rho \end{cases} \tag{2.1}$$

The vector fields in the equations are:

$\boldsymbol{E}$	Electric field strength [V/m]
$\boldsymbol{H}$	Magnetic field strength [A/m]
$\boldsymbol{D}$	Electric flux density [As/m^2]
$\boldsymbol{B}$	Magnetic flux density [Vs/m^2]
$\boldsymbol{J}$	Current density [A/m^2]

The boundary conditions in the case of a interface between two media are given by

$$\begin{cases} \boldsymbol{n} \times (\boldsymbol{E}_1 - \boldsymbol{E}_2) = \boldsymbol{0} \\ \boldsymbol{n} \times (\boldsymbol{H}_1 - \boldsymbol{H}_2) = \boldsymbol{J}_S \\ \boldsymbol{n} \cdot (\boldsymbol{B}_1 - \boldsymbol{B}_2) = 0 \\ \boldsymbol{n} \cdot (\boldsymbol{D}_1 - \boldsymbol{D}_2) = \rho_S \end{cases}$$

where $\boldsymbol{J}_S$ is the surface current density and ρ_S the surface charge density.
For time-harmonic fields

$$\begin{cases} \boldsymbol{E}(\boldsymbol{r},t) = \mathrm{Re}\{\boldsymbol{E}(\boldsymbol{r},\omega) e^{-i\omega t}\} \\ \boldsymbol{H}(\boldsymbol{r},t) = \mathrm{Re}\{\boldsymbol{H}(\boldsymbol{r},\omega) e^{-i\omega t}\} \end{cases} \tag{2.2}$$

the Fourier transform $\left(\dfrac{\partial}{\partial t} \rightarrow -i\omega t\right)$ of the fields becomes

$$\begin{cases} \nabla \times \boldsymbol{E}(\boldsymbol{r},\omega) = i\omega \boldsymbol{B}(\boldsymbol{r},\omega) \\ \nabla \times \boldsymbol{H}(\boldsymbol{r},\omega) = \boldsymbol{J}(\boldsymbol{r},\omega) - i\omega \boldsymbol{D}(\boldsymbol{r},\omega) \end{cases} \tag{2.3}$$

The polarization $\boldsymbol{P}(\boldsymbol{r},\omega)$ in a material is a measure of the bound-charge density deviation from equilibrium. In an isotropic material we suppose that the polarization is proportional to the outer macroscopic electric field $\boldsymbol{E}(\boldsymbol{r},\omega)$. In a corresponding way it is supposed that the magnetization $\boldsymbol{M}(\boldsymbol{r},\omega)$ of the material is proportional to the magnetic field $\boldsymbol{H}(\boldsymbol{r},\omega)$. The basic assumptions are

$$\begin{cases}\boldsymbol{P}(\boldsymbol{r},\omega)=\varepsilon_0\chi_e(\boldsymbol{r},\omega)\boldsymbol{E}(\boldsymbol{r},\omega)\\ \boldsymbol{M}(\boldsymbol{r},\omega)=\mu_0\chi_m(\boldsymbol{r},\omega)\boldsymbol{H}(\boldsymbol{r},\omega)\end{cases} \tag{2.4}$$

The functions $\chi_e(\boldsymbol{r},\omega)$ and $\chi_m(\boldsymbol{r},\omega)$ are called the electric and magnetic susceptibility functions and are generally dependent of $\boldsymbol{r}$ and ω. Since the definition of the polarization and magnetization is

$$\begin{cases}\boldsymbol{P}=\boldsymbol{D}-\varepsilon_0\boldsymbol{E}\\ \boldsymbol{M}=\dfrac{1}{\mu_0}\boldsymbol{B}-\boldsymbol{H}\end{cases} \tag{2.5}$$

the electric and magnetic flux densities $\boldsymbol{D}$ and $\boldsymbol{B}$ can be written as a set of equations that forms the constitutive relations of an isotropic medium

$$\begin{cases}\boldsymbol{D}(\boldsymbol{r},\omega)=\varepsilon_0\varepsilon(\boldsymbol{r},\omega)\boldsymbol{E}(\boldsymbol{r},\omega)\\ \boldsymbol{B}(\boldsymbol{r},\omega)=\mu_0\mu(\boldsymbol{r},\omega)\boldsymbol{H}(\boldsymbol{r},\omega)\end{cases} \tag{2.6}$$

We have here introduced the permittivity function $\varepsilon(\boldsymbol{r},\omega)$ and the permeability function $\mu(\boldsymbol{r},\omega)$

$$\begin{cases}\varepsilon(\boldsymbol{r},\omega)=1+\chi_e(\boldsymbol{r},\omega)\\ \mu(\boldsymbol{r},\omega)=1+\chi_m(\boldsymbol{r},\omega)\end{cases} \tag{2.7}$$

A material with losses is characterized by that ε and μ are complex quantities

$$\begin{cases}\varepsilon=\varepsilon'+i\,\varepsilon''\\ \mu=\mu'+i\,\mu''\end{cases} \tag{2.8}$$

If the material does not show any electric and magnetic properties the permittivity and permeability are set to unit, i.e. $\varepsilon,\mu=1$. With help of the constitutive relations Eq. (2.3) can be rewritten as

$$\nabla\times\boldsymbol{E}(\boldsymbol{r},\omega)=i\,\omega\mu_0\mu(\boldsymbol{r},\omega)\boldsymbol{H}(\boldsymbol{r},\omega) \tag{2.9a}$$
$$\nabla\times\boldsymbol{H}(\boldsymbol{r},\omega)=\boldsymbol{J}(\boldsymbol{r},\omega)-i\,\omega\varepsilon_0\varepsilon(\boldsymbol{r},\omega)\boldsymbol{E}(\boldsymbol{r},\omega) \tag{2.9b}$$

In materials with mobile charges a conductivity $\sigma(\boldsymbol{r},\omega)$ is defined to describe the dynamics of the charges. The current density $\boldsymbol{J}$ is in this model proportional to the electric field

$$\boldsymbol{J}(\boldsymbol{r},\omega)=\sigma(\boldsymbol{r},\omega)\boldsymbol{E}(\boldsymbol{r},\omega) \tag{2.10}$$

It is always possible to include these effects, of mobile charges, into a new permittivity function ε_{new} . We find

$$\varepsilon_{\text{new}} = \varepsilon_{\text{old}} + i\frac{\sigma}{\omega\varepsilon_0} \tag{2.11}$$

These effects can be included into the Eq. (2.9b) that yields

$$\begin{aligned}\nabla\times\boldsymbol{H}(\boldsymbol{r},\omega) &= (\sigma(\boldsymbol{r},\omega)-i\,\omega\varepsilon_0\varepsilon(\boldsymbol{r},\omega))\boldsymbol{E}(\boldsymbol{r},\omega)\\ &= -i\,\omega\varepsilon_0\left(\varepsilon(\boldsymbol{r},\omega)+i\frac{\sigma(\boldsymbol{r},\omega)}{\omega\varepsilon_0}\right)\boldsymbol{E}(\boldsymbol{r},\omega)\\ &= -i\,\omega\varepsilon_0\varepsilon_{\text{new}}(\boldsymbol{r},\omega)\boldsymbol{E}(\boldsymbol{r},\omega)\end{aligned} \tag{2.12}$$

Maxwell s equations, Eq. (2.9a) and (2.9b), for an isotropic medium, can now be restated

$$\nabla\times\boldsymbol{E}(\boldsymbol{r},\omega)=i\,\omega\mu_0\mu(\boldsymbol{r},\omega)\boldsymbol{H}(\boldsymbol{r},\omega) \tag{2.13a}$$

$$\nabla\times\boldsymbol{H}(\boldsymbol{r},\omega)=-i\,\omega\varepsilon_0\varepsilon(\boldsymbol{r},\omega)\boldsymbol{E}(\boldsymbol{r},\omega) \tag{2.13b}$$

A common case is when the medium is homogeneous. In that case the *r* dependence of the permittivity and the permeability functions expires. To obtain a solution for ***E***, in a homogeneous and isotropic medium, we take the curl of both sides of (2.13a)

$$\nabla\times(\nabla\times\boldsymbol{E})=i\,\omega\mu_0\mu(\nabla\times\boldsymbol{H}) \tag{2.14}$$

With help of the BAC-CAB rule

$$\nabla\times(\nabla\times\boldsymbol{E})=\nabla(\nabla\cdot\boldsymbol{E})-\nabla^2\boldsymbol{E} \tag{2.15}$$

we can substitute Eq. (2.13b) into (2.14) which yields

$$\nabla(\nabla\cdot\boldsymbol{E})-\nabla^2\boldsymbol{E}=k^2\,\boldsymbol{E} \tag{2.16}$$

We have here introduced the wave constant

$$k^2=\omega^2\varepsilon_0\mu_0\varepsilon\mu=\frac{\omega^2}{c_0^2}\varepsilon\mu \tag{2.17}$$

In a source free medium the divergence of the electric flux density is zero, $\nabla\cdot\boldsymbol{D}=0$. This means that Eq. (2.16) can be simplified and the result is

$$\nabla^2\boldsymbol{E}(\boldsymbol{r},\omega)+k(\omega)^2\,\boldsymbol{E}(\boldsymbol{r},\omega)=0 \tag{2.18}$$

Eq. (2.18) is established as Helmholtz s equation — also called the wave equation.
A possible solution to Helmholtz s equation is a plane wave (see appendix A.1)

$$\boldsymbol{E}(\boldsymbol{r},\omega) = \boldsymbol{E}_0\, e^{i\,\boldsymbol{k}\cdot\boldsymbol{r}} \tag{2.19}$$

If we select the wave s propagation direction to be the positive direction of the z-axis we get

$$\boldsymbol{E}(z,\omega) = \boldsymbol{E}_0\, e^{i\,k\,z} \tag{2.20}$$

Since the wave constant often is a complex quantity and thus can be written in the form

$$k = k' + ik'' \tag{2.21}$$

we can rewrite Eq. (2.20) which yields

$$\boldsymbol{E}(z,\omega) = \boldsymbol{E}_0\, e^{-\alpha\,z} e^{i\,\beta\,z} \tag{2.22}$$

where α is the attenuation constant and β is the phase constant. Comparison of Eq. (2.20) and Eq. (2.22) shows that

$$\alpha = k'' = \mathrm{Im}\left\{\frac{\omega}{c_0}\sqrt{\varepsilon\mu}\right\} \tag{2.23}$$

$$\beta = k' = \mathrm{Re}\left\{\frac{\omega}{c_0}\sqrt{\varepsilon\mu}\right\} \tag{2.24}$$

The corresponding real-time expression of the electric field can be calculated if we use Eq. (2.2)

$$\boldsymbol{E}(z,t) = \mathrm{Re}\left\{\boldsymbol{E}(z,\omega)e^{-i\omega t}\right\} \tag{2.25}$$

The electric field can be split up into two components parallel to the x- and y-axes, respectively

$$\boldsymbol{E}_0 = \boldsymbol{x}\,E_{0x} + \boldsymbol{y}\,E_{0y} = \boldsymbol{x}\left|E_{0x}\right|e^{i\theta_x} + \boldsymbol{y}\left|E_{0y}\right|e^{i\theta_y} \tag{2.26}$$

Since the electric field can be written in the form

$$\boldsymbol{E}(z,\omega) = \boldsymbol{x}\,E_x(z,\omega) + \boldsymbol{y}\,E_y(z,\omega) \tag{2.27}$$

we can use Eq. (2.22) and Eq. (2.26) to express $E_x(z,\omega)$ and $E_y(z,\omega)$ as

$$E_x(z,\omega) = \left|E_{0x}\right|e^{i\theta_x}e^{-\alpha\,z}e^{i\,\beta\,z} = \left|E_{0x}\right|e^{-\alpha\,z}e^{i(\beta\,z+\theta_x)} \tag{2.28a}$$

$$E_y(z,\omega) = \left|E_{0y}\right|e^{i\theta_y}e^{-\alpha\,z}e^{i\,\beta\,z} = \left|E_{0y}\right|e^{-\alpha\,z}e^{i(\beta\,z+\theta_y)} \tag{2.28b}$$

Similar expressions are obtained for the magnetic field. From Eq. (2.13a) we get

$$\boldsymbol{H}(z,\omega) = -\frac{i}{\omega\mu_0\mu}\nabla\times\boldsymbol{E}(z,\omega) \tag{2.29}$$

Use of Eq. (2.20) shows that the magnetic components H_x and H_y in the expression

$$\boldsymbol{H}(z,\omega) = \boldsymbol{x}H_x(z,\omega) + \boldsymbol{y}H_y(z,\omega) \tag{2.30}$$

is represented by

$$H_x(z,\omega) = -\frac{k}{\omega\mu_0\mu}E_y(z,\omega) = -\frac{1}{\eta_0\eta}E_y(z,\omega) \tag{2.31a}$$

$$H_y(z,\omega) = \frac{k}{\omega\mu_0\mu}E_x(z,\omega) = \frac{1}{\eta_0\eta}E_x(z,\omega) \tag{2.31b}$$

2.2 Poynting vector

From Eq. (2.27) and Eq. (2.30) it is obvious that $\boldsymbol{E}\times\boldsymbol{H}$ points in the *z*-direction, i.e. the direction of propagation. In consequence, ***E*** and ***H*** lie in a plane perpendicular to the direction of wave propagation. The quantity

$$\boldsymbol{S} = \boldsymbol{E}\times\boldsymbol{H} \tag{2.32}$$

is known as the Poynting vector, which defines the power density (W/m^2) associated with the electromagnetic field. It is obvious that for an isotropic medium the power propagation is directed perpendicular to the electric and magnetic field, i.e. in the wave propagation direction. The quantity that is of major interest, in the studying of time-harmonic fields, is the time-average value of the complex Poynting vector, $\boldsymbol{S}_{av}$, over one period of time. The time-average value is denoted by $\langle f(t)\rangle$ and for the product of two time-harmonic fields $f_1(t)$ and $f_2(t)$ we get

$$\begin{aligned}
\langle f_1(t)f_2(t)\rangle &= \frac{1}{T}\int_0^T \mathrm{Re}\left\{f_1(\omega)e^{-i\omega t}\right\}\mathrm{Re}\left\{f_2(\omega)e^{-i\omega t}\right\}dt \\
&= \frac{1}{4T}\int_0^T \left\{f_1(\omega)f_2(\omega)e^{-2i\omega t} + f_1^*(\omega)f_2^*(\omega)e^{2i\omega t} + f_1(\omega)f_2^*(\omega) + f_1^*(\omega)f_2(\omega)\right\}dt \\
&= \frac{1}{4}\left\{f_1(\omega)f_2^*(\omega) + f_1^*(\omega)f_2(\omega)\right\} = \frac{1}{2}\mathrm{Re}\left\{f_1(\omega)f_2^*(\omega)\right\}
\end{aligned}$$

If we now use this result in the calculation of the time-average value of the Poynting vector we get

$$\boldsymbol{S}_{av} = \langle\boldsymbol{S}(t)\rangle = \langle\boldsymbol{E}(t)\times\boldsymbol{H}(t)\rangle = \frac{1}{2}\mathrm{Re}\left\{\boldsymbol{E}(\omega)\times\boldsymbol{H}^*(\omega)\right\} \tag{2.33}$$

where $\boldsymbol{H}^*$ denotes the complex conjugate of the magnetic field vector. Eq. (2.33) is a general formula for computing the average power density of a propagating electromagnetic wave.

3 Existing models

In this section we present a brief overview of some of the established models used today. Since the different models have some limitations it is important to investigate under which circumstances the models can be used. The weaknesses and strengths of the different models will be elucidated and show which parts that are useful and which parts that have to be improved. Furthermore, data from earlier executed measurements will also be presented. This data is extremely valuable to us since it increases our understanding of how electromagnetic radiation is affected by vegetation. It also works as complementary information to the results of our own measurements.

3.1 Leaf model

Effective dielectric properties are modeled by dielectric mixing theory. In the case of vegetation elements, the components are liquid water with a high permittivity, organic material with moderate to low permittivity and air with unit permittivity. For such highly contrasting permittivities and large volume fractions physical mixing theory has, so far, failed. In the attempt to overcome this problem Ulaby and El-Rayes [6] assumed linear, i.e. empirical relationships between the permittivity and volume fractions of the different components. Dielectric measurements by Ulaby and El-Rayes indicate that the dielectric properties of vegetation can be modelled by representing vegetation as a mixture of saline water, bound water and dry vegetation. They derived a semi-empirical formula [6] from measurements at frequencies between 1 and 20 GHz on corn leaves with relatively high dry matter contents. The extrapolation of the formula to higher frequencies and lower dry matter contents leads to incorrect values. This was shown by M tzler and Sume [2]. From the data used in [6], and their own data at frequencies up to 94 GHz, they developed and improved a semi-empirical formula to calculate the dielectric constant of leaves. High and low dry matter contents were included. M tzler combined the data of Ulaby and El Rayes [6], El Rayes and Ulaby [9] and of M tzler and Sume [2] and derived a new dielectric formula [1]

$$\varepsilon_{\text{leaf}} = 0.522(1 - 1.32\, m_d)\varepsilon_{\text{sw}} + 0.51 + 3.84\, m_d$$

which is valid over the frequency range from 1 to 100 GHz. The formula is applicable to fresh leaves with m_d values in the range $0.1 \le m_d \le 0.5$. Here ε_{sw} is the dielectric permittivity for saline water according to the Debye model and m_d is the dry-matter fraction of leaves given by

$$m_d = \frac{\text{dry mass}}{\text{fresh mass}}$$

3.2 Canopy opacity model

Wegm ller, M tzler and Njoku [4] used the radiative transfer model, described by Kerr and Njoku [7], as a reference point for studying the vegetation attenuation and emission. The transfer model is a model for spaceborne observations of semi-arid land surfaces and it is based on the concept of temperature instead of the concept of electric and magnetic fields. It means that instead of analyzing how the magnitude of the electric and magnetic field is distributed to the different components one analyzes how the energy is distributed in terms of the temperature. Every component of the system — the land surface, air, leaves, branches etc. —

is considered as an object that emit, reflect and absorbs thermal radiation. For example is the soil-surface emission attenuated through the canopy and atmosphere given by

$$T = (1 - r_{sp})T_s e^{-(\tau_p + \tau_a)} \tag{3.1}$$

where r_{sp} is the reflectivity of the soil surface, T_s is temperature of the soil. The opacities of the atmosphere and the canopy are denoted by τ_a and τ_p where the polarization is denoted by p. The transfer model incorporates models of vegetation attenuation and emission that are valid at low frequencies only. It assumes that second and higher order scattering in the vegetation can be ignored and that there is no reflection of radiation at the vegetation-air interface. In [7] we find an equation for the canopy opacity

$$\tau_p = A_p k_0 \frac{W}{\rho_{\text{water}}} \varepsilon''_{\text{sw}} \frac{1}{\cos\theta} \tag{3.2}$$

where $\varepsilon''_{\text{sw}}$ is the imaginary part of the dielectric constant of saline water, k_0 is the wave number in air, W is the vegetation water content [kg/m^2], ρ_{water} is the density of water, and θ is the observation angle relative to nadir. The coefficient A_p depends on the canopy geometry. Originally, as introduced by Kirdyashev et al. [5], A_p appearing in Eq. (3.2) was a theoretically derived geometrical parameter. However, there is no simple way of deriving this parameter for actual vegetation such as grasses, trees or crops and the assumptions used in deriving Eq. (3.2) become invalid at higher frequencies. Hence, for comparing with satellite data, Kerr and Njoku [7] used Eq. (3.2) as an empirical formula and determined the parameter A_p individually for each frequency and canopy type.
M tzler et al. [4] examined the theoretical origin of Eq. (3.2), which is based on the Effective Medium theory , and showed that a more accurate frequency dependence can be obtained by considering the geometric optics theory. They derived a new, improved formula for the canopy opacity

$$\begin{cases} \tau_p = A_p k_0 \dfrac{B}{\rho_{\text{veg}}} \varepsilon''_{\text{veg}} \dfrac{1}{\cos\theta} t_p \\ B = \dfrac{W}{1 - m_d} \end{cases} \tag{3.3}$$

This result allows a direct connection of the low-frequency with the high-frequency approximation. The differences between Eq. (3.2) and Eq. (3.3) are the additional factor t_p that is the transmissivity of a single leaf at polarization p and the dry-matter fraction of leaves, m_d. The coefficient $\varepsilon''_{\text{veg}}$ is the imaginary part of the dielectric constant of leaves which is based on a combination of liquid water, organic material and air [1] (se section 3.1). The transmissivity t_p should not be confused with the transmission coefficient (that is derived in appendix A). As we mentioned before the derivation of the transmissivity is based on how the temperature is distributed in the system while the transmission coefficient is based on the magnitude of the electric and magnetic field in the different regions (we use the fact that the tangential components are continuous cross an interface between two media). Despite this we find that the two quantities are related. The transmissivity can be written as the square of the transmission coefficient.

$$\begin{cases} t_v = (t_{\parallel})^2 = T_{\parallel} \\ t_h = (t_{\perp})^2 = T_{\perp} \end{cases} \tag{3.4}$$

Here is $T_{\parallel}$ and $T_{\perp}$ the transmittance for the different states of polarization. This quantity is the ratio of the transmitted power to the incident power.

The validity of the Effective Medium theory is restricted to low microwave frequencies because of the assumption of homogeneous electromagnetic fields within the leaf. With the Geometric Optics theory the electric field within the vegetation components is no longer assumed to be constant which makes the range of validity extended to higher frequencies. It can be shown [4] that a criterion for the validity of the Effective Medium theory is $\lambda_0 > 200\,x$, with x being the smallest dimension of the leaf. For leaves with a thickness of 0.2 mm this leads to $\lambda_0 > 4$ cm or $f < 7.5$ GHz (the thickness of natural leaves often is between 0.1 and 0.3 mm). From this results Wegm ller et al [4] conclude that, for frequencies above 7.5 GHz, it is necessary to correct the model for the inhomogeneity of the electric field within the vegetation. Diffraction is neglected in the geometrical optics approach. This can be done as long as the area of single leaves is large compared to λ^2. If this condition is not met the more appropriate physical optics approach should be used.

3.3 Attenuation of a tree

A simple theoretical approach has been used by Torrico and Lang [8] to predict the specific attenuation of a tree for frequencies up to 2 GHz. At this frequency the wavelength is large compared to the maximum dimensions of the leaves (λ = 15 cm, radius = 5 cm) which means that the analysis will be based upon the approximation that the electric field can be considered as static over the entire leaf volume. The canopy of a tree is considered as a layer (or a wall) of thickness d which is modeled by a slab of leaves and branches as is shown in Figure 3.1. The slab is oriented in the y-z-plane. The leaves are modeled as randomly positioned flat-circular lossy dielectric discs and the branches as randomly positioned finitely-long lossy dielectric cylinders.

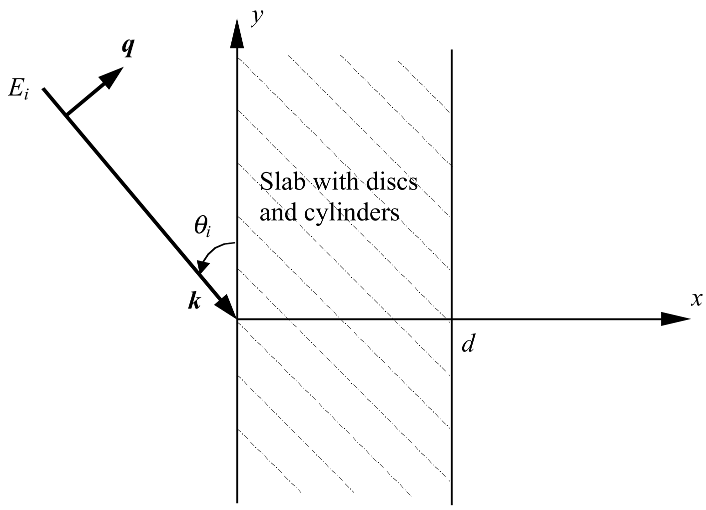

Figure 3.1: Incident plane wave with polarization $\boldsymbol{q}$ on a slab with thin discs and thin cylinders.

It is assumed that the cylinders and the discs are distributed uniformly in azimuthal coordinates ϕ, which are defined in the plane perpendicular to the slab (the x-y-plane). The canopy is thus a three-layered medium (as is shown in Figure 3.1). In the region $x < 0$ and $x > d$ we have free space with a free space permeability μ_0 and permittivity ε_0. In the region $0 < x < d$ we consider identical discs with a constant volume density ρ_d and identical cylinders with a constant volume density ρ_c. Furthermore a free space background medium is assumed in the slab and the interface between the slab and free-space is considered as smooth and does not introduce any reflections. In order to find the specific attenuation of the tree the mean field in the canopy has to be calculated. This is obtained by determining the dyadic scattering amplitudes of an arbitrarily oriented thin disc and of an arbitrarily oriented thin cylinder.

As a starting point we assume that a plane wave of unit amplitude and polarization $\boldsymbol{q}$ is incident upon the disc

$$\boldsymbol{E}_s(\boldsymbol{r},\boldsymbol{q}) = \boldsymbol{q}\, e^{ik_0(\boldsymbol{k}\cdot\boldsymbol{x})} \tag{3.5}$$

where $\boldsymbol{k}$ is the unit wave vector (direction of propagation) and k_0 is the free space propagation constant. Furthermore the disc is assumed to have cross-sectional shape S, a radius a, a thickness t and a complex relative permittivity ε_r. An expression for the vector scattered amplitude $\boldsymbol{f}$ can be found in [12]. The vector scattered amplitude $\boldsymbol{f}$ as observed in direction $\boldsymbol{o}$, can be related to the total field $\boldsymbol{E}_{ind}$ induced within the disc as follows

$$\boldsymbol{f}(\boldsymbol{o},\boldsymbol{k},\boldsymbol{q}) = \frac{k_0^2\,\chi_r}{4\pi}\left(\bar{\bar{\mathbf{I}}} - \boldsymbol{oo}\right)\int_V \boldsymbol{E}_{ind}(\boldsymbol{x}',\boldsymbol{q})\, e^{-ik_0(\boldsymbol{o}\cdot\boldsymbol{x}')}dv' \tag{3.6}$$

where $\chi_r = \varepsilon_r - 1$ is the susceptibility of the disc, $\bar{\bar{\mathbf{I}}}$ is a unit dyadic, and V is the volume of the disc. The relation between the vector scattered amplitude and the scattered electric field can be described by

$$\boldsymbol{E}(\boldsymbol{r}) = \frac{e^{ikr}}{r}\boldsymbol{f}(\boldsymbol{r}) \tag{3.7}$$

Compared to the far field expression Eq. (B.20)

$$\boldsymbol{E}_s(\boldsymbol{r}) = \frac{e^{ikr}}{kr}\boldsymbol{F}(\boldsymbol{r})$$

we note that the only difference between the two equations is that Eq. (3.7) does not have the wave propagation constant in the denominator. To find an expression for the induced field in the disc we assume that the disc radius a is much greater than the thickness of the disc t and the disc is electrically thin $k_{disc}t \ll 1$, where $k_{disc} = k_0\sqrt{|\varepsilon_r|}$. Moreover is the induced field within the disc approximated by the electric field in an unbounded slab that has the same orientation as the disc. These approximations lead to that we can employ the continuity conditions of the tangential field components across an arbitrary interface to express the induced field in terms of the incident field. We find

$$\boldsymbol{E}_{ind}(\boldsymbol{x}',\boldsymbol{q})=\left[\boldsymbol{q}-(\boldsymbol{n}\cdot\boldsymbol{q})\boldsymbol{n}+\frac{1}{\varepsilon_r}(\boldsymbol{n}\cdot\boldsymbol{q})\boldsymbol{n}\right]e^{ik_0(\boldsymbol{k}\cdot\boldsymbol{x}')} \tag{3.8}$$

Here $\boldsymbol{n}$ is the unit vector normal to the disc. Assuming that there is no-phase variation in the induced field normal to the disc ($k_{disc}t << 1$) and that the wave length is greater than the radius of the disc ($\lambda >> a$) the vector scattering amplitude can be obtained if Eq. (3.8) is substituted into Eq. (3.6)

$$\boldsymbol{f}(\boldsymbol{o},\boldsymbol{k},\boldsymbol{q})=\chi_r t\left(\frac{k_0 a}{2}\right)^2\left(\bar{\bar{\mathbf{I}}}-\boldsymbol{oo}\right)\left[\boldsymbol{q}-\left(\frac{\chi_r}{1+\chi_r}\right)(\boldsymbol{n}\cdot\boldsymbol{q})\boldsymbol{n}\right] \tag{3.9a}$$

The scalar scattering amplitude f_{pq} can be obtained by

$$f_{pq}=\boldsymbol{p}\cdot\boldsymbol{f}(\boldsymbol{o},\boldsymbol{k},\boldsymbol{q}) \tag{3.9b}$$

where $\boldsymbol{p}$ is the scattering polarization in direction $\boldsymbol{o}$.
The technique of calculating the dyadic scattering amplitude of an arbitrarily oriented thin cylinder is similar to the case of a thin disc. A plane way (Eq. (3.5)) is considered to be incident upon a cylinder of radius *a*, length *l* and complex relative permittivity ε_r . To find the vector scattering amplitude ***f*** we need to find the induced electric field within the cylinder. This is found by using a quasi-static technique. Under this approximation the electromagnetic boundary condition requiring the continuity of the tangential field components across an arbitrary interface can be employed to show that the induced electric field within the cylinder is given by

$$\boldsymbol{E}_{ind}(\boldsymbol{x}',\boldsymbol{q})=\left[\frac{2}{\varepsilon_r+1}\boldsymbol{q}+\frac{\varepsilon_r-1}{\varepsilon_r+1}(\boldsymbol{q}\cdot\boldsymbol{r})\boldsymbol{r}\right]e^{ik_0(\boldsymbol{x}'\cdot\boldsymbol{k})} \tag{3.10}$$

where $\boldsymbol{r}$ is the unit position vector directed along the symmetry axis of the cylinder. Finally, the vector scattering amplitude is obtained by substituting Eq. (3.10) into (3.6)

$$\boldsymbol{f}(\boldsymbol{o},\boldsymbol{k},\boldsymbol{q})=l\left(\frac{k_0 a}{2}\right)^2\chi_r\left(\bar{\bar{\mathbf{I}}}-\boldsymbol{oo}\right)\left[\frac{2}{\chi_r+2}\boldsymbol{q}+\frac{\chi_r}{\chi_r+2}(\boldsymbol{q}\cdot\boldsymbol{r})\boldsymbol{r}\right] \tag{3.11}$$

where $\chi_r=\varepsilon_r-1$ is the susceptibility of the disc and $\bar{\bar{\mathbf{I}}}$ is a unit dyadic.
The multiple scattering theory of Foldy [10] and Lax [11] is applied to derive the mean field in the canopy. Since the fractional volume occupied by the scatterers is small in comparison to the total volume *V* of the canopy the Foldy approximation — which assumes that the total field incident on a scatterer is equal to the mean field — can be used. The mean field in the canopy is obtained by solving the vector wave equation given in [13] and for a plane wave of unit amplitude and polarization $\boldsymbol{q}$ that is incident on the slab of scatters in the direction $\boldsymbol{k}$ as in Eq. (3.5) we get

$$\langle \boldsymbol{E}(x,z,\boldsymbol{q}) \rangle = \boldsymbol{q}\, e^{i \kappa_{qq} x - i k_0 \cos(\theta_i) z} \tag{3.12}$$

where

$$\kappa_{qq} = k_0 \sin(\theta_i) + \frac{2\pi}{k_0 \sin(\theta_i)} \sum_t \rho_t \left\langle f_{qq}^{(t)}(\boldsymbol{k},\boldsymbol{k}) \right\rangle \tag{3.13}$$

The incident plane wave makes an angle of θ_i with respect to the *z*-axis as is shown in Figure 3.1. Here κ_{qq} is the propagation constant in the *x*-direction of polarization $\boldsymbol{q}$ and $\left\langle f_{qq}^{(t)}(\boldsymbol{k},\boldsymbol{k}) \right\rangle$ is the mean forward scattering amplitude over the orientation of the scatterers. The sum is over scatterer type *t*. Because of the assumed independence of the distribution $\rho(\boldsymbol{s})$ on the transverse coordinates, the mean field in the canopy behaves like a plane wave in the transverse coordinates. The mean forward scattering amplitude can be written as

$$\left\langle f_{pq}^{(t)}(\boldsymbol{k},\boldsymbol{k}) \right\rangle = \frac{1}{2\pi} \int d\theta\, f_{pq}^{(t)}(\boldsymbol{k},\boldsymbol{k})\, p(\theta) \tag{3.14}$$

where $p(\theta)$ is the probability density function for the inclination angle and it is assumed that the probability density of the azimuthal angle is uniformly distributed from 0 to 2π. Because of the assumed azimuthal symmetry of the scatterers, the mean wave of the vertical and horizontal polarizations does not couple, so that no depolarization effects occur at the level of the mean wave. In general the wave propagation constant in the canopy κ has a real and imaginary component. This results from the fact that the scatterers have losses. The imaginary part of κ gives the specific attenuation in dB per meter and is given by

$$\alpha_{qq} \approx 8.686\, \mathrm{Im}(\kappa_{qq}) \quad \text{[dB/m]} \tag{3.15}$$

The propagation constant of an ensemble of thin discs is characterized in terms of the properties of an individual disc, which is found from the vector scattering amplitude given by Eq. (3.9a). By substituting Eq. (3.9a) in Eq. (3.9b) and then into Eq. (3.14) the four components of the mean forward scattering amplitude (*hh*, *hv*, *vh* and *vv*) for the ensemble of discs can be calculated. Using Eq. (3.13) and Eq. (3.15) we find that the specific attenuations for an ensemble of leaves in dB/m for different incident and scattering polarizations are given by

$$\alpha_{hh}^{d} = 8.686 \chi_r'' k_0\, \rho_d \frac{t a^2 \pi}{2 \sin\theta_i} \left[1 - \frac{1}{2} I_1 \right] \quad [\text{dB/m}] \tag{3.16}$$

$$\alpha_{vv}^{d} = 8.686 \chi_r'' k_0\, \rho_d \frac{t a^2 \pi}{2 \sin\theta_i} \left[1 - \left\{ \frac{1}{2} (\cos\theta_i)^2 I_1 + (\sin\theta_i)^2 I_2 \right\} \right] \quad [\text{dB/m}] \tag{3.17}$$

where

$$\begin{cases} I_1 = \int_{\theta_1}^{\theta_2} (sin\theta)^2 \, p(\theta) d\theta \\ I_1 = \int_{\theta_1}^{\theta_2} (cos\theta)^2 \, p(\theta) d\theta \end{cases} \tag{3.18}$$

We mentioned before that no depolarization effects occur at the level of the mean wave, which means that $\alpha_{hv}^{d} = \alpha_{vh}^{d} = 0$. The notation *d* is the type of scatterer (disc), *h* and *v* are the polarizations and $p(\theta)$ is the probability density in the polar coordinates of the leaves inclination. χ_r is the susceptibility of a disc given by $\chi_r = \chi' + i\,\chi''$ where the prime represents the real part and the double prime represents the imaginary part of the susceptibility. We have assumed that the real component of the susceptibility is much greater than its imaginary component. This is the case in general for thin discs.
The propagation constant of an ensemble of thin cylinders is calculated in a similar way as in the case of an ensemble of thin discs. This means that the propagation constant is characterized in terms of the properties of an individual cylinder. We find that the specific attenuation for an ensemble of branches for different incident and scattering polarizations are given in dB/m by

$$\alpha_{hh}^{c} = 8.686 \chi_r'' k_0 \, \rho_c \frac{l\, a^2 \pi}{2\, sin\theta_i} \frac{I_1}{2} \quad [\text{dB/m}] \tag{3.19}$$

$$\alpha_{vv}^{c} = 8.686 \chi_r'' k_0 \, \rho_c \frac{l\, a^2 \pi}{2\, sin\theta_i} \left[\frac{1}{2} (cos\theta_i)^2 I_1 + (sin\theta_i)^2 I_2 \right] \quad [\text{dB/m}] \tag{3.20}$$

Depolarization effects in the case of thin cylinders are negligible and thus $\alpha_{hv}^{c} = \alpha_{vh}^{c} = 0$. The type of scatterer is denoted by *c* (cylinder). We have here used the fact that the real part of the susceptibility of a thin cylinder, in general is much greater than its imaginary part. Finally, the specific attenuation of a tree is found by adding the specific attenuation of the branches and leaves of similar polarizations. We find

$$\begin{cases} \alpha_{hh} = \alpha_{hh}^{d} + \alpha_{hh}^{c} \\ \alpha_{vv} = \alpha_{vv}^{d} + \alpha_{vv}^{c} \end{cases} \tag{3.21}$$

The leaves are assumed to have a radius *a* = 5 cm and a thickness *t* = 0.5 mm, a dielectric constant of $\varepsilon_r = 26 + i\,7$ and a density of $\rho_l = 350 / \text{m}^3$. The branches are assumed to have a radius *a* = 1.6 cm and a branch length *l* = 50 cm, a dielectric constant $\varepsilon_r = 20 + i\,7$ and a density $\rho_l = 2 / \text{m}^3$. The probability density for the leaves and the branches in the azimuthal coordinate ϕ is assumed to be uniformly distributed from 0 to 360 deg. The probability density in the θ coordinate is dependent on vegetation type. For the branches and leaves it is considered to be uniformly distributed

$$p_\theta(\theta) = \frac{1}{\theta_1 - \theta_2} \tag{3.22}$$

where $\theta_2 = 180^\circ$ and $\theta_1 = 0^\circ$ for the leaves and $\theta_2 = 60^\circ$ and $\theta_1 = 0^\circ$ for the branches. Finally, it is important to note that the relative dielectric constants of the leaves and branches are frequency dependent [1]. In the analysis constant values for the permittivities of the leaves and the branches have been assumed because the permittivities of the leaves and the branches do not change much between 800 MHz to 2000 MHz.

3.4 Microwave transmissivity of a forest canopy

Microwave measurements have been executed by M tzler [3] for the microwave transmissivities and opacities of the crown of a beech (Fagus sylvatica L.). The technique used for measurements corresponds to the one explained in section 3.2. To avoid any prejudice on the type of microwave propagation model, M tzler limit the physical interpretation to obvious facts and to consistency tests of the multivariate dataset. The main instruments that have been used in the study are the five microwave radiometers of the PAMIR system.

The transmitted power has been recorded during a whole year. In this way it has been possible to get an apprehension of how much the attenuation is affected by the leaves alone since measurements were made both for a canopy containing leaves and branches and for a canopy without leaves. The microwave radiation at 4.9 GHz, 10.4 GHz, 21 GHz, 35 GHz and 94 GHz was measured about once every week between August 1987 and August 1988.

During the measurements the radiometer was placed to measure the transmissivity in a vertical direction through the beech. Thus it measures the brightness temperature T_{b1} of downwelling radiation from the beech. This temperature can be expressed by

$$T_{b1} = tT_{b2} + rT_{b0} + (1 - r - t)T_1 \qquad (3.23)$$

where *t* is the transmissivity and *r* the reflectivity of the vegetation layer. Here T_1 is the physical tree temperature and T_{b2} is the sky brightness temperature. That from the ground upwelling brightness temperature T_{b0} is given by

$$T_{b0} = e_0 T_0 + (1 - e_0)T_{b1} \qquad (3.24)$$

where e_0 is the emissivity of the ground surface and T_0 is the ground temperature.

Eq. (3.23) and Eq. (3.24) are the basic equations for the experiments and they can be used to get an expression for the transmissivity of the tree crown. After some algebra we find

$$t = \frac{T_1 + r\,\delta T - T_{b1}}{T_1 - T_{b2}} \qquad (3.25)$$

where $\delta T = T_{b0} - T_1$. Since the emissivity of the grass-covered ground below the beech is near 0.95 — over the entire frequency range — T_{b0} approaches T_0. This and the fact that the reflectivity of the beech is close to 0.1 lead to the following estimation

$$r\,\delta T = 0.1(T_0 - T_1)$$

Since T_0 and T_1 always are very similar (differences were typically within $\pm 2\ ^{\circ}\mathrm{C}$) we can neglect $r\,\delta\,T$ in Eq. (3.25) and write

$$t = \frac{T_1 - T_{b1}}{T_1 - T_{b2}} \tag{3.26}$$

In order to compute t we need values of the physical tree temperature T_1, of the brightness temperature T_{b1}, measured below the tree, and of the sky brightness temperature T_{b2}.
In the beech experiment T_{b2} was measured at zenith angles of 50° and 60°, and T_{b1} (the downwelling radiation of the beech) was measured at two linear (v) and (h) polarizations, at vertical direction, and through the center of the crown at 30° off zenith opposite the direction of the sky measurements. The tree temperature T_1 was measured with an infrared radiometer and compared with air and grass temperatures. We define the effective opacity of the vegetation layer

$$\tau = -ln(t) \tag{3.27}$$

in accordance with the Lambert-Beer law.
The temporal variation of the transmissivities at 4.9 GHz in vertical direction through the beech is shown in Figure 3.2 with the corresponding temperature measurements illustrated in Figure 3.3.

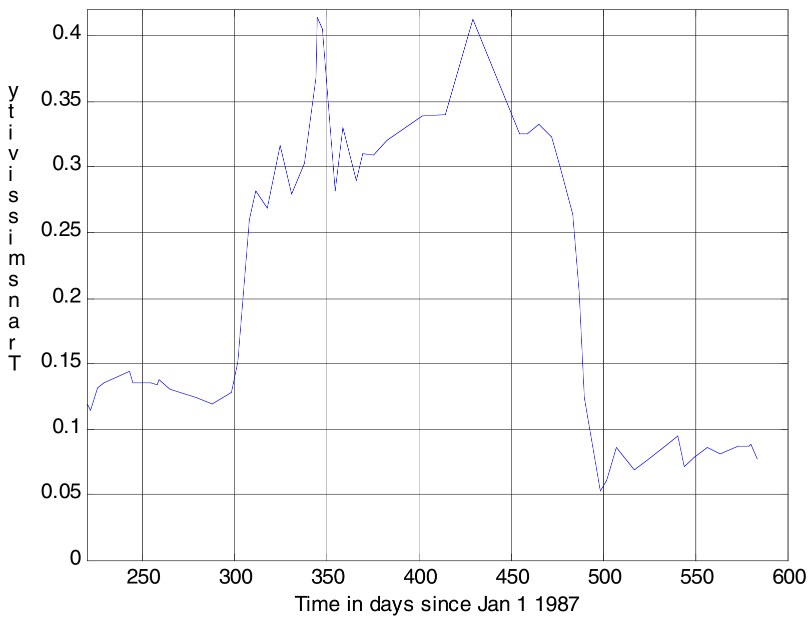

Figure 3.2: Transmissivity of a beech at 4.9 GHz versus time from August 1987 to August 1988.

The transmissivity data of Figure 3.2 clearly reflect the seasonal variation of the tree state with high t values during the defoliated period in winter and low values for the foliated beech.

The number of leaves remained nearly constant from August 1987 (Day 220) to mid-October (Day 290), when the leaves started to fall. Defoliation was most intense in early November (Day 306), and it was completed one month later when freezing began. Buds started to grow rapidly in April, they started to open on 23 April (Day 479), and 10 days later the leaves were almost fully open. No additional leaves were formed during the following observation period until August 1988.

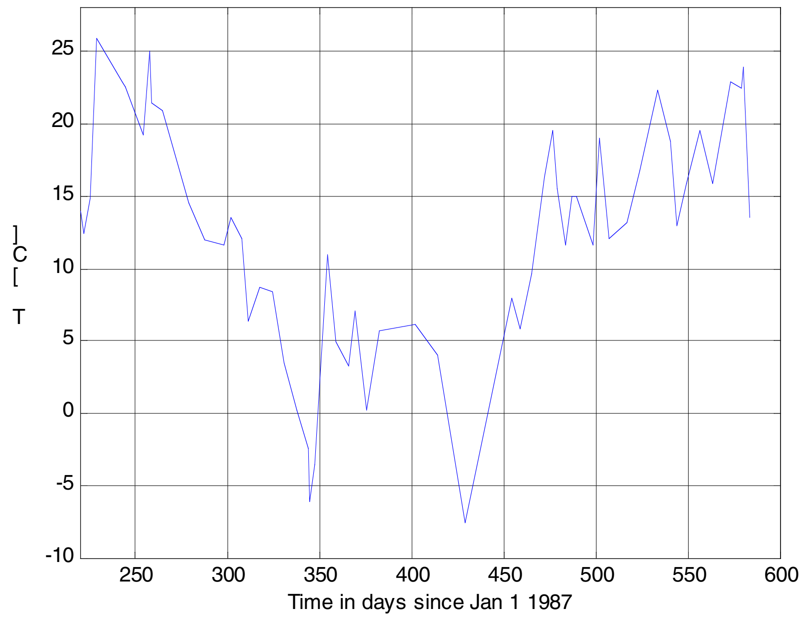

Figure 3.3: Tree temperature versus time from August 1987 to August 1988.

Variations of *t* during winter are related to changes in liquid water in the branches; thus the peaks of *t* are related to frozen conditions which is easy to confirm if we study Figure 3.3. Short-time variations during the foliated state are dominated by two factors: wind effect and temperature variation. Under the influence of wind the transmissivities were increased. This effect was most clearly felt when northeasterly winds hit the forest perpendicularly to its border. The transmissivity in a vertical direction through the beech increases with increased wind power. This effect can be explained by the change of the leaf orientation. For quiet conditions the leaves show a predominantly parallel, mostly horizontal orientation as forest trees often do. With increasing wind the distribution gets more and more isotropic. For strong wind it is also possible that the airflow opens channels in the canopy through which radiation can be guided.

The effects of freezing are shown in Figure 3.4. Freezing means reducing the liquid water content in the vegetation components, which leads to a decrease of the opacity. Liquid water increases the attenuation, i.e. a decrease of the transmissivity. A certain saturation of the freezing effect appears at -4 deg C.

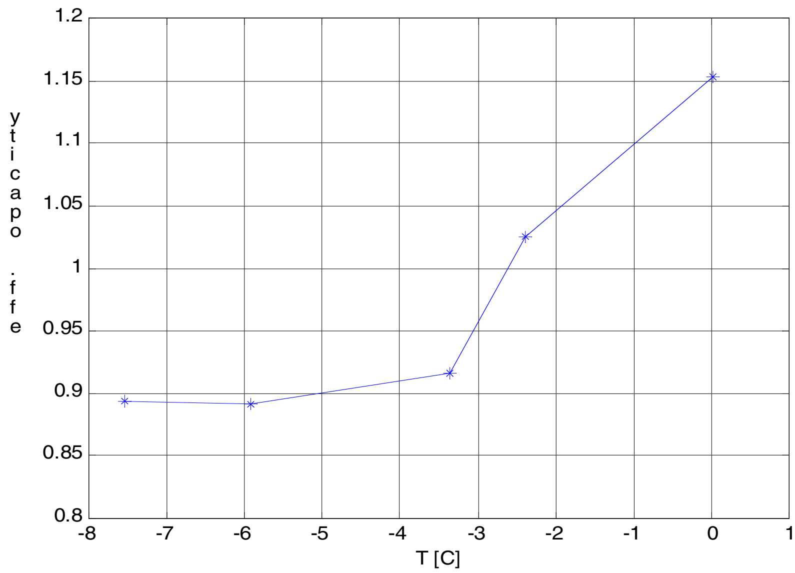

Figure 3.4: Opacities at 4.9 GHz versus temperature. Measured in vertical direction through the defoliated test beech in winter conditions.

The freezing effect is more pronounced at lower frequencies. At higher frequency values the branches remain opaque over the observed temperature range. For the defoliated test beech (at wintertime) the opacity is only weakly dependent on frequency. A maximum can be identified at 10 GHz with an effective opacity of about 1.3. With increasing frequency the opacity approaches 1.0. This value was also estimated from measurements of visible light. At low frequencies (1-3 GHz) the curves of the foliated and of the defoliated beech converge. This means that the influence of leaves becomes negligible. On the other hand, above 3 GHz the opacity increases strongly with increasing frequency for the foliated beech.

4 Tree modeling

In this section we analyze and model the dielectric properties of leaves and branches. We also analyze the structure of the crown of a tree. Despite the stochastic nature of this subject it is still possible to make some conclusions on the orientation and distribution of the leaves and branches. Since we have made our attenuation measurements on a Fagus sylvatica 'Pendula' (beech) the analysis is based on this tree. It is easy to adjust the results to another tree type since only a few parameters are related to the structure of the tree.

4.1 Dielectric model of Leaves

Leaves consist of a heterogeneous cell structure. Since frequencies are used with wavelengths corresponding to values around 0.5 to 1 dm the incident field is not able to resolve the cell structure. Thus the material of the leaves resembles a homogeneous material with effective medium properties. As was mentioned before (see section 3.1) the effective dielectric properties are modeled by dielectric mixing theory. In the technique of dielectric mixing theory the volume fractions of the different parts of the object are multiplied with the corresponding permittivity to obtain the effective permittivity of the object. If the object with the volume V consists of three components with the volumes V_1, V_2 and V_3, where the respective component has the permittivity ε_1, ε_2 and ε_3, we get

$$\varepsilon_{\mathrm{eff}} = \frac{1}{V}\{V_1\,\varepsilon_1 + V_2\,\varepsilon_2 + V_3\,\varepsilon_3\} = v_1\,\varepsilon_1 + v_2\,\varepsilon_2 + v_3\,\varepsilon_3 \tag{4.1}$$

where $V_i = v_i V$ and $v_1 + v_2 + v_3 = 1$. In the case of leaves[1] the components are liquid saline water with a high permittivity, organic material with moderate to low permittivity and air with unit permittivity. All attempts so far to use the physical mixing theory to create a formula for the effective permittivity of a leaf have failed. The reason is probably the large differences of volume fractions and permittivities between the different components — a leaf can consists of up to 90 percent of water (or even more) — which probably causes nonlinear effects.

To create a valid formula for the permittivity of a leaf we have to use another technique. Since the saline water of the leaf causes the largest contributions to the disturbance of the incident electromagnetic field, a model of the water content could serve as a basis. This model should thereafter be adjusted to the experimental values from leaves at different frequencies and at different dry matter fractions in order to compensate for the effects that the organic matter and air has on the permittivity.

A model that describes the dielectric properties of saline water is the Debye model [14]

$$\varepsilon_{\mathrm{sw}} = \varepsilon_\infty + \frac{\varepsilon_s - \varepsilon_\infty}{1 - i\omega\tau} + i\frac{\sigma}{\omega\varepsilon_0} \tag{4.2}$$

Here ε_∞ is the value of the dielectric function at high frequencies, ε_s is the corresponding value at $\omega = 0$ and τ is the relaxation time. The values of the different parameters are

[1] This is valid for all sorts of vegetation elements such as branches, herbs, trunks etc.

$$\begin{cases} \tau = 1.0 \cdot 10^{-11}\ \text{s} \\ \varepsilon_\infty = 5.27 \\ \varepsilon_s = 80.0 \end{cases} \qquad \begin{cases} c_0 = 299792458\ \text{m/s} \\ \mu_0 = 4\pi \cdot 10^{-7}\ \text{N/A}^2 \\ \varepsilon_0 = 1/\left(c_0^2\,\mu_0\right) \approx 8.854187817 \cdot 10^{-12}\ \text{F/m} \end{cases}$$

The conductivity σ for water is related to the salinity. A typical value for fresh water is $\sigma = 10^{-3}$ S/m and for salt water $\sigma = 3-6$ S/m. The average salinity of the world ocean is 3.5 % with a conductivity of σ = 5.8 S/m. Temperature can also have large effects on the conductivity for water. In contrast to metals, the conductivity for a solution like saline water, increases when the temperature increases. Normally, the value for conductivity is given at 20 deg C and since the conductivity of most solutions changes at approximately 2.2 % per deg C, this property should be taken into account.

M tzler and Sume [2] investigated the interaction of microwaves with individual leaves at 21, 35 and 94 GHz. Information of the dielectric properties of the leaves acquired radiometric measurements. The instruments were installed on a trailer and operated in Moosseedorf, near Bern (570 m above sea level). In order to measure the microwave parameters, the leaf area must at least cover the size of the horn antenna (the standard gain horns have aperture diameters of about 10 wavelengths). This resulted in that some of the leaves could not be measured at 21 GHz. A total of 33 leaves from 12 different plants were used. Some of the results are depicted in Table 4.1. M tzler [1] used the data from these measurements and together with other measurements (see section 3.1) to construct a semiempirical formula for the complex dielectric permittivity of leaves valid in the frequency range 1-100 GHz.

$$\varepsilon_{\text{leaf}} = 0.522\left(1 - 1.32\,m_d\right)\varepsilon_{\text{sw}} + 0.51 + 3.84\,m_d \tag{4.3}$$

He came to the conclusion that leaves from different plants at room temperature can be described by only two parameters: thickness d and dry matter content m_d. This conclusion should not be generalized to all plants since it is known that surface

Table 4.1: Results from measurements of leaves at 21, 35 and 94 GHz. The quantities that have been measured are: leaf thickness (d), dry-matter fraction (md), transmissivity (t) and reflectivity at horizontal and vertical polarization (rh and rv).

Plant	**Date**	**d [mm]**	**md**	**t21**	**t35**	**t94**	**rh21**	**rh35**	**rh94**	**rv21**	**rv35**	**rv94**
Beech	10-Aug-87	0.125	0.240	0.580	0.470	0.350		0.220	0.280		0.100	0.104
Maple	20-Aug-87	0.150	0.350	0.480	0.400							
Linden	1-Sep-87	0.175	0.410	0.540	0.460		0.170	0.260		0.060	0.100	
Walnut	10-Sep-87	0.210	0.333	0.446	0.423	0.310	0.190	0.310	0.390	0.100	0.110	0.120
Maple	10-Sep-87	0.170	0.370	0.550	0.460	0.350	0.190	0.270	0.330	0.065	0.080	0.070
Oak	10-Sep-87	0.145	0.400		0.560	0.440		0.164	0.260		0.060	0.080
Linden	21-Sep-87	0.145	0.340		0.413	0.322		0.256	0.366		0.075	0.088
Linden	21-Sep-87	0.140	0.240	0.492	0.420	0.344		0.235	0.339		0.082	0.084
Linden	21-Sep-87	0.145	0.320	0.528	0.460	0.363		0.213	0.357		0.064	0.067
Linden	21-Sep-87	0.145	0.390	0.543	0.457	0.363	0.171	0.209	0.336		0.070	0.071
Hazel	21-Sep-87	0.132	0.400	0.580	0.513	0.411	0.120	0.177	0.254	0.041	0.046	0.034
Hazel	21-Sep-87	0.145	0.370	0.546	0.473	0.370		0.177	0.303		0.062	0.041
Beech	16-May-88	0.090	0.260		0.580	0.450		0.100	0.140		0.030	0.035
Beech	16-May-88	0.110	0.260		0.500	0.400		0.150	0.210		0.050	0.060

roughness can reduce the reflectivity. But since most of the common trees contain leaves with smooth surface, Eq. (4.3) will be a useful in vegetated residential environments.

The dry matter fraction m_d for leaves varies over the whole summer. In the early summer, after the leaves have reached their maximum size, the dry matter fraction takes the value 0.1. This value increases during summer and will at the end of summer (or at the beginning of the autumn) take values between[2] 0.4 and 0.5. Since we made our measurements in the middle of September and some of the leaves already had start to change color, we estimate that a reasonable value for the dry matter fraction probably is $m_d = 0.4$. Even if the dry matter fraction changes the water content in the leaves stays rather constant during the life cycle. This means that the organic matter increases during the period and that there is a probability that the salinity changes. But since measurements indicate that the permittivity of leaves for a given frequency is affected linearly by a change in m_d the conductivity must stay rather constant (else the change would be exponential). This means that we can assume that the change of salinity is minimal during the whole life cycle.

To make explicit calculations on the absorption and the scattering we need to know the value of the conductivity of leaves. This can be done if we examine [1] and analyze the derivation of Eq. (4.3). A linear regression technique of the form

$$\begin{cases} \varepsilon' = A' + B' m_d \\ \varepsilon'' = A'' + B'' m_d \end{cases}$$

is used as a first step in the attempt of finding a dry-matter fraction dependent permittivity function. Here ε' is the real part and the imaginary part ε'' of the permittivity. From the experimental values the coefficients A' and A'' are determined for different frequencies. These coefficients are plotted in a diagram together with the corresponding frequency values. In the same diagram the Debye relaxation function

$$\varepsilon(m_d = 0) = \alpha \varepsilon_{\mathrm{sw}} + \beta$$

is fitted to the coefficients which gives

$$\varepsilon(m_d = 0) = A = A' + iA'' \cong 0.522 \varepsilon_{\mathrm{sw}} + 0.51 \tag{4.4}$$

Thereafter is the Debye relation, Eq. (4.2), used with numerical values inserted. This gives the frequency dependence of the coefficients

$$\begin{aligned} A' &\cong 3.07 + \frac{38}{1 + (f/f_0)^2} \\ A'' &\cong \frac{12.4 \cdot 10^9}{f} + \frac{38 f}{f_0 \left(1 + (f/f_0)^2\right)} \end{aligned} \tag{4.5}$$

If we now assume that $f_0 = 1/\tau = 10^{11}$ Hz and insert Eq. (4.5) and Eq. (4.2) into Eq. (4.4) we find

[2] Just before the leaves fall of the dry matter fraction takes values around 0.5.

$$\sigma = 1.32 \ [\mathrm{S/m}]$$

which corresponds to the value leaves. During the measurements the temperature was 20 deg C and the salinity in the leaves 0.9 %.

To assure that the calculated value for the conductivity is reasonable we can assume that the relation between the salinity and the conductivity is locally linear. This means that for a small change of the salinity ΔS the conductivity follows

$$\Delta\sigma = \kappa\Delta S$$

If we also assume that the conductivity is zero for zero salinity and at the same time use the values from the world ocean we find

$$\sigma(\mathrm{S}) = 1.67\,\mathrm{S} \tag{4.6}$$

where the salinity S is given in percent. This means that $\sigma = 1.50$ S/m for a salinity of 0.9 %. Since the difference between the two values of the conductivity is small we can assume that a proper value for the conductivity in leaves is $\sigma = 1.32\,\mathrm{S/m}$. The dielectric permittivity function has been calculated for the two values of the dry-matter fractions $m_d = 0.1$ and $m_d = 0.5$. In Figure 4.1 we find the real part of the

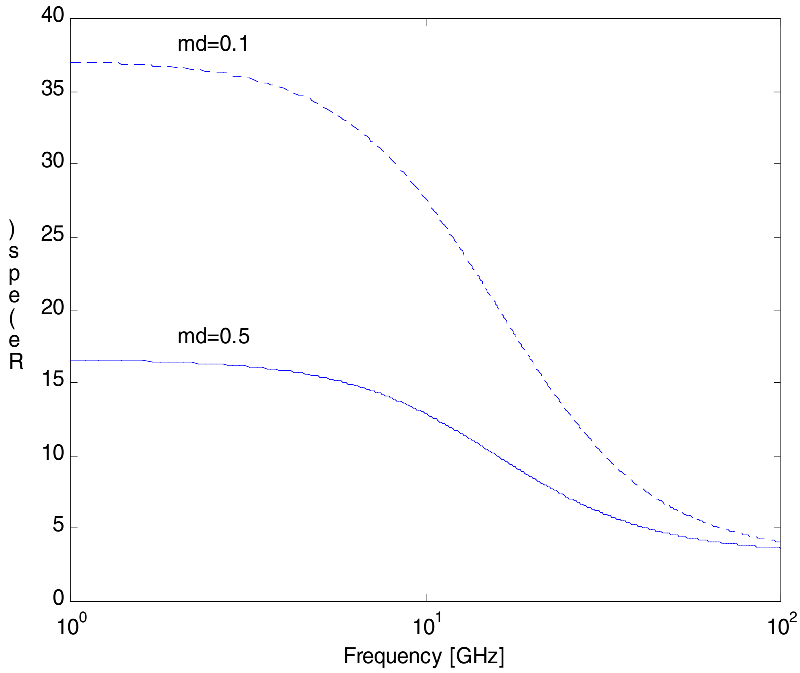

Figure 4.1: Real part of the dielectric permittivity for leaves plotted versus the frequency in the range 1-100 GHz for the dry-matter fractions $\mathrm{m_d} = 0.1$ and $\mathrm{m_d} = 0.5$.

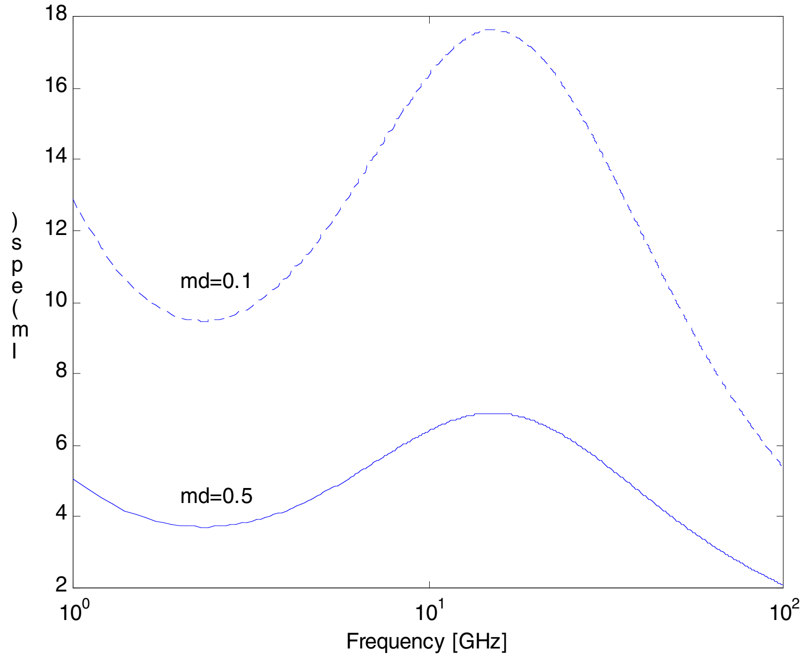

Figure 4.2: Imaginary part of the dielectric permittivity for leaves plotted versus the frequency in the range 1-100 GHz for the dry-matter fractions $m_d = 0.1$ and $m_d = 0.5$.

dielectric permittivity versus the frequency and in Figure 4.2 the imaginary parts of the corresponding calculations are shown. In Figure 4.3 and 4.4 the dielectric permittivity function has been calculated for the two frequencies 3.1 GHz and 5.8 GHz for different values of the dry-matter fraction, m_d.

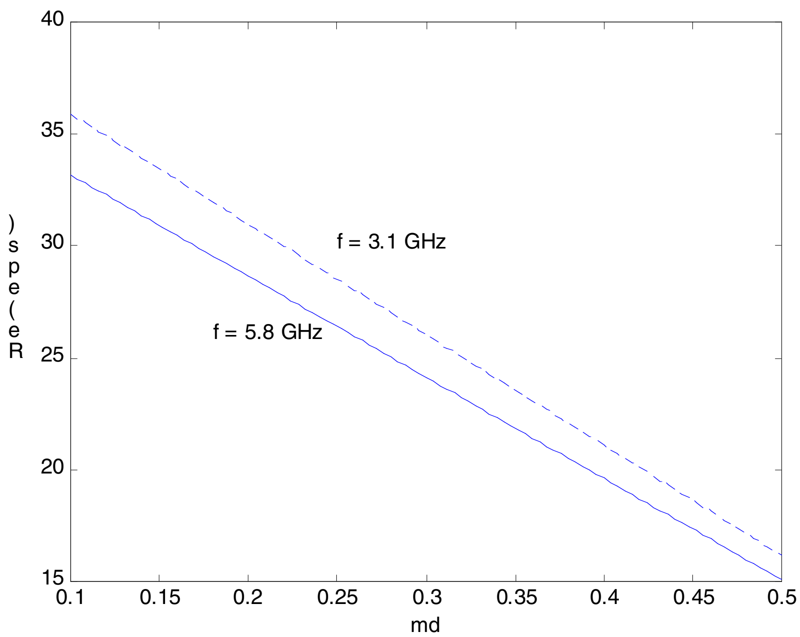

Figure 4.3: Real part of the dielectric permittivity for leaves plotted versus the dry-matter fraction. The two lines correspond to 3.1 GHz and 5.8 GHz.

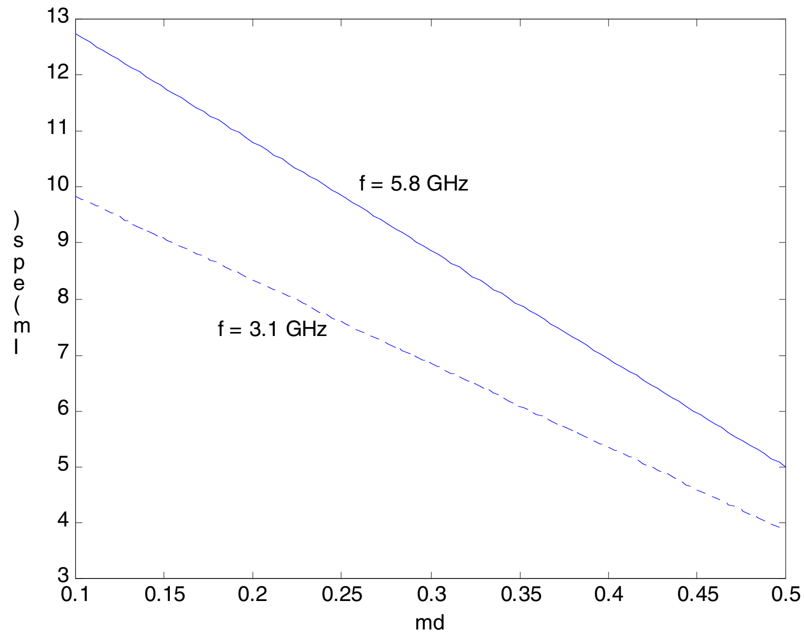

Figure 4.4: Imaginary part of the dielectric permittivity for leaves plotted versus the dry-matter fraction. The two lines correspond to 3.1 GHz and 5.8 GHz.

4.2 Dielectric Model of branches

Despite our efforts to find an existing model that describes the dielectric properties of branches we have so far not been successful. But since we in our research have found a lot of material about attenuation and wave propagation in general we are able to do some qualified guesses. For leaves we know that the influences of the organic matter to the power loss are minimal[3]. It is therefore reasonable to assume that the same effect is valid for the organic matter in branches too - Torrico and Lang [8] used the value $\varepsilon = 20 + i\,7$ for branches and the value $\varepsilon = 26 + i\,7$ for leaves in their prediction model of the attenuation of a tree at 2 GHz. Since leaves and branches have small values of the dry-matter fraction m_d we can assume that the saline water dominates the total power loss. The dry-matter content in the early part of the summer is 0.1 for leaves, which thereafter increases to 0.4-0.5 at the autumn just before the leaves fall of the trees. But since the trunk and the branches do not follow the same life cycle the dry-matter fraction stays more constant. Measured values are about 0.40 to 0.45 for the trunk and 0.35 to 0.40 for the branches. This indicates that the differences between the permittivity of leaves and branches — at the end of the summer — must be small[4]. Since the major difference between leaves and branches is their content of saline water, we can assume that the dielectric formula for the leaves, Eq. (4.3), can be used to estimate the permittivity of the branches. The error that this assumption generates can with some certainty be assumed to be small. M tzler [3] made some measurements on a beech over a whole year in the frequency range 4.9 GHz to 94 GHz. The transmissivity at 4.9 GHz in the summer was 0.12 to 0.14 and

[3] It is the saline water in the leaves that causes most of the losses.
[4] We have here assumed that the salinity is 0.9 % in the leaves as well as in the branches.

in the winter 0.30 to 0.40 (see Figure 3.2). This indicates that losses from leaves are 1.3 to 1.5 times larger than the losses from branches.
A proper value for the permittivity of the branches can thus be estimated if we use the fact that the dry-matter fraction of the branches stays rather constant during the whole year and use a value between 0.35 and 0.40 in the calculations. Since the leaves have values around 0.4 at the beginning of the autumn we assume that the same is valid for the branches. Insertion of $m_d = 0.4$ into Eq. (4.3) generates

$$\varepsilon_{\text{branch}} = 0.246\varepsilon_{\text{sw}} + 2.05 \qquad (4.7)$$

which thus describes the relative permittivity of a branch.

4.3 Crown structure

The crown of a tree can be thought of as an ensemble of leaves and branches with different size and orientation. Moreover the crown is not homogeneous which means that there will be regions with denser distribution and regions with sparser distribution. In the analysis of the vegetation attenuation (see section 5) we homogenize the crown of the tree and use the quantities N_l and N_b that gives the number of leaves and branches per unit volume on the average. This quantity is a measure of how dense a crown is. We know from section 3.4 that this value is not a constant in time. In Figure 3.2 we see that the value of the transmissivity is between 0.11 and 0.15 the first summer and between 0.05 and 0.1 the second summer. This means that the number of leaves and branches per unit volume was greater the second summer.
To simplify the analysis the leaves are modeled in two ways. In the case of long and short wave approximations, they are modeled as randomly positioned flat-circular lossy dielectric discs and in the resonance region (when the wavelength is of the same size as the leaves) they are modeled as randomly positioned thin lossy dielectric oblate spheroids. The branches are modeled as randomly positioned finitely-long lossy dielectric cylinders in all three models. Furthermore only the mean value of the geometry of the leaves is used. To get the mean value of the leaf area we first approximate the leaf by an ellipse with the area $\pi\, wl$, where w and l is the width and length of the leaf. If we thereafter let the area of the ellipse equal the area of the disc we get the relation

$$r = \sqrt{wl} \qquad (4.8)$$

which is used to describe the radii of the leaf. The leaf can in this way be approximated by a circular disc. The thickness of the leaves is quite independent of the size of the cross section of the leaves and a measured value of 0.1 mm is used in the calculations.
The orientation of leaves and branches is dependent on the type of tree that is analyzed and in which environment the tree stands. Trees in forest are often less illuminated than trees with free space around them. This leads to that the leaves in the lower part of the crown usually have a more horizontal orientation compared to the leaves in the upper parts. For trees that stand by themselves — i.e. trees in parks — it is different; the leaves get more illuminated which cause the leaf angle to be scarp also in the lower part of the crown and thus will the leaves take a more or less vertical orientation. The tree we have made our measurements on, the Fagus sylvatica Pendula (see Figure 4.5), stands in an environment where it get exposed by sunlight the whole day. Naturally will this have the effect that all the leaves are more or less vertical oriented. This fact is actually not disadvantage to us since wave propagation between

antennas on rooftops only is attenuated by the upper part of the tree crown, where all the leaves are more or less vertical oriented.
The orientation of the branches is strongly dependent on the tree type and not so much to the exposure. In this case we have a few branches that are long and thick (5 cm to 10 cm) with an almost horizontal orientation. From these branches a set of much thinner branches (1 mm to 10 mm) is hanging. Since the small branches totally outnumber the thick branches it is not a very large restriction to assume that the contribution to the scattered field, from the thick branches, is negligible and can be neglected. The branches in the crown are then modeled as thin cylinders with vertical orientation on average.

Figure 4.5: Photo of the test beech, the Fagus sylvatica Pendula.

5 Propagation and attenuation of the electromagnetic field

Electromagnetic waves propagating through foliages are attenuated because of absorption of power in the lossy dielectric medium represented by leaves and branches. There is also some losses in the direct transmitted wave because of scattering of power out of the beam by the components of the canopy. The theory for canopy attenuation and scattering is based on the calculation of the absorption and scattering cross sections of a single leaf and a single branch. The sum of the absorption and scattering cross sections is called the total cross section and is the quantity that will be of our interest. Three different methods have been used to derive expressions for the total cross section. These methods are valid in different frequency regions where different approximations have been used. The first method is based on a long wave approximation (Rayleigh scattering). The second method is based on the T-matrix method. With this method it is possible to get exact solutions to the scattering problem and thus an expression for the scattered electric field in the far zone can be calculated. The third method is based on a short wave approximation (physical optics) and should thus be used when it can be assumed that effects related to the boundary can be neglected — i.e. when the wavelength is much shorter than the size of the scattering body.
In section 1 we mentioned that if the medium is a weak scatterer the Born or Rytov approximation can be applied. To find out if this is the case here we first have to find explicit permittivity values for the branches and the leaves at 3.1 GHz and at 5.8 GHz. This can be achieved if we use the value for the conductivity for the saline water in organic matter (which was calculated in section 4.1). If this value is used and Eq. (4.2) at the same time is inserted into Eq. (4.3) we find $\varepsilon = 21.1 + \mathrm{i}\,7.4$ at 3.1 GHz and $\varepsilon = 19.6 + \mathrm{i}\,9.0$ at 5.8 GHz. A condition that has to be fulfilled for a medium in order to be classified as a weak scatterer is $\chi = \varepsilon - 1 << 1$ where χ is the susceptibility function of the material. Since this condition is not met here we find that neither of the two approximations — Born or Rytov — can be used to calculate the scattered electric field.

5.1 Attenuation by leaves and branches

To derive an expression for the attenuation of the field that propagates through the canopy of a tree we consider a volume, V, which is bounded by a cone of the power flux lines and two spherical surfaces, see Figure 5.1. That to the volume incident power, P_i, corresponds to the power emitted from the transmitter, P_0, minus some power loss. Some of the power is absorbed in the volume while some of the power is scattered by the different components in the volume.

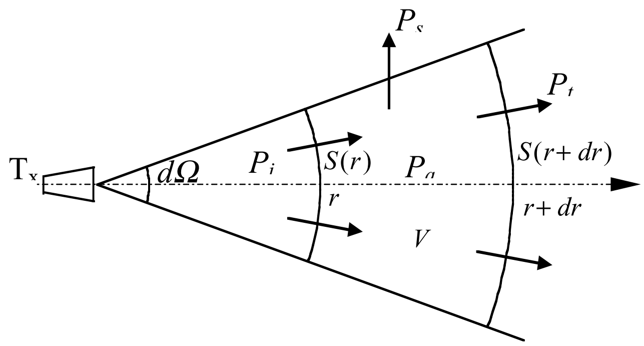

Figure 5.1: The cross-section of a spherical beam cone formed by the emitted power.

First we consider the power[5] balance in the volume

$$P_i = P_a + P_s + P_t \tag{5.1}$$

where the different components are

P_i	Incident power
P_a	Absorbed power
P_s	Scattered power
P_t	Transmitted power

The time-average value of the Poynting vector (see Eq. (2.33))

$$\boldsymbol{S}_{av}(\boldsymbol{r}) = \langle \boldsymbol{S}(\boldsymbol{r},t) \rangle = \frac{1}{2}\mathrm{Re}\{\boldsymbol{E}(\boldsymbol{r},\omega) \times \boldsymbol{H}^*(\boldsymbol{r},\omega)\} \tag{5.2}$$

gives a value of the power density (W/m^2). The incident power can be written in terms of $\boldsymbol{S}_{av}(\boldsymbol{r})$ which yields

$$P_i = \boldsymbol{S}_{av}(\boldsymbol{r}) \cdot \boldsymbol{n}\, r^2 d\,\Omega \tag{5.3}$$

Here $\boldsymbol{n}$ is the normal of the first surface and $r^2 d\,\Omega$ is the spherical surface area where $d\,\Omega$ is the differential solid angle, $d\,\Omega = \sin\theta\, d\,\theta\, d\,\phi$. Since the symmetry is spherical the projection of the average power density is the same as the magnitude of the average power density.

$$S_{av}(\boldsymbol{r}) = \boldsymbol{S}_{av}(\boldsymbol{r}) \cdot \boldsymbol{n}$$

The symmetry also leads to that we can use the argument *r* instead of the position vector ***r*** and thus can the power components in Eq. (5.1) be restated as

$$\begin{cases} P_i = S(r) r^2 d\,\Omega \\ P_t = S(r+dr)(r+dr)^2\, d\,\Omega \\ P_s = S(r) V \left(N_l \langle \sigma_{ls} \rangle + N_b \langle \sigma_{bs} \rangle\right) \\ P_a = S(r) V \left(N_l \langle \sigma_{la} \rangle + N_b \langle \sigma_{ba} \rangle\right) \end{cases} \tag{5.4}$$

From now on we denote the average power density as $S(r)$ instead of $S_{av}(r)$ to simplify the notation. The number of leaves per unit volume is denoted by N_l and the number of branches per unit volume is denoted by N_b . The scattering cross section (which is elucidated in the next section) of leaves is denoted by $\langle \sigma_{ls} \rangle$ and for branches by $\langle \sigma_{bs} \rangle$. The absorption cross section of leaves and branches is in a corresponding way denoted by $\langle \sigma_{la} \rangle$ and $\langle \sigma_{ba} \rangle$. The

[5] With power we refer to the time-average radiated power $P = \langle P(t) \rangle = \frac{1}{T}\int_0^T P(t)dt$.

bracket around the cross sections denotes expectation value. Now we introduce the total cross section

$$\langle \sigma_t \rangle = \langle \sigma_s \rangle + \langle \sigma_a \rangle \tag{5.5}$$

which leads to that the total power loss can be written as

$$\begin{aligned} P_l = P_s + P_a &= S(r)V\left(N_l\langle \sigma_{ls} \rangle + N_b\langle \sigma_{bs} \rangle\right) + S(r)V\left(N_l\langle \sigma_{la} \rangle + N_b\langle \sigma_{ba} \rangle\right) \\ &= S(r)V\left(N_l\langle \sigma_{lt} \rangle + N_b\langle \sigma_{bt} \rangle\right) \end{aligned} \tag{5.6}$$

Substitution of Eq. (5.4) and Eq. (5.6) into Eq. (5.1) yields

$$S(r)r^2 d\,\Omega = S(r+dr)(r+dr)^2\, d\,\Omega + S(r)V\left(N_l\langle \sigma_{lt} \rangle + N_b\langle \sigma_{bt} \rangle\right) \tag{5.7}$$

Since the volume can be approximated by $r^2\, drd\,\Omega$ Eq. (5.7) becomes

$$S(r)r^2 d\,\Omega = S(r+dr)(r+dr)^2\, d\,\Omega + S(r)\left(N_l\langle \sigma_{lt} \rangle + N_b\langle \sigma_{bt} \rangle\right)r^2 drd\,\Omega$$

which simplifies to

$$\frac{S(r+dr)(r+dr)^2 - S(r)r^2}{dr} + \left(N_l\langle \sigma_{lt} \rangle + N_b\langle \sigma_{bt} \rangle\right)S(r)r^2 = 0 \tag{5.8}$$

Further simplifications can be achieved by Taylor expansion

$$(r+dr)^2 = r^2\left(1+\frac{dr}{r}\right)^2 \approx r^2\left(1+2\frac{dr}{r}\right) = r^2 + 2rdr, \quad \frac{dr}{r} << 1$$

and Eq. (5.8) can now be restated as

$$\frac{\left(S(r+dr) - S(r)\right)r^2}{dr} + 2rS(r+dr) + \left(N_l\langle \sigma_{lt} \rangle + N_b\langle \sigma_{bt} \rangle\right)S(r)r^2 = 0$$

If we let $dr \to 0$ we get a differential equation for the transmitted power density

$$\frac{dS(r)}{dr}r^2 + 2rS(r) + \left(N_l\langle \sigma_{lt} \rangle + N_b\langle \sigma_{bt} \rangle\right)S(r)r^2 = 0$$

which can be written as

$$\frac{d}{dr}\left(S(r)r^2\right) + \left(N_l\langle \sigma_{lt} \rangle + N_b\langle \sigma_{bt} \rangle\right)S(r)r^2 = 0 \tag{5.9}$$

Eq. (5.9) has the solution

$$S(r) = C\frac{e^{-(N_l\langle\sigma_{lt}\rangle + N_b\langle\sigma_{bt}\rangle)r}}{r^2}, \qquad r \neq 0 \tag{5.10}$$

where C is an arbitrary constant. To find the value of this constant we consider the emitted power density in a spherical wave generated by an isotropic[6] antenna with a time-average radiated power P_0 (source power).

$$S_{iso}(r) = \frac{P_0}{4\pi r^2}, \qquad r \neq 0$$

If we compare this expression with Eq. (5.10) in the case when the signal is propagating in free space, i.e. $N_l\langle\sigma_{lt}\rangle + N_b\langle\sigma_{bt}\rangle = 0$, we find

$$S(r) = \frac{C}{r^2} = S_{iso}(r) = \frac{P_0}{4\pi r^2}, \qquad r \neq 0$$

which gives

$$C = \frac{P_0}{4\pi}$$

Thus it is possible to rewrite Eq. (5.10) as

$$S(r) = \frac{P_0 e^{-(N_l\langle\sigma_{lt}\rangle + N_b\langle\sigma_{bt}\rangle)r}}{4\pi r^2}, \qquad r \neq 0 \tag{5.11}$$

Since a perfect isotropic antenna does not exist in practice we have to take into account the antennas ability to direct the gain. For a more realistic antenna the radiation is not only transmitted in the desirable direction but also in other less desirable directions. The radiation can be split up into two categories — the main beam and the sidelobes. The region of maximum radiation between the first null points around the maximum is the main beam, and the regions of minor maxima are sidelobes. The main beam always point in the direction where the antenna is designed to have its maximum radiation. The width of the main beam (or simply the beamwidth) describes the sharpness of the main radiation region. It is generally taken to be the angular width of a pattern between the half-power, or —3 dB, points. The beamwidth of an antenna pattern specifies the sharpness of the main beam, but it does not provide us with any information about the rest of the pattern. For example, the sidelobes may be very high — an undesirable feature. A commonly used parameter to measure the overall ability of an antenna to direct radiated power in a given direction is a dimensionless quantity called directive gain. The directive gain is defined in terms of radiation intensity. The radiation intensity, $I(\theta,\phi)$, is the time-average power per unit solid angle and the SI unit is watt per steradian (W/sr). Since there are r^2 square meters of spherical surface area for each unit of solid angle, radiation intensity, $I(\theta,\phi)$, equals r^2 times the time-average power per unit area or r^2 times the magnitude of the time-average Poynting vector, S

[6] An isotropic or omnidirectional antenna is an antenna that radiates uniformly in all directions.

$$I(\theta,\phi)=r^2 S(r,\theta,\phi) \tag{5.12}$$

The total radiated time-average power is

$$P_0 = \oint \boldsymbol{S}(\boldsymbol{r})\cdot d\,\boldsymbol{s} = \oint I(\theta,\phi)d\,\Omega \tag{5.13}$$

The directive gain, $G_D(\theta,\phi)$, of an antenna pattern is the ratio of the radiation intensity in the direction (θ,ϕ) to the average radiation intensity

$$G_D(\theta,\phi)=\frac{I(\theta,\phi)}{P_0/4\pi}=\frac{4\pi\, I(\theta,\phi)}{\oint I(\theta,\phi)d\,\Omega} \tag{5.14}$$

Obviously, the directive gain of an isotropic antenna is unity. The maximum directive gain of an antenna is called the directivity of the antenna. It is the ratio of the maximum radiation intensity to the average radiation intensity and is defined as

$$D=\frac{I(\theta,\phi)_{\max}}{I(\theta,\phi)_{av}}=\frac{4\pi\, I(\theta,\phi)_{\max}}{P_0} \tag{5.15}$$

Since the radiation from an antenna is not uniformly distributed the expression of the attenuated time-average power density, Eq. (5.11), has to be improved to consider this property. If we substitute Eq. (5.12) into Eq. (5.14) we get

$$S(r,\theta,\phi)=\frac{P_0}{4\pi\, r^2}G_D(\theta,\phi) \tag{5.16}$$

which is an expression for the transmitted time-average power density in free space. We can now use this expression to restate Eq. (5.11) that yields

$$S(r,\theta,\phi)=\frac{P_0 e^{-\left(N_l\langle\sigma_{lt}\rangle+N_b\langle\sigma_{bt}\rangle\right)r}}{4\pi\, r^2}G_D(\theta,\phi), \qquad r\neq 0 \tag{5.17}$$

If a receiving antenna is used to measure that through the canopy transmitted power, P_t, at a distance r from the transmitter the properties of the receiving antenna have to be considered. The incident waves are be received in an area that is not the same as the physical area of the receiving antenna. It is therefore convenient to define a quantity called the effective area[7]. The effective area, $A_e(\theta,\phi)$, of a receiving antenna is the ratio of the average power delivered to a matched load to the time-average power density (time-average Poynting vector) of the incident electromagnetic wave at the antenna. We write

$$P_L = A_e S \tag{5.18}$$

where P_L is the maximum average power transferred to the load (under matched conditions) with the receiving antenna properly oriented with respect to the polarization of the incident

[7] Also called effective aperture or receiving cross section.

wave. It can be proved that the ratio of the directive gain and the effective area of an antenna is a universal constant and follows the relation

$$G_D(\theta,\phi) = \frac{4\pi}{\lambda^2} A_e(\theta,\phi) \tag{5.19}$$

An expression for the received power can be achieved if we use the expression for the transmitted time-average power density, Eq. (5.17), and multiply it with the receiving antennas effective area, $A_e(\theta,\phi)$. We get

$$P_r = \frac{P_0 e^{-(N_l\langle\sigma_{lt}\rangle + N_b\langle\sigma_{bt}\rangle)r}}{4\pi r^2} G_{Dt} A_{er}$$

Making use of Eq. (5.19) yields

$$\frac{P_r}{P_0} = \frac{\lambda^2 G_{Dt} G_{Dr}}{(4\pi r)^2} e^{-(N_l\langle\sigma_{lt}\rangle + N_b\langle\sigma_{bt}\rangle)r}, \qquad r \neq 0 \tag{5.20}$$

where G_{Dt} is the directive gain of the transmitting antenna and G_{Dr} is the directive gain of the receiving antenna. Eq. (5.20) considers the case when leaves and branches represent all space between the transmitting and receiving antenna. To get a more realistic expression for the attenuation of the emitted radiation we have to consider the case when some part of the distance between the two antennas consists of free space. If the total distance between the transmitting and receiving antenna is *r* and the distance through the canopy is *d* the improved formula becomes

$$\frac{P_r}{P_0} = \frac{\lambda^2 G_{Dt} G_{Dr}}{(4\pi r)^2} e^{-(N_l\langle\sigma_{lt}\rangle + N_b\langle\sigma_{bt}\rangle)d}, \qquad r \neq 0 \tag{5.21}$$

A desirable property during transmission between two antennas is that the ratio between the transmitted and received power should be as big as possible. This happens when the two antennas are directed to have the maximum value of the directive gain. As we mentioned before the maximum value of G_{Dt} and G_{Dr} is represented by the directivity of each antenna. In this case Eq. (5.21) is restated as

$$\frac{P_r}{P_0} = \frac{\lambda^2 D_t D_r}{(4\pi r)^2} e^{-(N_l\langle\sigma_{lt}\rangle + N_b\langle\sigma_{bt}\rangle)d}, \qquad r \neq 0 \tag{5.22}$$

where D_t and D_r is the directivity of the transmitting and receiving antenna. From this expression it is possible to get an expression for the attenuation of a tree crown. We find

$$L = 10\,lg(e)\left(N_l\langle\sigma_{lt}\rangle + N_b\langle\sigma_{bt}\rangle\right) \approx 4.343\left(N_l\langle\sigma_{lt}\rangle + N_b\langle\sigma_{bt}\rangle\right) \tag{5.23}$$

5.2 The total cross section

In the preceding section we introduced and explained the concept of the effective area. This concept has much in common with the concept of the cross section since it is a quantity that indicates how much of the incident power density that is delivered to a load in the receiving antenna (see Eq. (5.18)). The cross section is instead a quantity that indicates the ability of an object to scatter or absorb incident power density. A quantity that informs about the ability for a body, with the volume V_s, to scatter is the differential scattering cross section.

$$\frac{d\sigma}{d\Omega} = r^2 \frac{\langle \boldsymbol{S}_s(t)\rangle \cdot \boldsymbol{r}}{\langle \boldsymbol{S}_i(t)\rangle \cdot \boldsymbol{k}_i} \tag{5.24}$$

This quantity is the ratio between the power density of the scattered wave and the power density of the incident wave. In Eq. (5.24) the radius, r, of the sphere — on which the scattering power is calculated — has been used as a normalization variable. The total power P_s that the volume V_s scatters is the integral of $\langle \boldsymbol{S}_s(t)\rangle \cdot \boldsymbol{r}$ over a sphere with the radius r. We get

$$P_s = \iint_{\text{Sphere}} \langle \boldsymbol{S}_s(t)\rangle \cdot \boldsymbol{r}\, dS = \iint \langle \boldsymbol{S}_s(t)\rangle \cdot \boldsymbol{r}\, r^2 d\Omega \tag{5.25}$$

where $d\Omega = sin\theta\, d\theta\, d\phi$ is the differential solid angle. The total scattering cross section can now be defined as

$$\sigma_s(\boldsymbol{k}_i) = \frac{P_s}{\langle \boldsymbol{S}_i(t)\rangle \cdot \boldsymbol{k}_i} = \iint \frac{d\sigma}{d\Omega} d\Omega \tag{5.26}$$

The scattering body does not only scatter the incident wave, it will in most cases absorb electromagnetic energy. The total power that the scattering body absorbs can be expressed by the Poynting vector (see Eq. (2.33))

$$P_a = -\iint_{S_s} \frac{1}{2} \mathrm{Re}\left\{\boldsymbol{E}(\boldsymbol{r}') \times \boldsymbol{H}^*(\boldsymbol{r}')\right\} \boldsymbol{n}(\boldsymbol{r}') dS' \tag{5.27}$$

Here S_s is the surface area of the scattering body with volume V_s. Eq. (5.27) gives us the total power that penetrates the body and gets absorbed — i.e. it will be transformed to other states of energy. The total absorbed power defines the total absorption cross section σ_a.

$$\sigma_a(\boldsymbol{k}_i) = \frac{P_a}{\langle \boldsymbol{S}_i(t)\rangle \cdot \boldsymbol{k}_i} \tag{5.28}$$

The total scattering cross section and the total absorption cross section is often combined for the total cross section which is defined by

$$\sigma_t(\boldsymbol{k}_i) = \sigma_s(\boldsymbol{k}_i) + \sigma_a(\boldsymbol{k}_i) = \frac{P_s + P_a}{\langle \boldsymbol{S}_i(t)\rangle \cdot \boldsymbol{k}_i} \tag{5.29}$$

If the scattering body consists of an isotropic medium the total scattered and absorbed power can be described by

$$P_s + P_a = \frac{1}{2}\mathrm{Re}\left\{\iiint_{V_s} \boldsymbol{E}_i^* \cdot \boldsymbol{J}\, dv'\right\} \tag{5.30}$$

If the incident wave is a plane wave

$$\boldsymbol{E}(\boldsymbol{r}) = \boldsymbol{E}_0\, e^{ik\,\boldsymbol{k}_i \cdot \boldsymbol{r}}$$

then Eq. (5.30) becomes

$$P_s + P_a = -\frac{2\pi}{k^2 \eta_0 \eta}\mathrm{Re}\left\{\boldsymbol{E}_0^* \cdot \boldsymbol{F}(\boldsymbol{k}_i)\right\} \tag{5.31}$$

where $\boldsymbol{F}(\boldsymbol{k}_i)$ is the far field amplitude of the scattered field (see appendix B). The total cross section can now be restated if Eq. (5.31) is inserted into Eq. (5.29) which gives

$$\begin{aligned}\sigma_t(\boldsymbol{k}_i) &= \frac{P_s + P_a}{\langle \boldsymbol{S}_i(t)\rangle \cdot \boldsymbol{k}_i} = \frac{-\frac{2\pi}{k^2 \eta_0 \eta}\mathrm{Re}\left\{\boldsymbol{E}_0^* \cdot \boldsymbol{F}(\boldsymbol{k}_i)\right\}}{\frac{|\boldsymbol{E}_0|^2}{2\eta_0\eta}} \\ &= -\frac{4\pi}{k^2}\mathrm{Re}\left\{\frac{i}{|\boldsymbol{E}_0|^2}\boldsymbol{E}_0^* \cdot \boldsymbol{F}(\boldsymbol{k}_i)\right\}\end{aligned} \tag{5.32}$$

Here k is the wave constant for the incident wave. After further simplifications we find the optical theorem

$$\sigma_t(\boldsymbol{k}_i) = \frac{4\pi}{k^2}\mathrm{Im}\left\{\frac{\boldsymbol{E}_0^*}{|\boldsymbol{E}_0|^2} \cdot \boldsymbol{F}(\boldsymbol{k}_i)\right\} \tag{5.33}$$

In the case of an incident plane wave the power density becomes

$$\langle \boldsymbol{S}_i(t)\rangle = \frac{1}{2}\mathrm{Re}\left\{\boldsymbol{E}_i \times \boldsymbol{H}_i^*\right\} = \frac{1}{2\eta_0\eta}\mathrm{Re}\left\{\boldsymbol{E}_i \times (\boldsymbol{k}_i \times \boldsymbol{E}_i^*)\right\} \tag{5.34}$$

Using the BAC-CAB rule and the fact that $\boldsymbol{k}_i \cdot \boldsymbol{E}_i = 0$ gives

$$\langle \boldsymbol{S}_i(t)\rangle = \frac{\boldsymbol{k}_i}{2\eta_0\eta}|\boldsymbol{E}_0|^2 \tag{5.35}$$

In a common way the scattered power density in the far zone can be calculated. Making use of the far field expression for the scattered field (see appendix B)

$$\boldsymbol{E}_s(\boldsymbol{r}) = \frac{e^{ikr}}{kr}\boldsymbol{F}(\boldsymbol{r}) \tag{5.36}$$

the scattered power density becomes

$$\langle \boldsymbol{S}_s(t) \rangle = \frac{1}{2}\mathrm{Re}\{\boldsymbol{E}_s \times \boldsymbol{H}_s^*\} = \frac{\boldsymbol{r}}{2\eta_0 \eta\, k^2 r^2}|\boldsymbol{F}(\boldsymbol{r})|^2 \tag{5.37}$$

We have here used the expression

$$\boldsymbol{H}_s(\boldsymbol{r}) = \frac{1}{ik\eta_0\eta}\nabla \times \boldsymbol{E}_s(\boldsymbol{r}) \tag{5.38}$$

which is a relation between the scattered magnetic and electric field. In the far zone it becomes

$$\boldsymbol{H}_s(\boldsymbol{r}) = \frac{1}{\eta_0\eta}\frac{e^{ikr}}{kr}\boldsymbol{r} \times \boldsymbol{F}(\boldsymbol{r}) \tag{5.39}$$

The differential scattering cross section can now be restated. Substitution of Eq. (5.35) and Eq. (5.37) into Eq. (5.24) yields

$$\frac{d\sigma}{d\Omega} = r^2 \frac{\left(\dfrac{\boldsymbol{r}}{2\eta_0\eta\, k^2 r^2}|\boldsymbol{F}(\boldsymbol{r})|^2\right)\cdot \boldsymbol{r}}{\left(\dfrac{\boldsymbol{k}_i}{2\eta_0\eta}|\boldsymbol{E}_0|^2\right)\cdot \boldsymbol{k}_i} = \frac{|\boldsymbol{F}(\boldsymbol{r})|^2}{k^2|\boldsymbol{E}_0|^2} \tag{5.40}$$

where k is the wave constant for the surrounding medium. If we insert this equation into Eq. (5.26) we find an expression for the total scattered cross section

$$\sigma_s(\boldsymbol{k}_i) = \frac{1}{k^2|\boldsymbol{E}_0|^2}\iint |\boldsymbol{F}(\boldsymbol{r})|^2\, d\Omega \tag{5.41}$$

These expressions are valid when the incident electric field is represented by a plane wave and the scattered field is analyzed in the far zone.

5.2.1 Long wave approximation

When the size of the scatterer is small in comparison to the wavelength, i.e. $ka < 0.1$ where a is the maximum size of the scattering object, the incident field will be experienced as uniform. The scattering object sense the electric field as a function of time, only. Under these semi-static conditions Rayleigh scattering can be applied. To find an expression for the total cross section we start with the expression for the scattered electric field in the far zone, Eq. (B.23)

$$\boldsymbol{E}_s(\boldsymbol{r}) = k_0^2\,\chi_e \iiint_{V_s} \left[\bar{\bar{\boldsymbol{I}}} - \boldsymbol{rr}\right]\frac{e^{ik(r-\boldsymbol{r}\cdot\boldsymbol{r}')}}{4\pi r}\boldsymbol{E}_{ind}(\boldsymbol{r}')dv' \tag{5.42}$$

Here k is the wave constant for free space, k_0 , since the surrounding medium is air, and $\boldsymbol{E}_{ind}(\boldsymbol{r}')$ is that in the scattering body induced electric field. Equation (5.42) is simplified and we find

$$\boldsymbol{E}_s(\boldsymbol{r}) = \frac{e^{ik_0 r}}{r} \frac{k_0^2 \chi_e}{4\pi} \left[\bar{\bar{\boldsymbol{I}}} - \boldsymbol{rr}\right] \iiint_{V_s} e^{-ik_0 \boldsymbol{r}\cdot\boldsymbol{r}'} \boldsymbol{E}_{ind}(\boldsymbol{r}') dv' \tag{5.43}$$

If we compare this equation with Eq. (5.36) we find that the far field amplitude can be expressed as

$$\boldsymbol{F}(\boldsymbol{r}) = \frac{k_0^3 \chi_e}{4\pi} \left[\bar{\bar{\boldsymbol{I}}} - \boldsymbol{rr}\right] \iiint_{V_s} e^{-ik_0 \boldsymbol{r}\cdot\boldsymbol{r}'} \boldsymbol{E}_{ind}(\boldsymbol{r}') dv' \tag{5.44}$$

where χ_e is the susceptibility of the scattering medium and $\boldsymbol{r}$ is the direction of observation. This expression can be used to calculate the scattered field in the far zone for a scattering body of arbitrarily volume, V_s . Since the induced field, in Eq. (5.44), is unknown we have to find a way to overcome this problem, to be able to calculate the scattered field. This was done in section 3.3. Here the leaves are modeled as flat-circular lossy dielectric discs and the branches as finitely-long lossy dielectric cylinders. The induced electric field within the disc is approximated by the electric field in an unbounded slab that has the same orientation as the disc. If the incident electric field is represented by a plane wave

$$\boldsymbol{E}_i(\boldsymbol{r}) = \boldsymbol{E}_0 e^{ik_0 \boldsymbol{k}\cdot\boldsymbol{r}} \tag{5.45}$$

and the continuity conditions of the tangential components of the electric field and the normal components of the D-field, across the interface of the disc, are employed

$$\begin{cases} \boldsymbol{n}\times\boldsymbol{E}_i = \boldsymbol{n}\times\boldsymbol{E}_{ind} \\ \boldsymbol{n}\cdot\boldsymbol{D}_i = \boldsymbol{n}\cdot\boldsymbol{D}_{ind} \end{cases}$$

the induced field reads

$$\boldsymbol{E}_{ind}(\boldsymbol{r}') = \left[\boldsymbol{E}_0 - (\boldsymbol{n}\cdot\boldsymbol{E}_0)\boldsymbol{n} + \frac{1}{\varepsilon}(\boldsymbol{n}\cdot\boldsymbol{E}_0)\boldsymbol{n}\right] e^{ik_0 \boldsymbol{k}\cdot\boldsymbol{r}'} \tag{5.46}$$

Here ε is the relative permittivity of the medium and $\boldsymbol{n}$ the normal of the disc. We have assumed that reflections of the incident field can be neglected. This can be done if the disc is electrically thin, i.e. $k_0\sqrt{\varepsilon}\, d << 1$. We realize this if we use the reflection coefficients from appendix A

$$r_{\parallel} = \frac{r_{0\parallel} + r_{d\parallel} e^{2ik_{2z}d}}{1 + r_{0\parallel} r_{d\parallel} e^{2ik_{2z}d}} \qquad r_{\perp} = \frac{r_{0\perp} + r_{d\perp} e^{2ik_{2z}d}}{1 + r_{0\perp} r_{d\perp} e^{2ik_{2z}d}}$$

Here $r_{\|}$ is the reflection coefficient for the electric field parallel to plane of incidence and $r_{\perp}$ is the corresponding coefficient for the field perpendicular to it. Both of the field components are furthermore parallel to the surface between the two media. Since $r_{0\|} = -r_{d\|}$ and $r_{0\perp} = -r_{d\perp}$, when the surrounding medium is air, both $r_{\|}$ and $r_{\perp}$ are close to zero and thus the reflected field is negligible. Insertion of Eq. (5.46) into Eq. (5.44) yields

$$\boldsymbol{F}(\boldsymbol{r}) = \frac{k_0^3 \chi_e}{4\pi}\left[\bar{\bar{\boldsymbol{I}}} - \boldsymbol{rr}\right]\left[\boldsymbol{E}_0 + \left(\frac{1}{\varepsilon_r} - 1\right)(\boldsymbol{n}\cdot\boldsymbol{E}_0)\boldsymbol{n}\right]\iiint_{V_s} e^{ik_0(\boldsymbol{k}-\boldsymbol{r})\boldsymbol{r}'}\, dv' \qquad (5.47)$$

The thickness of the disc is represented by d and the radius by a and if these quantities are inserted into Eq. (5.47) we find

$$\begin{aligned}\boldsymbol{F}(\boldsymbol{r}) &= \frac{k_0^3 \chi_e}{4\pi}\left[\bar{\bar{\boldsymbol{I}}} - \boldsymbol{rr}\right]\left[\boldsymbol{E}_0 + \left(\frac{1}{\varepsilon_r} - 1\right)(\boldsymbol{n}\cdot\boldsymbol{E}_0)\boldsymbol{n}\right] \\ &\int_{-d/2}^{d/2}\int_0^{2\pi}\int_0^{a} e^{ik_0(\boldsymbol{k}-\boldsymbol{r})(x\rho'\cos\phi' + y\rho'\sin\phi' + z\,z')}\,\rho'\,d\rho'\,d\phi'\,dz'\end{aligned} \qquad (5.48)$$

If we now assume that the wavelength is much greater than the radius of the disc ($\lambda >> a$) and that the radius is much greater than the thickness of the disc ($a >> d$) we finally get

$$\boldsymbol{F}(\boldsymbol{r}) = k_0^3 \chi_e d\left(\frac{a}{2}\right)^2\left(\bar{\bar{\boldsymbol{I}}} - \boldsymbol{rr}\right)\left[\boldsymbol{E}_0 - \left(\frac{\chi_e}{1+\chi_e}\right)(\boldsymbol{n}\cdot\boldsymbol{E}_0)\boldsymbol{n}\right] \qquad (5.49)$$

which represents the far field amplitude in the case of scattering from a thin disc. The analysis of finding the far field amplitude in the case of scattering from a finite-length cylinder, is very similar to the case of a thin disc. The electromagnetic boundary conditions, requiring the continuity of the tangential field components across the interface, are used together with a quasi-static technique to show that the electric field within the cylinder is given by

$$\boldsymbol{E}_{ind}(\boldsymbol{r}') = \left[\frac{2}{\varepsilon+1}\boldsymbol{E}_0 + \frac{\varepsilon-1}{\varepsilon+1}(\boldsymbol{E}_0\cdot\boldsymbol{m})\boldsymbol{m}\right]e^{ik_0\,\boldsymbol{k}\cdot\boldsymbol{r}'} \qquad (5.50)$$

Here $\boldsymbol{m}$ is the unit position vector directed along the symmetry axis of the cylinder. The far field amplitude is obtained by substituting Eq. (5.50) into Eq. (5.44)

$$\boldsymbol{F}(\boldsymbol{r}) = k_0^3 l\left(\frac{a}{2}\right)^2 \chi_e\left(\bar{\bar{\boldsymbol{I}}} - \boldsymbol{rr}\right)\left[\frac{2}{\chi_e+2}\boldsymbol{E}_0 + \frac{\chi_e}{\chi_e+2}(\boldsymbol{E}_0\cdot\boldsymbol{m})\boldsymbol{m}\right] \qquad (5.51)$$

where l is the length and a is the radius of the cylinder.
The total cross section for a leaf and a branch can now be achieved if we use the optical theorem.

$$\sigma_t(\boldsymbol{k}_i) = \frac{4\pi}{k_0^2}\,\mathrm{Im}\left\{\frac{\boldsymbol{E}_0^*}{|\boldsymbol{E}_0|^2}\cdot\boldsymbol{F}(\boldsymbol{k}_i)\right\} \tag{5.52}$$

If we assume that the incident electric field is linearly polarized and represented by

$$\boldsymbol{E}_0 = E_0\,\boldsymbol{q} \tag{5.53}$$

the total cross section for a leaf can be written as

$$\sigma_t(\boldsymbol{k}_i) = k_0\,\chi_e\pi\,a^2 d\,\mathrm{Im}\left\{\boldsymbol{q}\cdot\left(\mathbf{I}-\boldsymbol{k}_i\boldsymbol{k}_i\right)\left[\boldsymbol{q}-\left(\frac{\chi_e}{1+\chi_e}\right)(\boldsymbol{q}\cdot\boldsymbol{n})\boldsymbol{n}\right]\right\} \tag{5.54}$$

and for a branch as

$$\sigma_t(\boldsymbol{k}_i) = k_0\,\chi_e\pi\,a^2 l\,\mathrm{Im}\left\{\boldsymbol{q}\cdot\left(\mathbf{I}-\boldsymbol{k}_i\boldsymbol{k}_i\right)\left[\frac{2}{\chi_e+2}\boldsymbol{q}+\frac{\chi_e}{\chi_e+2}(\boldsymbol{q}\cdot\boldsymbol{m})\boldsymbol{m}\right]\right\} \tag{5.55}$$

5.2.2 Resonance region

The theory for the electromagnetic interaction for bodies in the resonance region is discussed in appendix C. The T-matrix method is used to derive an expression for the total cross section in the far zone. From Eq. (C.41) we get

$$\sigma_t(\boldsymbol{k}_i) = \frac{4\pi}{k^2}\,\mathrm{Im}\left\{\frac{\boldsymbol{E}_0^*}{|\boldsymbol{E}_0|^2}\cdot\sum_{l=1}^{\infty}\sum_{m=0}^{l}\sum_{\sigma=\mathrm{e,o}}\sum_{\tau=1}^{2} i^{-l-2+\tau} f_{\tau\sigma ml}\,\boldsymbol{A}_{\tau\sigma ml}(\boldsymbol{k}_i)\right\} \tag{5.56}$$

where $f_{\tau\sigma ml}$ are the expansion coefficients of the scattered field and $\boldsymbol{A}_{\tau\sigma ml}$ are the spherical vector surface functions. Since the surrounding medium is air the wave constant becomes $k = k_0$. To find the expansion coefficients for the scattered field Eq. (C.53)

$$f_{\tau\sigma ml} = \sum_{l'=1}^{\infty}\sum_{m'=0}^{l'}\sum_{\sigma'=\mathrm{e,o}}\sum_{\tau'=1}^{2} T_{\tau\sigma ml,\tau'\sigma'm'l'}\,a_{\tau'\sigma'm'l'} \tag{5.57}$$

is used. Here we find the T-matrix and the expansion coefficients for the incident field. To generate the different elements of the T-matrix, a surface integral has to be calculated.
In this model the leaves are modeled as dielectric oblate spheroids and the branches as cylinders of finite length. These symmetries lead to that it is hard to do any simplifications (especially in the case of an oblate spheroid) and thus must the surface integrals be calculated numerically.

5.2.3 Short wave approximation

When the frequency increases and the wavelength becomes small in comparison to the size of the scattering object, i.e. $ka > 10$, the field will be much more sensitive to surface irregularities. If we can assume that the radius of curvature of the surface can be considered as much larger than the wavelength, i.e. each small portion of the surface behaves as if it were plane, and the surface can be considered as smooth some valid approximations can be done, i.e. physical optics approach for dielectric scatterers. The leaves are modeled as flat dielectric discs with radius a and thickness d. To calculate the total cross section of the leaves we start with the general expression for the far field amplitude, Eq. (5.44).

$$\boldsymbol{F}(\boldsymbol{r}) = \frac{k_0^3\,\chi_e}{4\pi}\left[\bar{\bar{\mathbf{I}}} - \boldsymbol{rr}\right]\iiint_{V_s} e^{-ik_0\,\boldsymbol{r}\cdot\boldsymbol{r}'}\,\boldsymbol{E}_{ind}(\boldsymbol{r}')dv'$$

To be able to evaluate this integral the fields inside the disc, $\boldsymbol{E}_{ind}$, are needed. Unfortunately, these are not known, and approximations are necessary to obtain the solution. The approximation used here is to assume that the fields inside the disc are the same as in a dielectric slab of the same thickness and orientation as the disc. Thus the approximation is

$$\boldsymbol{F}(\boldsymbol{r}) = \frac{k_0^3\,\chi_e}{4\pi}\left[\bar{\bar{\mathbf{I}}} - \boldsymbol{rr}\right]\iiint_{V_s} e^{-ik_0\,\boldsymbol{r}\cdot\boldsymbol{r}'}\,\boldsymbol{E}_{slab}(\boldsymbol{r}')dv' \tag{5.58}$$

This approximation is an extension of the Kirchhoff approximation (Kirchhoff boundary condition) employed in diffraction theory and in scattering from perfectly conducting irregular surfaces. The extended principle is to replace the object (aperture, disc or surface) by a canonical form for which the fields are known and then to use these fields in the original object (the same principle as in appendix B). In the case of the disc, the canonical form is a slab and the approximation in Eq. (5.58) amounts to using the slab to calculate approximate equivalent source distributions inside the disc. These equivalent sources can thereafter be used to calculate the scattered amplitude in the far zone. The approximation in Eq. (5.58) work fine as long as the edges of the disc do not appreciably change the fields inside the disc, i.e. when the minimum dimension of the cross section of the disc is large compared to the wavelength ($2a >> \lambda$) and large compared to the thickness of the disc ($2a >> d$). This approximation has the advantage of not requiring the thickness to be small compared to the wavelength and not imposing restrictions on the dielectric constant of the disc (see section 5.2.1). The internal fields in a slab are analyzed in appendix A. The field in the slab (region 2 in Figure A.3) contains two parts; one part that propagates in the positive *z*-direction and one part that propagates in the negative *z*-direction. The induced field in the slab can thus be written as

$$\boldsymbol{E}_{ind}(\boldsymbol{r}) \approx \boldsymbol{E}_{slab}(\boldsymbol{r}) = \boldsymbol{E}^{+}(\boldsymbol{r}) + \boldsymbol{E}^{-}(\boldsymbol{r}) \tag{5.59}$$

where the two field components are (see Eq. (A.49))

$$\begin{cases} \boldsymbol{E}^{+}(\boldsymbol{r},\omega) = \left\{\bar{\bar{\mathbf{I}}} - \boldsymbol{z}\dfrac{1}{k_{2z}}\boldsymbol{k}_t\right\}\cdot \boldsymbol{E}_{xy}^{+}\, e^{ik_{2z}z} e^{i\boldsymbol{k}_t\cdot\boldsymbol{\rho}} \\ \boldsymbol{E}^{-}(\boldsymbol{r},\omega) = \left\{\bar{\bar{\mathbf{I}}} + \boldsymbol{z}\dfrac{1}{k_{2z}}\boldsymbol{k}_t\right\}\cdot \boldsymbol{E}_{xy}^{-}\, e^{-ik_{2z}z} e^{i\boldsymbol{k}_t\cdot\boldsymbol{\rho}} \end{cases} \tag{5.60}$$

The transversal vectorial amplitudes are defined as

$$\begin{cases} \boldsymbol{E}_{xy}^{+} = E_{\|}^{+}\,\boldsymbol{e}_{\|} + E_{\perp}^{+}\,\boldsymbol{e}_{\perp} = \left(e_{\|}^{+}\,\boldsymbol{e}_{\|}\boldsymbol{e}_{\|} + e_{\perp}^{+}\,\boldsymbol{e}_{\perp}\boldsymbol{e}_{\perp}\right)\cdot \boldsymbol{E}_{0} \\ \boldsymbol{E}_{xy}^{-} = E_{\|}^{-}\,\boldsymbol{e}_{\|} + E_{\perp}^{-}\,\boldsymbol{e}_{\perp} = \left(e_{\|}^{-}\,\boldsymbol{e}_{\|}\boldsymbol{e}_{\|} + e_{\perp}^{-}\,\boldsymbol{e}_{\perp}\boldsymbol{e}_{\perp}\right)\cdot \boldsymbol{E}_{0} \end{cases} \tag{5.61}$$

where the different coefficients are

$$\begin{cases} e_{\|}^{+} = \dfrac{t_{0\|}}{1+r_{0\|}r_{d\|}e^{2ik_{2z}d}} \\ e_{\perp}^{+} = \dfrac{t_{0\perp}}{1+r_{0\perp}r_{d\perp}e^{2ik_{2z}d}} \end{cases} \qquad \begin{cases} e_{\|}^{-} = \dfrac{t_{0\|}r_{d\|}e^{2ik_{2z}d}}{1+r_{0\|}r_{d\|}e^{2ik_{2z}d}} \\ e_{\perp}^{-} = \dfrac{t_{0\perp}r_{d\perp}e^{2ik_{2z}d}}{1+r_{0\perp}r_{d\perp}e^{2ik_{2z}d}} \end{cases} \tag{5.62}$$

Here is t_{0p} the transmission coefficient at the first surface and r_{0p} and r_{dp} the reflection coefficients at the first and second surface. The subscript p corresponds to the polarization parallel ($\boldsymbol{e}_{\|}$) or perpendicular ($\boldsymbol{e}_{\perp}$) to the plane of incidence. Furthermore is k_{2z} the longitudinal wave constant in the slab (region 2) and $\boldsymbol{k}_{t}$ the corresponding wave vector in the tangential direction. The vectorial amplitude of the incident field, $\boldsymbol{E}_{0}$, can be divided into three parts due to the dyadic $\boldsymbol{e}_{\|}\boldsymbol{e}_{\|}$ and $\boldsymbol{e}_{\perp}\boldsymbol{e}_{\perp}$. We find

$$\boldsymbol{E}_{0} = \boldsymbol{e}_{\|}\,E_{0\|} + \boldsymbol{e}_{\perp}\,E_{0\perp} + \boldsymbol{z}\,E_{0z} \tag{5.63}$$

The first dyadic in Eq. (5.61) will thus project $\boldsymbol{E}_{0}$ on the line that intersects the surface of the slab and the plane of incidence. This component is parallel to the plane of incidence. The second dyadic projects the vectorial amplitude on a line orthogonal to the plane of incidence and is parallel to the surface of the slab. Since the different unit vectors are orthogonal, i.e. $\boldsymbol{z} = \boldsymbol{e}_{\|} \times \boldsymbol{e}_{\perp}$, the last part in Eq. (5.63) does not contribute to the calculations and can therefore be omitted. All details about the different components of Eq. (5.60) are elucidated in appendix A.

Since that to the slab surrounding medium is air and the material in the slab is nonmagnetic ($\mu = 1$) some of the components in Eq. (5.60) can be simplified. We find

$$\begin{cases} r_{0\|} = \dfrac{k_{2z} - \varepsilon\,k_{1z}}{k_{2z} + \varepsilon\,k_{1z}} = -r_{d\|} \\ r_{0\perp} = \dfrac{k_{1z} - k_{2z}}{k_{1z} + k_{2z}} = -r_{d\perp} \end{cases} \qquad \begin{cases} t_{0\|} = 1 + r_{0\|} \\ t_{0\perp} = 1 + r_{0\perp} \end{cases} \qquad \begin{cases} k_{1z} = k_{0}\,cos\,\delta \\ k_{2z} = k_{0}\,\sqrt{\varepsilon}\,cos\,\gamma \\ \boldsymbol{k}_{t} = \boldsymbol{e}_{\|}\,k_{0}\,sin\,\delta \end{cases} \tag{5.64}$$

where ε is the relative permittivity of the medium in the slab, δ is the angle of incidence and γ is the angle of transmission (see Figure 5.2).

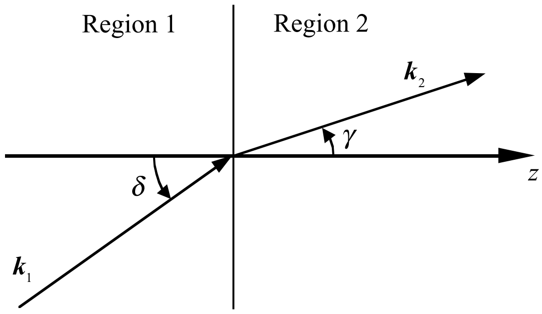

Figure 5.2: Plane wave incident on a plane dielectric boundary.

The angle γ can be calculated if we use Snell s law of refraction, Eq. (A.52)

$$k_1 \sin\delta = k_2 \sin\gamma \tag{5.65}$$

We can now apply the simplifications on Eq. (5.62), which become

$$\begin{cases} e_{\|}^{+} = \dfrac{1+r_{0\|}}{1-r_{0\|}^{2}e^{2ik_{2z}d}} \\ e_{\perp}^{+} = \dfrac{1+r_{0\perp}}{1-r_{0\perp}^{2}e^{2ik_{2z}d}} \end{cases} \qquad \begin{cases} e_{\|}^{-} = -\dfrac{(1+r_{0\|})r_{0\|}e^{2ik_{2z}d}}{1-r_{0\|}^{2}e^{2ik_{2z}d}} \\ e_{\perp}^{-} = -\dfrac{(1+r_{0\perp})r_{0\perp}e^{2ik_{2z}d}}{1-r_{0\perp}^{2}e^{2ik_{2z}d}} \end{cases} \tag{5.66}$$

We have here achieved an approximate expression for the induced electric field in the disc. But to evaluate the integral in Eq. (5.58) the origin of the coordinate system has to be placed at the center of the slab. This has not been the case so far. During the derivation of the internal fields the assumption of that the first and second surface was placed at $z=0$ and $z=d$, respectively, was done. When the origin is moved the first surface will instead be placed at $z=-d/2$ and the second surface at $z=d/2$. The new expressions become

$$\begin{cases} e_{\|}^{+} = \dfrac{(1+r_{0\|})e^{-i(k_{1z}-k_{2z})d/2}}{1-r_{0\|}^{2}e^{2ik_{2z}d}} \\ e_{\perp}^{+} = \dfrac{(1+r_{0\perp})e^{-i(k_{1z}-k_{2z})d/2}}{1-r_{0\perp}^{2}e^{2ik_{2z}d}} \end{cases} \qquad \begin{cases} e_{\|}^{-} = -\dfrac{(1+r_{0\|})r_{0\|}e^{2ik_{2z}d}e^{-i(k_{1z}+k_{2z})d/2}}{1-r_{0\|}^{2}e^{2ik_{2z}d}} \\ e_{\perp}^{-} = -\dfrac{(1+r_{0\perp})r_{0\perp}e^{2ik_{2z}d}e^{-i(k_{1z}+k_{2z})d/2}}{1-r_{0\perp}^{2}e^{2ik_{2z}d}} \end{cases} \tag{5.67}$$

We have now the necessary tools to solve the integral in Eq. (5.58) and thus be able to calculate the vectorial amplitude in the far zone. If Eq. (5.60) is inserted into Eq. (5.59) and the result thereafter is inserted into Eq. (5.58) we get

$$\boldsymbol{F}(\boldsymbol{r}) = \frac{k_0^3\chi_e}{4\pi}\left[\bar{\bar{\mathbf{I}}} - \boldsymbol{rr}\right]$$
$$\cdot \iiint_{V_s} e^{-ik_0\boldsymbol{r}\cdot\boldsymbol{r}'}\left(\left\{\bar{\bar{\mathbf{I}}} - \boldsymbol{z}\frac{1}{k_{2z}}\boldsymbol{k}_t\right\}\cdot\boldsymbol{E}_{xy}^{+}\,e^{ik_{2z}z'}e^{i\boldsymbol{k}_t\cdot\,'} + \left\{\bar{\bar{\mathbf{I}}} + \boldsymbol{z}\frac{1}{k_{2z}}\boldsymbol{k}_t\right\}\cdot\boldsymbol{E}_{xy}^{-}\,e^{-ik_{2z}z'}e^{i\boldsymbol{k}_t\cdot\rho'}\right)dv'$$

which can be simplified to

$$\boldsymbol{F}(\boldsymbol{r})=\frac{k_0^3\,\chi_e}{4\pi}\left[\bar{\bar{\mathbf{I}}}-\boldsymbol{rr}\right]\left(\left\{\bar{\bar{\mathbf{I}}}-\boldsymbol{z}\frac{1}{k_{2z}}\boldsymbol{k}_t\right\}\cdot\boldsymbol{E}_{xy}^{+}\,I_1+\left\{\bar{\bar{\mathbf{I}}}+\boldsymbol{z}\frac{1}{k_{2z}}\boldsymbol{k}_t\right\}\cdot\boldsymbol{E}_{xy}^{-}\,I_2\right) \tag{5.68}$$

The two integrals I_1 and I_2 are given by the expressions

$$\begin{aligned} I_1 &= \iiint_{V_s} e^{-ik_0\boldsymbol{r}\cdot\boldsymbol{r}'}e^{ik_{2z}z'}e^{i\boldsymbol{k}_t\cdot\boldsymbol{\rho}'}\,dv' \\ I_2 &= \iiint_{V_s} e^{-ik_0\boldsymbol{r}\cdot\boldsymbol{r}'}e^{-ik_{2z}z'}e^{i\boldsymbol{k}_t\cdot\boldsymbol{\rho}'}\,dv' \end{aligned} \tag{5.69}$$

These two integrals are calculated in appendix D and the results are

$$I_1=\frac{4\pi\,a}{(k_0q)^4\,sin^3\beta\,cos\,\beta}sin\left(k_0qcos\,\beta\,\frac{d}{2}\right)J_1\left(\frac{a}{k_0qsin\,\beta}\right) \tag{5.70}$$

$$I_2=\frac{4\pi\,a}{(k_0p)^4\,sin^3\varphi\,cos\,\varphi}sin\left(k_0pcos\,\varphi\,\frac{d}{2}\right)J_1\left(\frac{a}{k_0psin\,\varphi}\right) \tag{5.71}$$

where q and p are the magnitudes of the two vectors

$$\begin{aligned} \boldsymbol{q} &= \sqrt{\varepsilon}\boldsymbol{k}_2-\boldsymbol{r}=q\{\boldsymbol{x}\,cos\,\alpha\,sin\,\beta+\boldsymbol{y}\,sin\,\alpha\,sin\,\beta+\boldsymbol{z}\,cos\,\beta\} \\ \boldsymbol{p} &= \sqrt{\varepsilon}\left(\boldsymbol{k}_t\,sin\,\gamma-\boldsymbol{z}\,cos\,\gamma\right)-\boldsymbol{r}=p\{\boldsymbol{x}\,cos\,\xi\,sin\,\varphi+\boldsymbol{y}\,sin\,\xi\,sin\,\varphi+\boldsymbol{z}\,cos\,\varphi\} \end{aligned}$$

where $\alpha=\xi$. The wave vector of the incident field, $\boldsymbol{k}_1$, the wave vector inside the disc, $\boldsymbol{k}_2$, and the position vector directed to the observation point, $\boldsymbol{r}$, are given by

$$\begin{aligned} \boldsymbol{k}_1 &= \boldsymbol{x}\,cos\,\psi\,sin\,\delta+\boldsymbol{y}\,sin\,\psi\,sin\,\delta+\boldsymbol{z}\,cos\,\delta \\ \boldsymbol{k}_2 &= \boldsymbol{x}\,cos\,\psi\,sin\,\gamma+\boldsymbol{y}\,sin\,\psi\,sin\,\gamma+\boldsymbol{z}\,cos\,\gamma \\ \boldsymbol{r} &= \boldsymbol{x}\,cos\,\phi\,sin\,\theta+\boldsymbol{y}\,sin\,\phi\,sin\,\theta+\boldsymbol{z}\,cos\,\theta \end{aligned}$$

where the relation

$$sin\,\delta=\sqrt{\varepsilon}\,sin\,\gamma$$

is used to calculate γ if δ is known. The tangential part of the wave vector is defined as

$$\boldsymbol{k}_t=\boldsymbol{x}\,cos\,\psi+\boldsymbol{y}\,sin\,\psi$$

and the two angles β and φ in Eq. (5.70) and Eq. (5.71) are given by

$$cos\,\beta = \frac{1}{q}\left[\sqrt{\varepsilon}\,cos\,\gamma - cos\,\theta\right]$$

$$cos\,\varphi = -\frac{1}{p}\left[\sqrt{\varepsilon}\,cos\,\gamma + cos\,\theta\right]$$

It is now possible to calculate the total cross section of a leaf if we use the optical theorem and insert the expression for the far field amplitude into it. We get

$$\sigma_t(\boldsymbol{k}_i) = k_0\,\mathrm{Im}\left\{\frac{\boldsymbol{E}_0^*}{|\boldsymbol{E}_0|^2}\cdot\chi_e\left[\bar{\bar{\mathbf{I}}} - \boldsymbol{k}_i\boldsymbol{k}_i\right]\left(\left\{\bar{\bar{\mathbf{I}}} - \boldsymbol{z}\frac{1}{k_{2z}}\boldsymbol{k}_t\right\}\cdot\boldsymbol{E}_{xy}^+ I_1 + \left\{\bar{\bar{\mathbf{I}}} + \boldsymbol{z}\frac{1}{k_{2z}}\boldsymbol{k}_t\right\}\cdot\boldsymbol{E}_{xy}^- I_2\right)\right\} \quad (5.72)$$

To simplify this expression we use the same technique as in section 5.2.1 and assume that the incident electric field is linearly polarized and thus represented by

$$\boldsymbol{E}_0 = E_0\,\boldsymbol{q}$$

After insertion of this expression in Eq. (5.72) the total cross section for a leaf finally becomes

$$\sigma_t(\boldsymbol{k}_i) = k_0\,\mathrm{Im}\left\{\boldsymbol{q}\cdot\chi_e\left[\bar{\bar{\mathbf{I}}} - \boldsymbol{k}_i\boldsymbol{k}_i\right]\left(\begin{aligned}&\left\{\bar{\bar{\mathbf{I}}} - \boldsymbol{z}\frac{1}{k_{2z}}\boldsymbol{k}_t\right\}\cdot\left(e_\parallel^+\,\boldsymbol{e}_\parallel\boldsymbol{e}_\parallel + e_\perp^+\,\boldsymbol{e}_\perp\boldsymbol{e}_\perp\right)\boldsymbol{q}\,I_1\\ &+\left\{\bar{\bar{\mathbf{I}}} + \boldsymbol{z}\frac{1}{k_{2z}}\boldsymbol{k}_t\right\}\cdot\left(e_\parallel^-\,\boldsymbol{e}_\parallel\boldsymbol{e}_\parallel + e_\perp^-\,\boldsymbol{e}_\perp\boldsymbol{e}_\perp\right)\boldsymbol{q}\,I_2\end{aligned}\right)\right\} \quad (5.73)$$

5.2.4 Expectation value of the total cross section

We have so far derived expressions for the total cross section valid in different frequency regions. The value of the total cross section in these expressions is dependent on the direction and polarization of the incident wave. Furthermore is the orientation of the scattering body of significant importance. In order to be able to calculate the expectation value of the total cross section in the case of an electromagnetic field propagating through a canopy, a statistic distribution of the orientation of the leaves and branches will be necessary. In Figure 5.3 we find an incident wave propagating towards a single disc (leaf) or a single cylinder (branch).

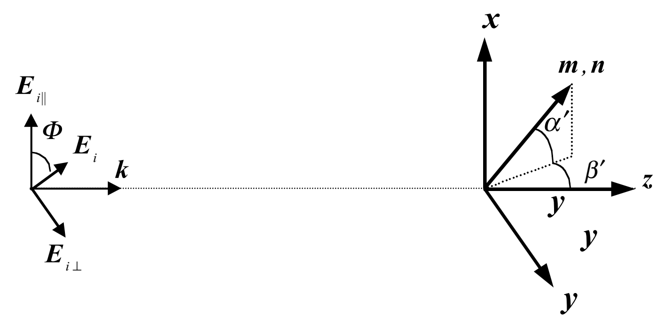

Figure 5.3: The normal of the disc is denoted by $\boldsymbol{n}$ and the symmetry axis of the cylinder by $\boldsymbol{m}$. The two angles α' and β' represents the orientation in vertical and horizontal direction. The parallel and perpendicular electric field polarizations are shown for the incident field together with its magnitude and azimuth angle Φ.

The normal of the disc is denoted by $\boldsymbol{n}$ and the symmetry axis of the cylinder by $\boldsymbol{m}$. The angle between the normal and the *y*-*z*-plane is denoted by α' and gives the deviation in the vertical plane. In a corresponding way is β' the angle between the projection of the normal on the *y*-*z*-plane and the *z*-axis and gives thus the horizontal deviation. The two angles are defined in the region $-\frac{\pi}{2} < \alpha' < \frac{\pi}{2}$ and $0 < \beta' < 2\pi$. The normal vector can be written as

$$\boldsymbol{n} = \boldsymbol{x}\sin\alpha' - \boldsymbol{y}\cos\alpha'\sin\beta' + \boldsymbol{z}\cos\alpha'\cos\beta' \tag{5.74}$$

which also is valid for the symmetry axis of the cylinder.
A general expression for the expectation value of the total cross section is

$$\langle\sigma_t\rangle = \iint \sigma_t(\alpha',\beta')\,p(\alpha',\beta')\,d\,\Omega' \tag{5.75}$$

where $d\,\Omega' = \cos\alpha'\,d\alpha'\,d\beta'$ is the solid angle and $p(\alpha',\beta')$ the probability function for the statistical distribution of the normal of a leaf or the symmetry axis of a branch. In Eq. (5.75) it is assumed that the total cross section is a function of the two angles α' and β' only and not a function of the size of the scattering body. The reason is that that the size of the leaves and the branches can be considered as normal distributed which means that the mean values of the statistical distributions can be used. This was discussed in section 4.3. In order to find a probability function that describes the $\boldsymbol{n}$ and $\boldsymbol{m}$ distributions in a realistic way we use the fact that the leaves and branches are more or less vertical oriented (see section 4.3). This means that there will be a high probability to find a leaf or a branch in a vertical orientation and a low probability to find them in a horizontal orientation. Moreover should the probability to find a leaf or a branch at a specific angle $\alpha' = \alpha_0$ be the same for every value of β'. This means that the angle β' has a uniform distribution and the probability function can thus be written as

$$p(\alpha',\beta') = \frac{A}{2\pi}\,p(\alpha') \tag{5.76}$$

where A is a normalization constant. Expressions that fit the requirements for the vertical orientation of the normal of the leaves and the symmetry axis of the branches are

$$p_l(\alpha') = \cos^n(\alpha') \tag{5.77}$$

$$p_b(\alpha') = \sin^{2n}(\alpha') \tag{5.78}$$

Here is n a positive integer. These two functions are plotted in Figure 5.4 and Figure 5.5 for some values of n. It should be mentioned that these two probability functions only are valid

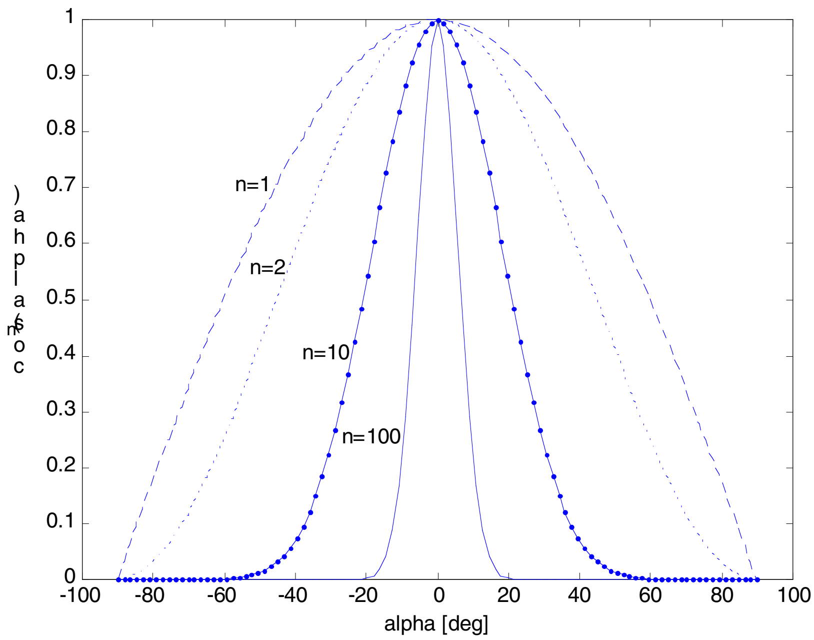

Figure 5.4: Probability function for the vertical distribution of the normal of the leaves. The probability function is plotted against the angle α' for four different values of n.

when a tree type that corresponds to the test beech, the Fagus sylvatica Pendula, are used. Insertion of Eq. (5.77) and Eq. (5.76) into Eq. (5.75) gives the expectation value of the leaves

$$\langle \sigma_{lt} \rangle = \frac{A}{2\pi} \int_{0}^{2\pi} \int_{-\pi/2}^{\pi/2} \sigma_{lt}(\alpha', \beta') cos^{n}(\alpha') cos(\alpha') d\,\alpha' \, d\,\beta' \qquad (5.79)$$

where the normalization constant is given by

$$A = \left[\frac{1}{2\pi} \int_{0}^{2\pi} \int_{-\pi/2}^{\pi/2} cos^{n+1}(\alpha') d\,\alpha' \, d\,\beta' \right]^{-1} \qquad (5.80)$$

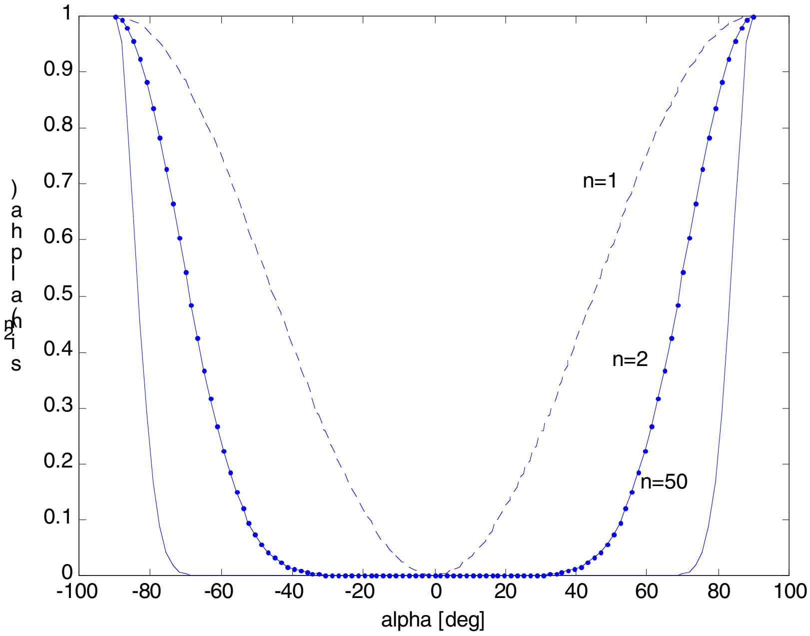

Figure 5.4: Probability function for the vertical distribution of the symmetry axis of the branches. The probability function is plotted against the angle α' for three different values of *n*.

And in the same way can the expectation value of the branches be calculated if Eq. (5.76) and Eq. (5.78) is inserted into Eq. (5.75). We find

$$\langle \sigma_{bt} \rangle = \frac{A}{2\pi} \int_0^{2\pi} \int_{-\pi/2}^{\pi/2} \sigma_{bt}(\alpha', \beta') sin^{2n}(\alpha') cos(\alpha') d\alpha' d\beta' \tag{5.81}$$

where the normalization constant is given by

$$A = \left[\frac{1}{2\pi} \int_0^{2\pi} \int_{-\pi/2}^{\pi/2} sin^{2n}(\alpha') cos(\alpha') d\alpha' d\beta' \right]^{-1} \tag{5.82}$$

Since the T-matrix program that is used has the limitation that it does not generate continues values of the total cross section a discrete form of the total cross section will be needed. For the leaves this becomes

$$\langle \sigma_{\mathrm{lt}} \rangle = \frac{\mathrm{A}}{2\pi} \sum_{\mathrm{i=1}}^{\mathrm{N_1}} \sum_{\mathrm{j=1}}^{\mathrm{N_2}} \sigma_{\mathrm{lt}}(\alpha'_{\mathrm{i}}, \beta'_{\mathrm{j}}) \cos^{\mathrm{n+1}}(\alpha'_{\mathrm{i}}) \tag{5.83}$$

where the constants $\mathrm{N_1}$ and $\mathrm{N_2}$ are the number of sample points. The normalization constant is

$$A = \left[\frac{1}{2\pi} \sum_{i=1}^{N_1} \sum_{j=1}^{4N_2} \cos^{n+1}(\alpha_i') \right]^{-1} \tag{5.84}$$

And for the branches it becomes

$$\langle \sigma_{bt} \rangle = \frac{A}{2\pi} \sum_{i=1}^{N_1} \sum_{j=1}^{N_2} \sigma_{bt}(\alpha_i', \beta_j') \sin^{2n}(\alpha_i') \cos(\alpha_i') \tag{5.85}$$

where the normalization constant is

$$A = \left[\frac{1}{2\pi} \sum_{i=1}^{N_1} \sum_{j=1}^{N_2} \sin^{2n}(\alpha_i') \cos(\alpha_i') \right]^{-1} \tag{5.86}$$

6 Measurements

The results from the measurements on the test beech (see Figure 4.5) at 3.1 and 5.8 GHz are presented in this section. The results from the inventories of the leaves and branches in the tree are included. The inventory serves as a basis for the determination of the densities of the leaves and branches, i.e. the *N* values.
In order to get a good comprehension of the attenuation of the tree, several measurements have been made. The emitted radiation has mainly been vertical polarized and the transmitted field has been measured both for vertical and horizontal polarization. An ordinary horn antenna has been used as a transmitting antenna and the receiving antenna has been a log periodic sector antenna used for broadband applications. During a measurement the transmitting antenna is held at a fixed point while the receiving antenna is moved to different positions along a straight line. This line is directed in an orthogonal direction compared to the wave vector and has a horizontal orientation. When the measurement started the receiving antenna is standing for some time (1.4 sec) at one point where it record information about the transmitted power. Thereafter the receiving antenna moves 13 mm, along the horizontal line, until the next point has been reached where it continues with the next recording. This will proceed until all 21 recording points have been reached. The whole procedure is repeated three times for every case (i.e. for different values of the vegetation thickness) in order to receive a proper mean value of the transmitted power and to minimize the errors. The two antennas are directed toward each other during the measurement, so that a maximum value of the directive gain (see section 5) is obtained. The distance between the two antennas has in all measurements been 30 m while the distance through vegetation has been changed. In this way it is possible to alter the vegetation attenuation while the attenuation of free space remains at a constant level. Four different vegetation lengths have been used: 6, 9, 12 and 15 m.
Measurements was also done in the case of line of sight (LOS), i.e. when the electromagnetic field is propagating in free space and is attenuated only by the path length. The results from the LOS measurements have been used to compensate the vegetation measurements for the attenuation of free space and for the properties of the two antennas. In this way it is possible to isolate the part that just belongs to the vegetation attenuation, only. In table 6.1 we find the results from the measurements of the attenuation of the beech at 3.1 and 5.8 GHz for different values of the thickness of vegetation.

Table 6.1: Results from measurements of the vertical part of the transmitted field at 3.1 and 5.8 GHz. The distance between the two antennas has been 30 m in all measurements. The quantities in the table are the mean value and the standard deviation of the attenuation for different values of the vegetation length through the beech.

Veg length [m]	**Mean value** [dB] 3.1 GHz	**Std dev** [dB] 3.1 GHz	**Mean value** [dB] 5.8 GHz	**Std dev** [dB] 5.8 GHz
LOS	49.3	0.1	52.7	2.2
6	68.7	1.8	70.2	3.4
9	66.4	2.9	67.0	1.2
12	61.0	1.5	65.5	1.9
15	66.2	0.5	76.4	3.3

The receiving antenna has been adjusted to measure vertical polarized radiation. In table 6.2 we find the corresponding results for the measurements of the horizontal field. These results give a good comprehension of the effects of cross polarization. The presence of the beech cause twisting effects on the incident field and thus the contribution to the horizontal polarization increases. If we compare the results at LOS with the results at 6 m in Table 6.2 we find that the attenuation is less at 6 m than in the case of LOS. The emitted field has mainly

Table 6.2: Results from measurements of the horizontal part of the transmitted field at 3.1 and 5.8 GHz. The distance between the two antennas has been 30 m in all measurements. The quantities in the table are the mean value and the standard deviation of the attenuation for different values of the vegetation length through the beech.

Veg length [m]	**Mean value** [dB] 3.1 GHz	**Std dev** [dB] 3.1 GHz	**Mean value** [dB] 5.8 GHz	**Std dev** [dB] 5.8 GHz
LOS	74.0	1.3	70.1	2.9
6	71.0	0.9	79.7	2.9
9	74.9	2.4	83.1	1.9
12	79.1	3.3	79.7	3.4
15	79.4	1.6	87.4	3.5

been vertical polarized throughout all of the measurements. The results from the measurements of the vertical polarized field were compensated for the attenuation of free space and for the properties of the two antennas. In this way it were possible to get the magnitude of the attenuation that is related to the vegetation. This can be achieved if the results from the vegetation measurements are subtracted from the results at the LOS measurements. The values specific to vegetation attenuation are given in Table 6.3. From

Table 6.3: The mean value and the standard deviation for the vegetation attenuation per meter at 3.1 and 5.8 GHz. Results from the measurements of the transmitted vertical polarized field.

Veg length [m]	**Mean value** [dB/m] 3.1 GHz	**Std dev** [dB/m] 3.1 GHz	**Mean value** [dB/m] 5.8 GHz	**Std dev** [dB/m] 5.8 GHz
6	3.2	0.3	2.9	0.7
9	1.9	0.3	1.6	0.3
12	1.0	0.1	1.1	0.2
15	1.12	0.04	1.6	0.3

these values it is possible to calculate a mean value of the vegetation attenuation of the beech. Since the different values in Table 6.3 represent the attenuation at different parts of the tree crown the mean value is a measure of the attenuation of the test beech on average. The results are given in Table 6.4. The results from the measurements at 6 m are excluded in the calculation of the mean value. The reason is that during the measurements the emitted wave was propagating through a part of the crown that was extremely dense — much denser than the other parts of the crown — which is reflected in the attenuation values in Table 6.3. Since the values of the attenuation at 6 m is not representative for the whole crown and since the number of measurements were too few these results will be excluded. The values in

Table 6.4: The mean value and standard deviation for the vegetation attenuation of the test beech per meter at 3.1 and 5.8 GHz. Results from the measurements of the transmitted vertical

Frequency [GHz]	**Mean value** [dB/m]	**Std dev** [dB/m]
3.1	1.3	0.4
5.8	1.4	0.5

Table 6.4 correspond to the mean value and the standard deviation of the vegetation attenuation per meter for a vertical polarized transmitted field. To estimate the number of leaves and branches per unit volume in the tree crown a number of branches have first been selected. The lengths of the branches are measured and at the same time the number of leaves that are attached to the respective branch is counted. From this information it is possible to estimate a mean value for the number of leaves per meter in the tree crown. To get an

apprehension on the number of leaves and branches per unit volume we just select some parts of the crown where we count the number of branches that cross one horizontal square meter. If the values for the leaves per meter are multiplied with these new values we find an estimation of the number of leaves per unit volume. The value for the number of branches per unit volume will be taken to be the same as the number of branches that cross one square meter. The results are given in Table 6.5. In Table 6.6 the mean value of the size of a leaf (the radius of a leaf) is given together with the information of the mean value of the length

Table 6.5: The number of leaves and branches per unit volume in the test beech.

Category	**Mean value** [1/m^3]	**Std dev** [1/m^3]
Leaves	2403	1025
Branches	26	4

of a branch. We have also included information about the leaf and branch thicknesses. The reason why the information about the standard deviations is excluded in Table 6.6 is that we were not able to measure these thicknesses with a sufficiently high resolution to determine the standard deviation.

Table 6.6: The mean value of the leaf size and the length of the branch is given together with the standard deviation.

Category	**Mean value** [m]	**Std dev** [m]
Leaf size	0.063	0.004
Branch length	0.8	0.2
Leaf thickness	0.0002	----
Branch thickness	0.002	----

7 Results

The results from the calculations of the total cross section of a single leaf and a branch are presented in this section. The calculations are based on the T-matrix method, explained in appendix C. In order to achieve values for the expectation value of the total cross section the total cross section must be calculated for different orientations. This will be done for 121 points on a surface that cover an eighth of a sphere — i.e. the two angles in Figure 5.3 take values in the regions $0 < \alpha < 90^{\circ}$ and $0 < \beta < 90^{\circ}$. Due to the spherical symmetry the total cross section on the other parts of the sphere can be achieved from these values, which is necessary in order to calculate the expectation value.
The solution for the total cross section is written as an infinite sum (see appendix C), but only a finite number of terms can be computed. Enough terms must be included for the total cross section to converge to the correct solution with the required accuracy. Therefor the minimum number of terms necessary to obtain a converged solution must be determined. It is also necessary to find the number of sample points required for accurate numerical integration. There is no standard technique that can be applied to find the number of modes and sample points. It is a little bit tricky and some trial and error is needed. After several calculations we have found that a value for the number of sample points that can be used is 500. This value is sufficiently large to cover all of the cases that will occur. It has been a more severe problem though to determine the number of modes — i.e. to pass the convergence test — which has to be done in order to be able to proceed with the calculations for the expectation value of the total cross section. The reason is that the spheroid is very thin in comparison to the diameter (*2b*). The spheroidal particle has the dimensions of 2*a* along the symmetry axis (*z*-axis) and 2*b* across the equatorial plane (the *x*-*y*-plane) where the center of the spheroidal is placed at the origin of the coordinate system. The values that were used in the calculations are 2*a* = 0.2 mm and 2*b* = 6.3 cm which corresponds to *a*/*b* = 0.00316. From this we find that *ka* = 0.0065 and *kb* = 2.055 at 3.1 GHz and *ka* = 0.0122 and *kb* = 3.844 at 5.8 GHz. The first problem that we run into is that it is not possible — with the computer program that is used — to calculate the total cross section for these values. We therefor have to try another way to tackle the problem.

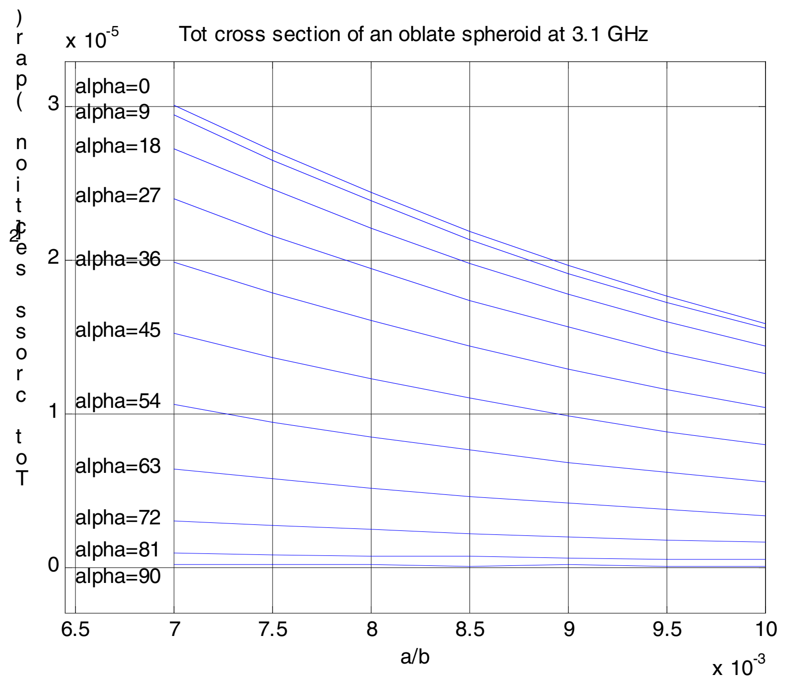

Figure 7.1: Calculation of the tot cross section for an oblate spheroid at 3.1 GHz for different values of b and alpha. The thickness of the spheroid (2a) is constant and the beta angle is zero. The polarization is parallel to the plane of incidence.

Instead of using the actual values we use the values that pass through the convergence test, i.e. small values of 2*b*. Thereafter the *a*/*b* values are decreased until convergence no longer is achieved. If the results from the calculations of the total cross section are plotted as a function of *a*/*b* there might be a possibility to extrapolate the requested values. We start with the given value of *ka* and alter the 2*b* value until we no longer obtain a converged solution. In Figure 7.1 we find the results from the calculations of the total cross section at 3.1 GHz for different values of the angle α and the size 2*b*. The values of the thickness and the horizontal angle have been 2*a* = 0.2 mm and $\beta = 0$ during the calculations. The incident field is represented by a plane wave of vertical polarization. In Figure 7.2 the corresponding results for the calculations of the total cross section at 5.8 GHz are plotted. We find that the closest we get to the value *a*/*b* = 0.00316 is *a*/*b* = 0.007

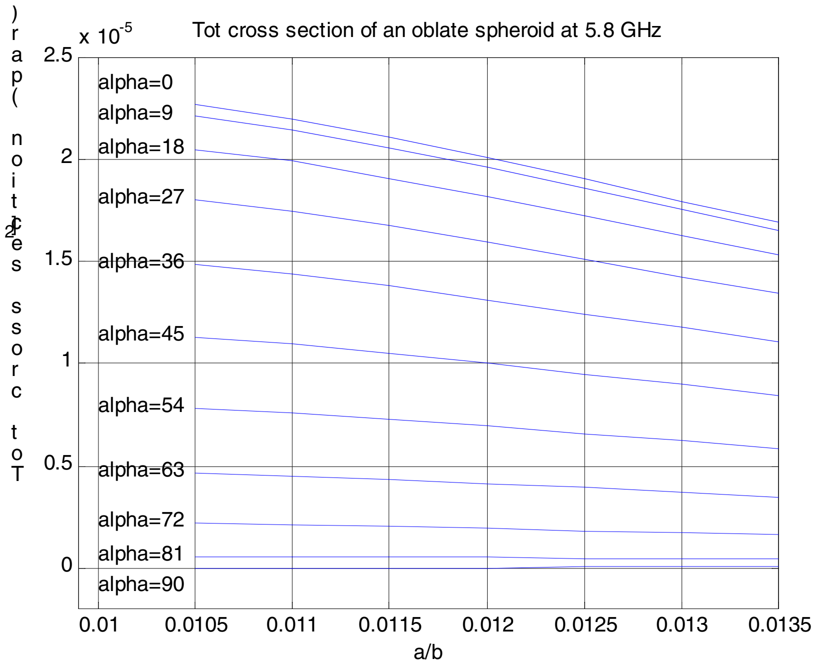

Figure 7.2: Calculation of the tot cross section for an oblate spheroid at 5.8 GHz for different values of b and alpha. The thickness of the spheroid (2a) is constant and the beta angle is zero. The polarization is parallel to the plane of incidence.

at 3.1 GHz and *a*/*b* = 0.0105 at 5.8 GHz. This corresponds to a leaf size of 2*b* = 2.86 cm at 3.1 GHz and 2*b* = 1.90 cm at 5.8 GHz. Furthermore the *kb* values are between 0.650 and 0.928 in Figure 7.1 and between 0.900 and 1.158 in Figure 7.2. We can now use these results to extrapolate the values of the total cross section to estimate the values at *a*/*b* = 0.00316. The problem is that the shape of the curves in Figure 7.1 and Figure 7.2 are not similar. This means that we can not be sure which behavior the curves will have outside the current region. This is a typical behavior in the resonance region. We simply have to accept that we can not calculate the total cross section of a leaf with the actual dimensions with the presented computer program. We instead use the values 2*b* = 2.86 cm at 3.1 GHz and 2*b* = 1.90 cm at 5.8 GHz in order to estimate the attenuation of the tree crown. The results from the calculations of the total cross section at 3.1 GHz for different values of α and β are plotted in Figure 7.3. The incident field

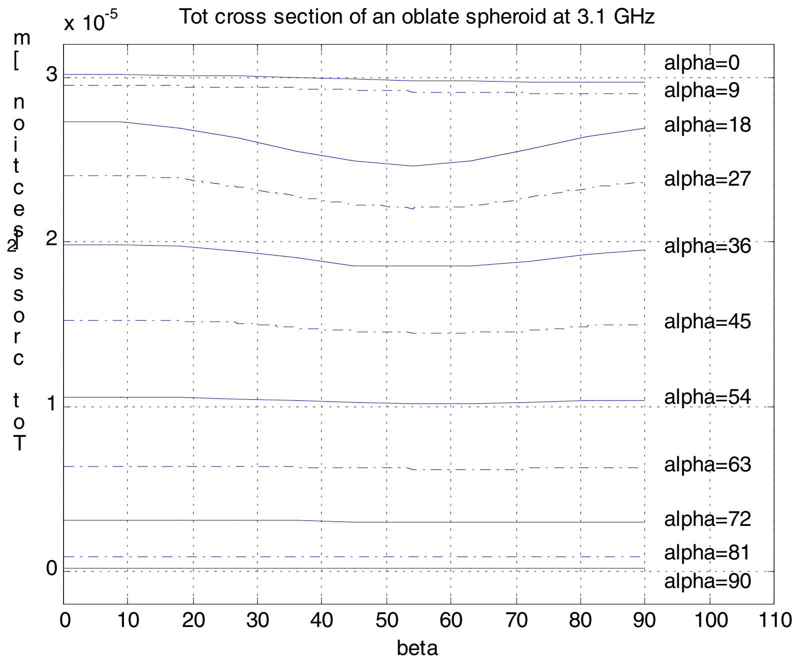

Figure 7.3: The total cross section for an oblate spheroid at 3.1 GHz for different values of alpha and beta. The polarization of the incident field is parallel to the plane of incidence.

is parallel to the plane of incidence. In Figure 7.4 is the corresponding results for the frequency 5.8 GHz are plotted. The incident field is here also parallel to the plane of incidence.

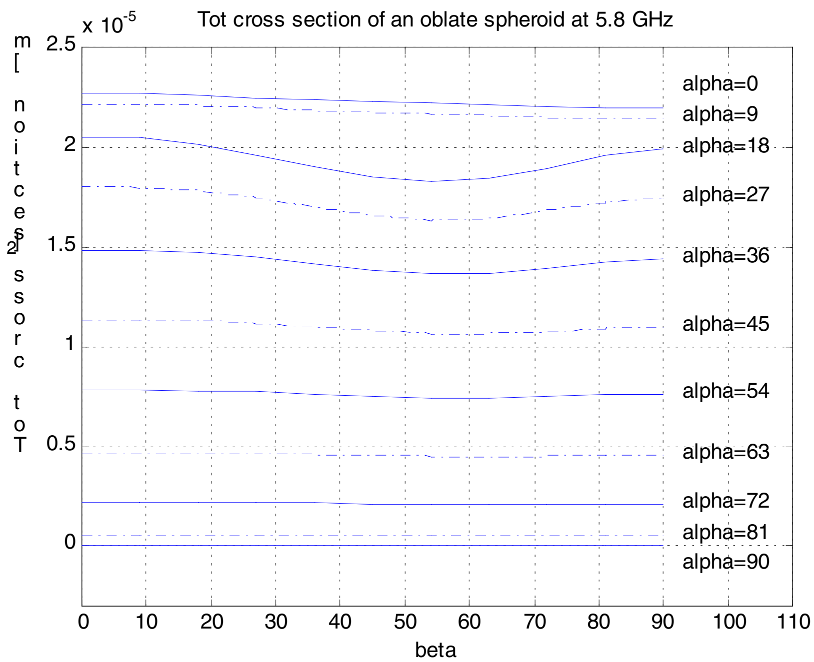

Figure 7.4: The total cross section for an oblate spheroid at 5.8 GHz for different values of alpha and beta. The polarization of the incident field is parallel to the plane of incidence.

To get a better overview of the results in Figure 7.3 the results are plotted in a three-dimensional diagram in Figure 7.5. In Figure 7.6 the results from the calculation of the

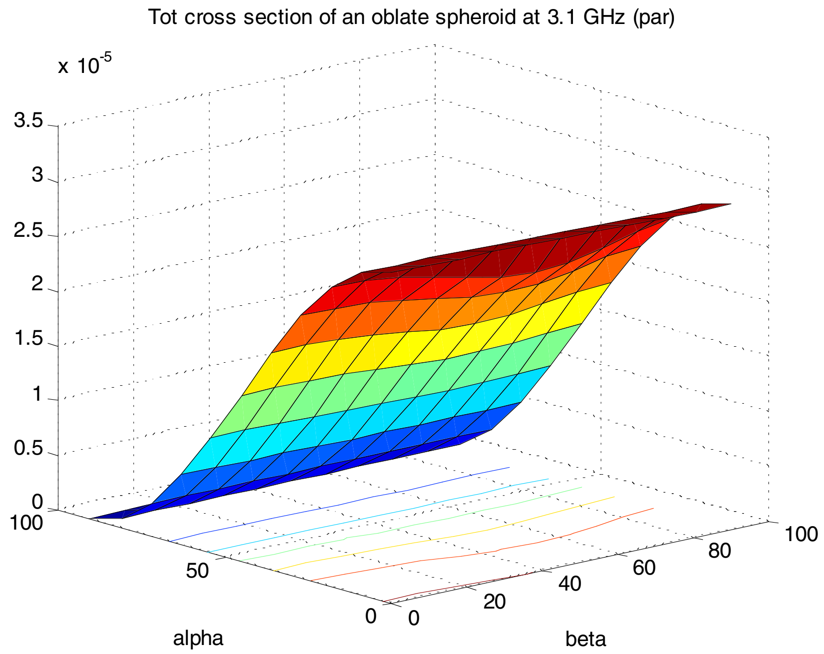

Figure 7.5: The total cross section for an oblate spheroid at 3.1 GHz for different values of alpha and beta. The polarization of the incident field is parallel to the plane of incidence.

total cross section at 3.1 GHz are plotted for horizontal polarization of the incident field, i.e. the polarization of the incident field is orthogonal to the plane of incidence. The

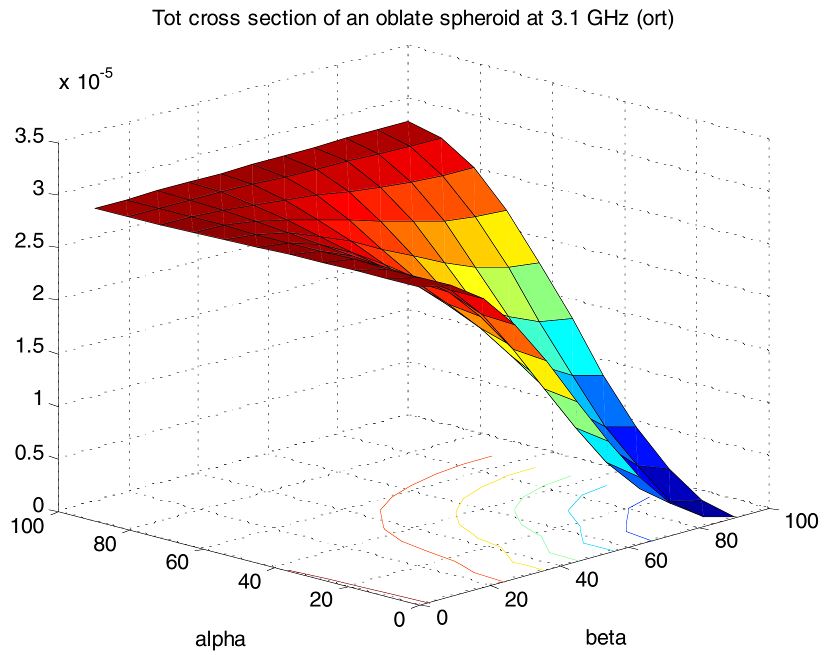

Figure 7.6: The total cross section for an oblate spheroid at 3.1 GHz for different values of alpha and beta. The polarization of the incident field is orthogonal to the plane of incidence.

corresponding calculations are at 5.8 GHz and the results are given in Figure 7.7 and Figure 7.8.

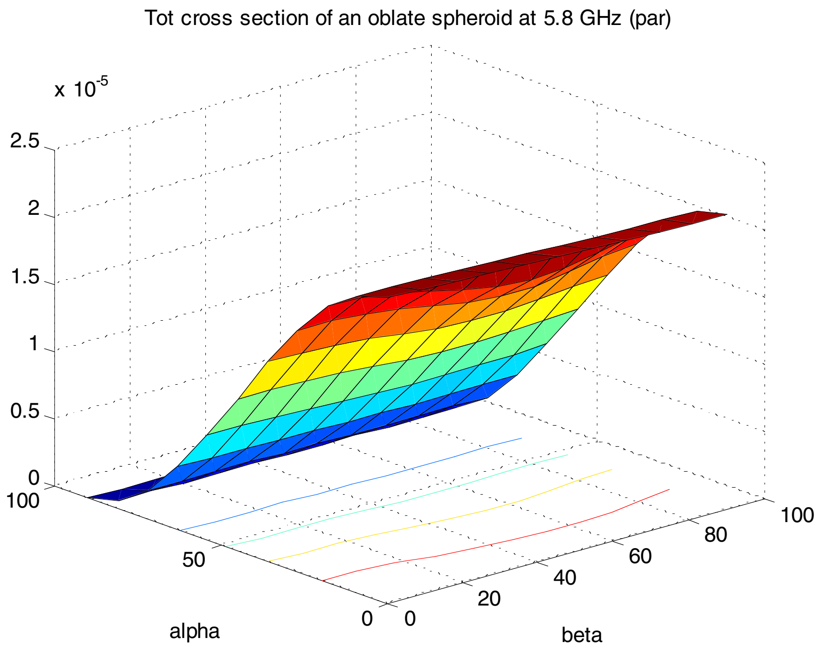

Figure 7.7: The total cross section for an oblate spheroid at 5.8 GHz for different values of alpha and beta. The polarization of the incident field is parallel to the plane of incidence.

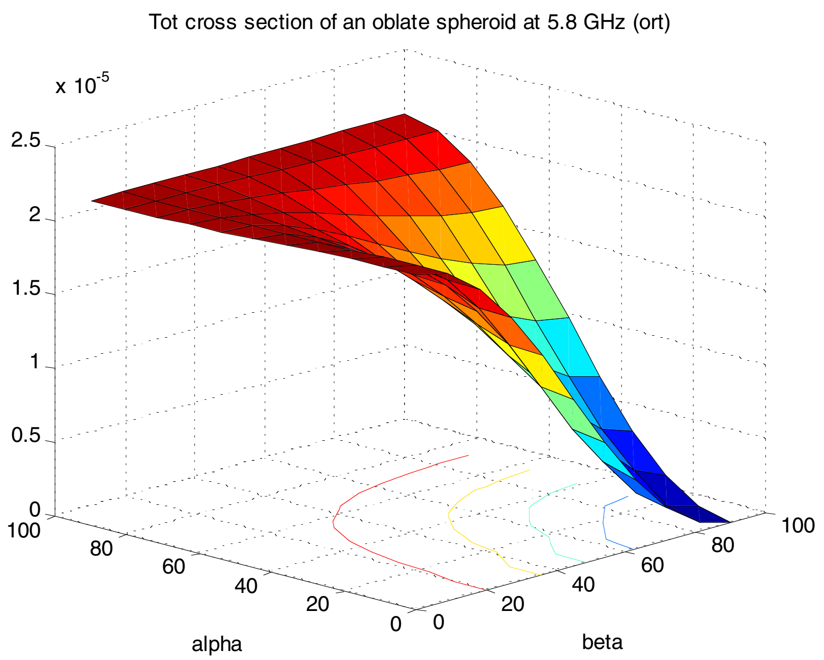

Figure 7.8: The total cross section for an oblate spheroid at 5.8 GHz for different values of alpha and beta. The polarization of the incident field is orthogonal to the plane of incidence.

The expectation value of the total cross section of an oblate spheroid can now be calculated. The results are given in Figures 7.9-12 and they are based on the results presented in Figures 7.5-8. The *n* value corresponds to the exponent of the probability function. When the value of the exponent is increased the probability of finding the leaf in a vertical orientation is increased (see Figure 5.4 and Figure 5.5).

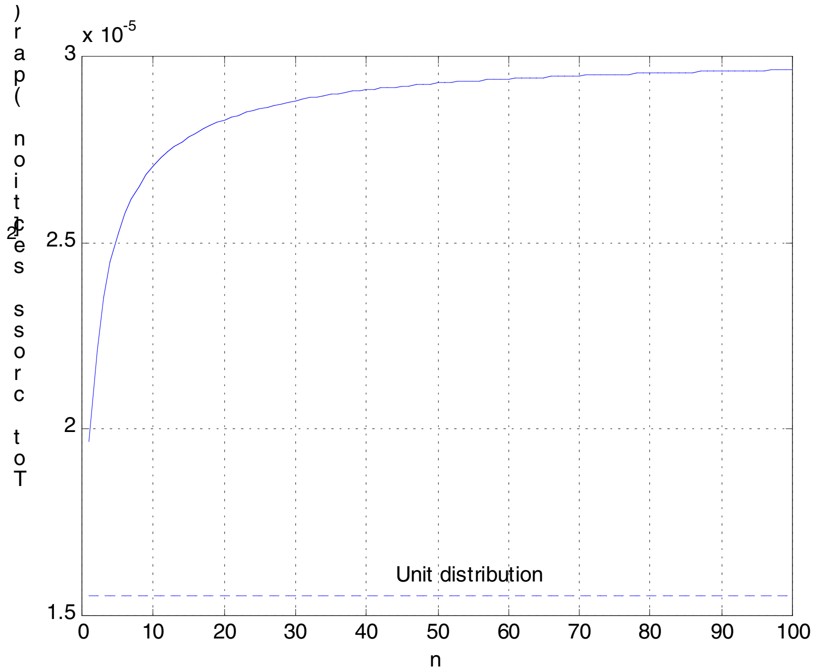

Figure 7.9: The expectation value of the total cross section for an oblate spheroid at 3.1 GHz for different values of the exponent *n*. The polarization of the incident field is parallel to the plane of incidence.

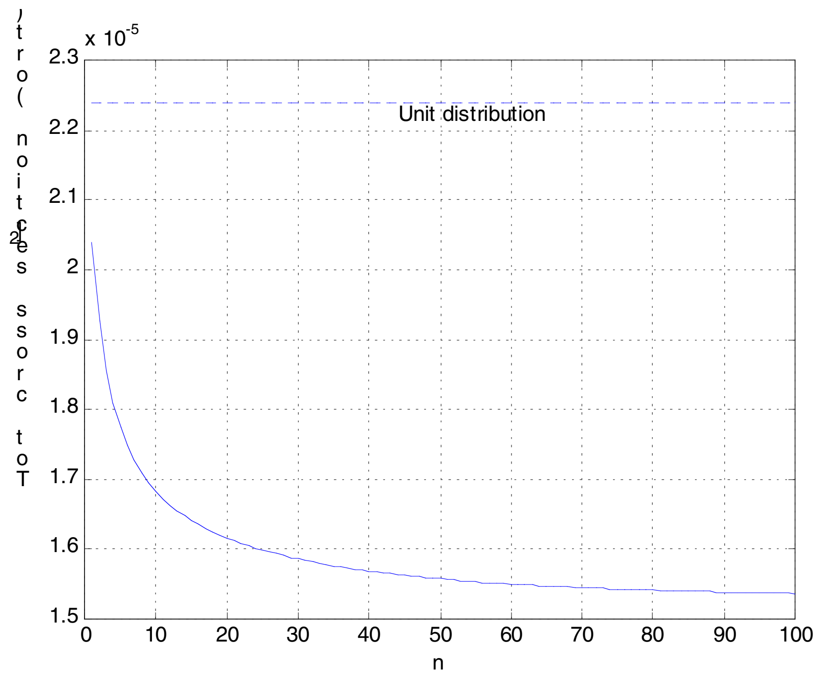

Figure 7.10: The expectation value of the total cross section for an oblate spheroid at 3.1 GHz for different values of the exponent *n*. The polarization of the incident field is orthogonal to the plane of incidence.

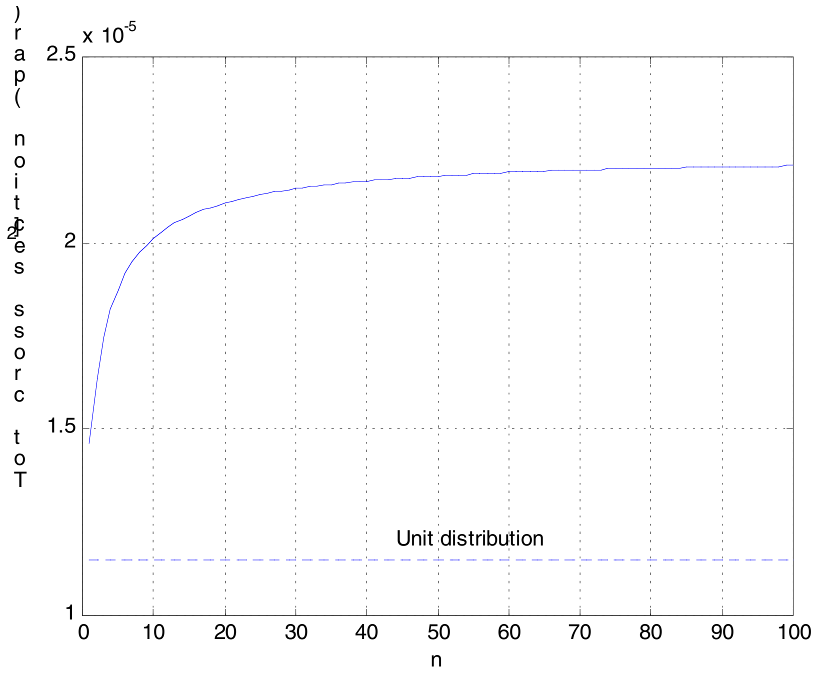

Figure 7.11: The expectation value of the total cross section for an oblate spheroid at 5.8 GHz for different values of the exponent *n*. The polarization of the incident field is parallel to the plane of incidence.

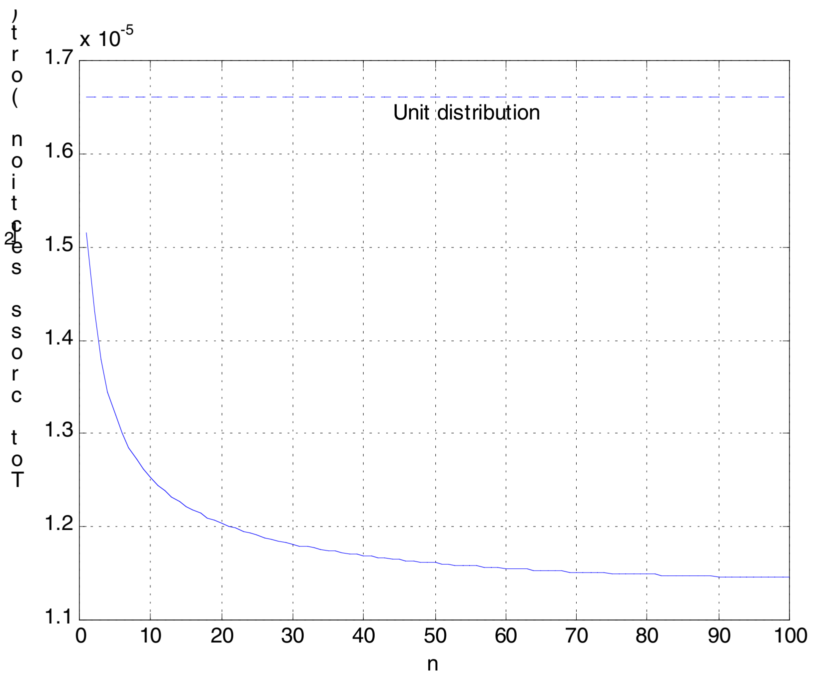

Figure 7.12: The expectation value of the total cross section for an oblate spheroid at 5.8 GHz for different values of the exponent *n*. The polarization of the incident field is orthogonal to the plane of incidence.

In the case of calculating the total cross section for a cylinder the problems that occurred during the convergence test of the total cross section for a spheroid also occurs here. The mean value of the length of a branch is $2a = 0.8$ m and the thickness is $2b = 2$ mm (see section 6) where $2a$ is the length and $2b$ is the diameter of a cylinder. With these values no convergence was achieved. To solve this problem we divide the cylinder into several small cylinders for which it is possible to achieve convergence. We assume that the electromagnetic interaction between the small cylinders is negligible which is a rough approximation. After some trial and error we find that convergence is achieved for $2b = 3$ cm at 3.1 GHz and $2b = 2$ cm at 5.8 GHz which corresponds to the approximation conditions. The results from the calculations of the total cross section for a cylinder at 3.1 GHz are plotted in Figure 7.13. The polarization of the incident field is parallel to the plane of incidence. In Figure 7.14 the corresponding results for the calculation of the total cross section for a cylinder at 5.8 GHz are plotted.

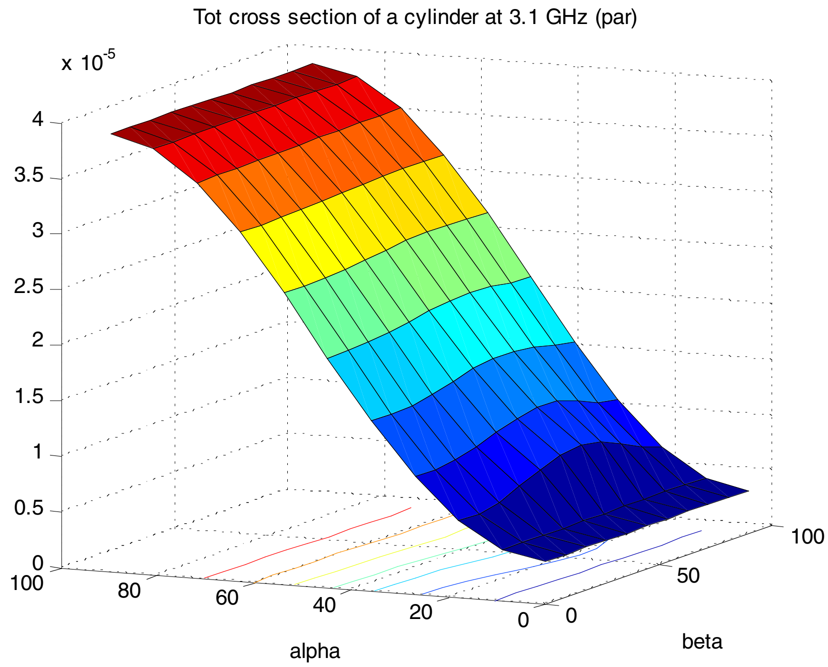

Figure 7.13: The total cross section for a cylinder at 3.1 GHz for different values of alpha and beta. The polarization of the incident field is parallel to the plane of incidence.

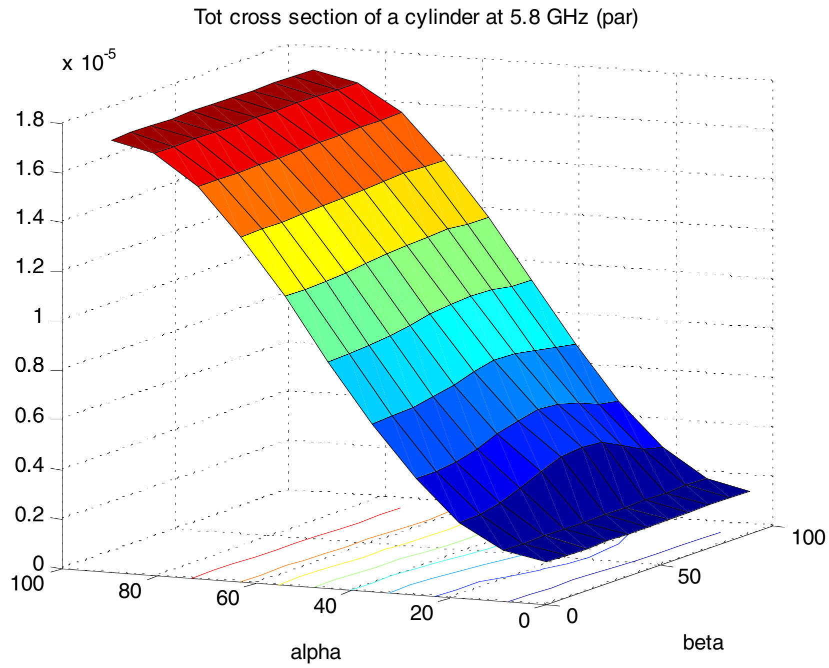

Figure 7.14: The total cross section for a cylinder at 5.8 GHz for different values of alpha and beta. The polarization of the incident field is parallel to the plane of incidence.

In Figure 7.15 and Figure 7.16 the expectation values of the total cross section for a cylinder at 3.1 GHz and 5.8 GHz have been plotted as a function of the exponent n. When the value of the exponent is increased the probability of finding the branch in a vertical position increases.

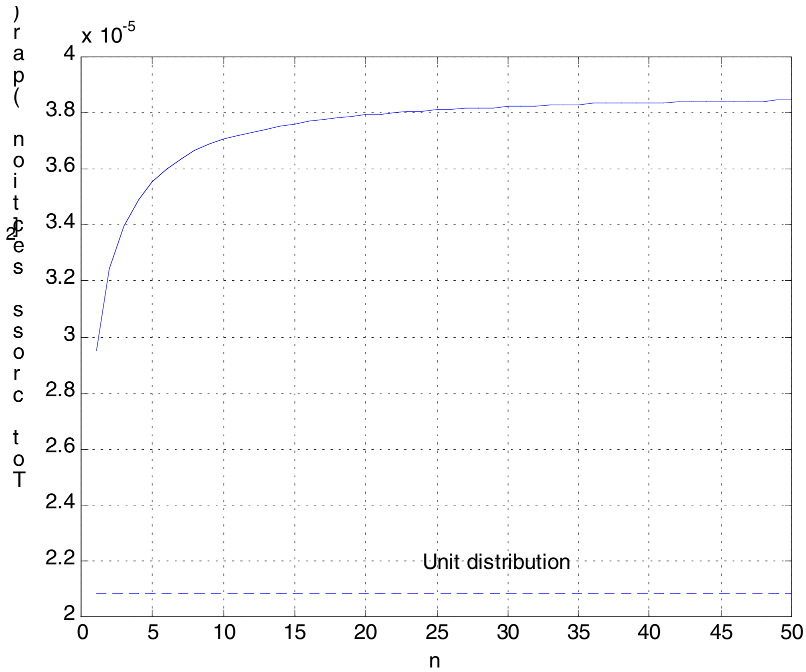

Figure 7.15: The expectation value of the total cross section for a cylinder at 3.1 GHz for different values of the exponent n. The polarization of the incident field is parallel to the plane of incidence.

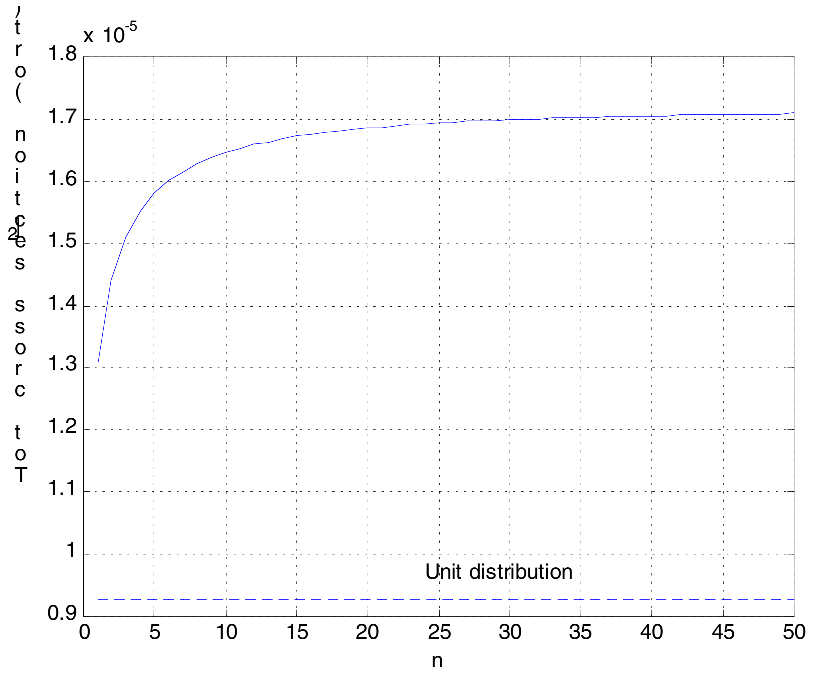

Figure 7.16: The expectation value of the total cross section for a cylinder at 5.8 GHz for different values of the exponent *n*. The polarization of the incident field is parallel to the plane of incidence.

The expectation value of the total cross section for the large cylinder can be calculated by multiplying the results in Figure 7.15 and 7.16 with the number of small cylinders that the large cylinder has been divided into. In Table 7.1 the results from the calculations of the expectation value of the total cross section are presented. The results that are presented are the maximum value of the expectation value of the total cross section. The Large cylinder and the Large spheroid correspond to an average branch and leaf, respectively. The expectation value of the total cross section for the large spheroid at 3.1 GHz has been estimated to be approximately twice the value of the small spheroid. The expectation value at 5.8 GHz has been estimated to be three times the value of the small spheroid. These relations should not be taken too seriously since they are based on the difference in size between the small and large spheroid. In Table 7.2 the attenuation for the branches and the leaves are presented. These values are based on Eq. (5.23) and the *N* values calculated in section 6.

Table 7.1: The maximum expectation value of the total cross section for a cylinder and an oblate spheroid. The polarization of the incident field is parallel to the plane of incidence.

Category	$<\sigma>$ 3.1 GHz [m^2]	$<\sigma>$ 5.8 GHz [m^2]
Small cylinder	3.9E-5	1.7E-5
Large cylinder	1.1E-3	7.0E-4
Small spheroid	3.0E-5	2.2E-5
Large spheroid	6.0E-5	6.6E-5

Table 7.2: The results from the calculations of the maximum attenuation for a branch and two different sizes of leaves. These values are used to calculate the vegetation attenuation of the beech.

Category	***L*** (3.1 GHz) [dB/m]	***L*** (5.8 GHz) [dB/m]
Branch, mean value	0.12	0.08
Branch, std dev	0.02	0.01
Small leaf, mean value	0.3	0.2
Small leaf, std dev	0.1	0.1
Large leaf, mean value	0.6	0.7
Large leaf, std dev	0.3	0.3
Small leaf + branch, mean val	0.4	0.3
Small leaf + branch, std dev	0.2	0.1
Large leaf + branch, mean val	0.7	0.8
Large leaf + branch, std dev	0.3	0.3

8 Discussion and conclusions

During this work we have made a review of existing models. We have found that the existing models do not cover the case of resonance effects, which means that we have to find a way to improve the model of vegetation attenuation. The same concepts as in the case of rain attenuation has been used and thus the problem of vegetation attenuation has been minimized to find the two quantities N and $\langle\sigma\rangle$; the number of scattering bodies per unit volume and the expectation value of the total cross section. To calculate the N-values a test tree has been chosen in which the number of leaves and branches per unit volume on average have been counted. The total cross section for the leaves and branches has been calculated with a computer program based on the T-matrix method in the resonance region. We have not been able though to use the real symmetries because of restrictions in the computer program. Convergence for the oblate spheroids (the leaves) was achieved for $2b$ = 2.86 cm at 3.1 GHz and $2b$ = 1.90 cm at 5.8 GHz. The oblate spheroid has the dimensions of $2a$ along the symmetry axis (z-axis) and $2b$ across the equatorial plane (the x-y-plane) where the center of the spheroidal is placed at the origin of the coordinate system. The correct value should be $2b$ = 6.30 cm. For the cylinders (the branches) convergence was achieved for $2a$ = 3 cm at 3.1 GHz and $2a$ = 2 cm at 5.8 GHz. Here $2a$ is the length and $2b$ is the diameter of the cylinder. Since we could not use the real values we instead used the values that gave convergence. From these values we calculated the attenuation of the tree. We used these values to estimate the real values for the attenuation of the tree crown. To do that we assumed that the difference between the sizes of the leaves reflected the difference in attenuation. We therefor increased the attenuation values at 3.1 GHz with a factor of two and the attenuation values at 5.8 GHz by a factor of three. But it turned out that the results still were to low compared to the measurements. The calculated values were 0.7 (0.3) dB/m at 3.1 GHz and 0.8 (0.3) dB/m at 5.8 GHz (the standard deviation is given inside the parenthesis). The measured values were 1.3 (0.4) dB/m at 3.1 GHz and 1.4 (0.5) dB/m at 5.8 GHz. The predicted values are thus too low. If we compare the results we find that they overlap and thus are the deviations from the correct values small. To decrease the uncertainties more measurements have to be done. This means that further work is needed but the modeling approach can be used

8.1 Future work

More measurements have to be done on the same test beech in order to increase the accuracy of the mean value and the standard deviation of the attenuation. The inventory of the test beech must be done with a greater accuracy since the values of the standard deviation are much too high. The total cross section should be calculated for different sizes of the branches and leaves. In that way a better estimation can be performed. If it is possible the computer program based on the T-matrix method must be improved in order to be able to calculate oblate spheroids and cylinders with extreme symmetries or alternatively find another method to calculate the total cross section. Since the results of the vegetation attenuation will be used in a prediction tool it is necessary to investigate the attenuation from other trees so that a mean value of the attenuation can be estimated. This prediction tool is used to investigate wave propagation in general at residential environments. It is therefor important to investigate the attenuation of many different types of trees. It is also important to investigate the frequency of tree types in cities. If this factor can be determined a model for every single tree type can be constructed and used together with this factor as a statistical weight to get a better estimation of the vegetation attenuation in general. Of course measurements must be made on all different types of trees in order to verify the validity of the theoretical model.

9 Acknowledgements

First of all, I would like to thank my supervisors Christian Bergljung and Anders Karlsson for their good advice and their positive attitudes.

Special thanks to Professor Gerhard Kristensson at the Department of Applied Electronics, Lund Institute of Technology, for some brilliant ideas and also for letting me use the derivations from his books.

I am also very grateful to my family who supported me during my work.

Finally, I would like to thank the staff members at Telia Research and at the Department of Applied Electronics for many pleasant conversations.

10 References

[1] C. M tzler, Microwave (1-100 GHz) dielectric model of leaves, (IEEE Trans Geosci Remote Sens, vol 32, No 5, pp 947-949, (1994)).
[2] C. M tzler and A. Sume, Microwave radiometry of leaves, (in Microwave Radiometry and Remote Sensing Applications, P. Pampaloni, Ed. Utrecht, The Netherlands: VSP, pp. 133-148 (1989)).
[3] C. M tzler, Microwave transmissivity in forest canopy: Experiments made with a beech, (Remote Sens. Environ ., in press (1994)).
[4] U. Wegm ller, C. M tzler and E. Njoku, Canopy opacity models, (in Proc. ESA-NASA Workshop Passive Microwave Remote Sens. Res. Related Land-Atmosphere Interact., St. Lary, France, Jan. 10-15, (1993)).
[5] K. P. Kirdyashev, A. A. Chuckhlantsev and A. M. Shutko. Microwave radiation of the Earth s surface in the presence of vegetation cover, (Radio Science and Electronics, 24, 256-264 (1979)) (or: Radio Eng. Electron. Phys., 24, 37-44, (1979)).
[6] F. Ulaby and M El-Rayes. Microwave dielectric spectrum of vegetation. Part II: Dual-dispertion model, (IEEE Trans. Geosci. Remote Sens., GE-25 (5), 550-556, (1987)).
[7] Y. H. Kerr and E. G. Njoku. A semi-empirical model for interpreting microwave emission from semiarid land surfaces as seen from space, (IEEE Trans. Geosci. Remote Sensing, GE-28 (3), 384-393, (1990)).
[8] S. A. Torrico and R. H. Lang. Simple engineering expressions to predict the specific attenuation of a tree, COST259TO(99)5
[9] M. El-Rayes and F. Ulaby. Microwave dielectric behaviour of vegetation material, (NASA GSFC Rep., Contract NAG 5-480, Jan. (1987)).
[10] L. L. Foldy, The multiple scattering of waves, (Phys. Rev., vol. 67, No. 3, pp. 107-119, (1945)).
[11] M. X. Lax, Multiple scattering of waves, (Rev. Mod. Phys., vol. 23, No. 4, pp. 287-310, (1951)).
[12] D. M. LeVine, R. Meneghini, R. H. Lang, and S.S. Seker, Scattering from arbitrary oriented dielectric discs in the physical optics regime, (J. Opt. Soc. Amer., vol. 73, pp. 1255-1262, (1983)).
[13] R. H. Lang, Electromagnetic backscattering from a sparse distribution of lossy dielectric scatterers, (Radio Science, vol. 16, No. 1, pp. 15-30, (1981)).
[14] G. Kristensson, Spridningsteori med antenntill mpningar, (Lund, 1999) (in Swedish).
[15] P. W. Barber and S. C. Hill, Light scattering by particles: Computational Methods, (Word Scientific Publishing Co. Pte. Ltd. Singapore, (1990)).

Appendix A

Wave propagation in multiple dimensions

In the following analysis we will consider the case when the propagated waves are represented by plane waves. Since waves usually take this shape, at least at a distance from the transmitter, the results can be used in many applications. Furthermore it has been assumed that the size of the obstacles are sufficiently large (actually approximately infinite large) to cover the incident wave, i.e. no part of the incident wave will pass on the outside of the obstacles, and that the different materials are homogenous. This means that the constitutive relations are independent of the room coordinates. To be able to calculate the reflected and transmitted waves we first have to know the solutions Maxwell s equations generate in an arbitrary region. This is done in the following section. When we have the solutions we can use them to calculate the reflected and transmitted fields, which is done in the other sections.

A.1 Basic derivations

As a starting point we use Maxwell s equations for a region without sources. We assume that all conducting currents are included in the constitutive relations (see Eq. (2.6) and Eq. (2.11)).

$$\begin{cases} \nabla \times \boldsymbol{E}(\boldsymbol{r},\omega) = i\,\omega \boldsymbol{B}(\boldsymbol{r},\omega) \\ \nabla \times \boldsymbol{H}(\boldsymbol{r},\omega) = -i\,\omega \boldsymbol{D}(\boldsymbol{r},\omega) \end{cases} \tag{A.1}$$

During reflection and transmission at a plane surface, $z = \text{const}$, the z-axis takes an exceptional position since the field sources are placed on one of the sides of a plane, $z = \text{const}$ (see Figure A.1).

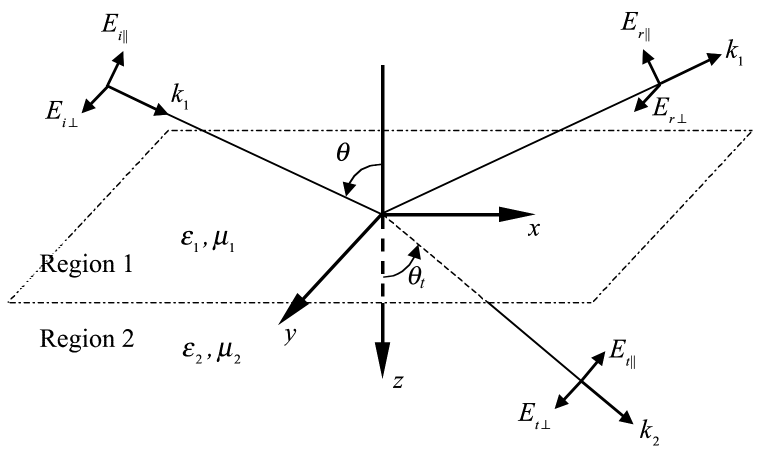

Figure A.1: Reflection and transmission between two isotropic materials.

The placement of the sources leads to that the fields propagate in either the positive or negative z-direction. For the presence we will keep the z-dependence of the fields, whereas we Fourier transform the fields in the other two spatial variables, x- and y-variables.
The Fourier transform is defined as

$$\boldsymbol{E}(z,\boldsymbol{k}_t,\omega) = \int_{-\infty}^{\infty}\int_{-\infty}^{\infty} \boldsymbol{E}(\boldsymbol{r},\omega) e^{-i\boldsymbol{k}_t\cdot\rho}\, dx\, dy$$

with the inverse transform

$$\boldsymbol{E}(\boldsymbol{r},\omega) = \frac{1}{4\pi^2}\int_{-\infty}^{\infty}\int_{-\infty}^{\infty} \boldsymbol{E}(z,\boldsymbol{k}_t,\omega) e^{i\boldsymbol{k}_t\cdot\rho}\, dk_x dk_y$$

We have here defined a vector $\boldsymbol{k}_t$ and the position vector in the x-y-plane (see Figure A.2)

$$\boldsymbol{k}_t = \boldsymbol{x}\, k_x + \boldsymbol{y}\, k_y = k_t\, \boldsymbol{e}_\parallel \qquad \rho = \boldsymbol{x}\, x + \boldsymbol{y}\, y$$

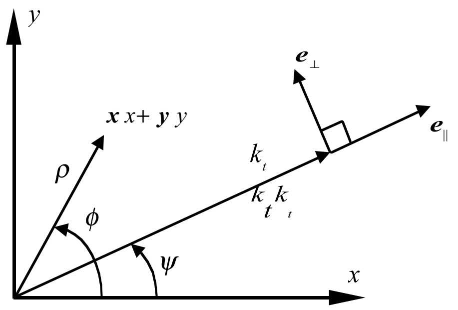

Figure A.2: Definition of cylindrical coordinates.

The representation of the electric field $\boldsymbol{E}$ has here been used to represent the time harmonic field $\boldsymbol{E}(\boldsymbol{r},\omega)$ as well as its Fourier transform $\boldsymbol{E}(z,\boldsymbol{k}_t,\omega)$ to avoid clumsy notations. The argument clarifies which form that is considered. Whenever it is possible the arguments $\boldsymbol{k}_t$ and ω are omitted. This means that the notation $\boldsymbol{E}(z)$ instead of $\boldsymbol{E}(z,\boldsymbol{k}_t,\omega)$ is used.
We will now study the Fourier coefficients $\boldsymbol{E}(z,\boldsymbol{k}_t,\omega)$ and their properties. Maxwell s equations without sources $(\boldsymbol{J} = \boldsymbol{0})$ for harmonic waves, see Eq. (A.1), are transformed into the following equations (use $\nabla \to i\,\boldsymbol{k}_t + \boldsymbol{z}\frac{d}{dz}$)

$$\begin{cases} \boldsymbol{z}\times\dfrac{d}{dz}\boldsymbol{E}(z) + i\,\boldsymbol{k}_t \times \boldsymbol{E}(z) = i\,\omega \boldsymbol{B}(z) \\ \boldsymbol{z}\times\dfrac{d}{dz}\boldsymbol{H}(z) + i\,\boldsymbol{k}_t \times \boldsymbol{H}(z) = -i\,\omega \boldsymbol{D}(z) \end{cases} \tag{A.2}$$

The exceptionality of the z-axis makes it advantageous to separate the fields into one transversal and one longitudinal part, $\boldsymbol{E} = \boldsymbol{E}_{xy} + \boldsymbol{z}\, E_z$. If we operate with $-\boldsymbol{z}\times$ on both sides of Eq. (A.2)

$$\begin{cases} -\boldsymbol{z}\times\left(\boldsymbol{z}\times\dfrac{d}{dz}\left(\boldsymbol{E}_{xy}+\boldsymbol{z}E_z\right)\right)-\boldsymbol{z}\times\left(i\boldsymbol{k}_t\times\left(\boldsymbol{E}_{xy}+\boldsymbol{z}E_z\right)\right) \\ \qquad\qquad\qquad\qquad = -\boldsymbol{z}\times\left(i\omega\left(\boldsymbol{B}_{xy}+\boldsymbol{z}B_z\right)\right)=-i\omega\,\boldsymbol{z}\times\boldsymbol{B}_{xy} \\ -\boldsymbol{z}\times\left(\boldsymbol{z}\times\dfrac{d}{dz}\left(\boldsymbol{H}_{xy}+\boldsymbol{z}H_z\right)\right)-\boldsymbol{z}\times\left(i\boldsymbol{k}_t\times\left(\boldsymbol{H}_{xy}+\boldsymbol{z}H_z\right)\right) \\ \qquad\qquad\qquad\qquad = \boldsymbol{z}\times\left(i\omega\left(\boldsymbol{D}_{xy}+\boldsymbol{z}D_z\right)\right)=i\omega\,\boldsymbol{z}\times\boldsymbol{D}_{xy} \end{cases}$$

and use the BAC-CAB rule

$$(\boldsymbol{a}\times(\boldsymbol{b}\times\boldsymbol{c}))=\boldsymbol{b}(\boldsymbol{a}\cdot\boldsymbol{c})-\boldsymbol{c}(\boldsymbol{a}\cdot\boldsymbol{b})$$

it will be possible to get the transversal components of the fields.

$$\begin{cases} \dfrac{d}{dz}\boldsymbol{E}_{xy}(z)=i\boldsymbol{k}_t\,E_z(z)-i\omega\,\boldsymbol{z}\times\boldsymbol{B}_{xy}(z) \\ \dfrac{d}{dz}\boldsymbol{H}_{xy}(z)=i\boldsymbol{k}_t\,H_z(z)+i\omega\,\boldsymbol{z}\times\boldsymbol{D}_{xy}(z) \end{cases} \tag{A.3}$$

In the same way we operates with $\boldsymbol{z}\cdot$ to get the longitudinal components. We get

$$\begin{cases} \boldsymbol{z}\cdot\left(\boldsymbol{k}_t\times\boldsymbol{E}_{xy}(z)\right)=\omega B_z(z) \\ \boldsymbol{z}\cdot\left(\boldsymbol{k}_t\times\boldsymbol{H}_{xy}(z)\right)=-\omega D_z(z) \end{cases} \tag{A.4}$$

If we now use the Constitutive relations (Eq. (2.6)) we can rewrite Eq. (A.3) and Eq. (A.4)

$$\begin{cases} \dfrac{d}{dz}\boldsymbol{E}_{xy}(z)=i\boldsymbol{k}_t\,E_z(z)-\dfrac{i\omega\mu_0\mu}{\eta_0}\,\boldsymbol{z}\times\eta_0\boldsymbol{H}_{xy}(z) \\ \dfrac{d}{dz}\eta_0\boldsymbol{H}_{xy}(z)=i\boldsymbol{k}_t\eta_0\,H_z(z)+i\omega\varepsilon_0\varepsilon\eta_0\,\boldsymbol{z}\times\boldsymbol{E}_{xy}(z) \end{cases} \tag{A.5}$$

$$\begin{cases} \boldsymbol{z}\cdot\left(\boldsymbol{k}_t\times\boldsymbol{E}_{xy}(z)\right)=-\boldsymbol{k}_t\cdot\left(\boldsymbol{z}\times\boldsymbol{E}_{xy}(z)\right)=\dfrac{\omega\mu_0\mu}{\eta_0}\eta_0\,H_z(z) \\ \boldsymbol{z}\cdot\left(\boldsymbol{k}_t\times\eta_0\boldsymbol{H}_{xy}(z)\right)=-\boldsymbol{k}_t\cdot\left(\boldsymbol{z}\times\eta_0\boldsymbol{H}_{xy}(z)\right)=-\omega\varepsilon_0\varepsilon\eta_0\,E_z(z) \end{cases} \tag{A.6}$$

We have here introduced the wave impedance of vacuum

$$\eta_0=\sqrt{\frac{\mu_0}{\varepsilon_0}}=\mu_0\,c_0=\frac{1}{\varepsilon_0\,c_0}$$

By using these relations it s possible to restate Eq. (A.5) and Eq. (A.6)

$$\begin{cases} \dfrac{d}{dz}\boldsymbol{E}_{xy}(z) = i\,\boldsymbol{k}_t\,E_z(z) - \dfrac{i\,\omega\mu}{c_0}\,\boldsymbol{z}\times\eta_0\boldsymbol{H}_{xy}(z) \\ \dfrac{d}{dz}\eta_0\boldsymbol{H}_{xy}(z) = i\,\boldsymbol{k}_t\eta_0\,H_z(z) + \dfrac{i\,\omega\varepsilon}{c_0}\,\boldsymbol{z}\times\boldsymbol{E}_{xy}(z) \end{cases} \tag{A.7}$$

$$\begin{cases} E_z(z) = \dfrac{c_0}{\omega\varepsilon\mu}\mu\,\boldsymbol{k}_t\cdot\left(\boldsymbol{z}\times\eta_0\boldsymbol{H}_{xy}(z)\right) \\ \eta_0\,H_z(z) = -\dfrac{c_0}{\omega\varepsilon\mu}\varepsilon\,\boldsymbol{k}_t\cdot\left(\boldsymbol{z}\times\boldsymbol{E}_{xy}(z)\right) \end{cases} \tag{A.8}$$

Before we go any further in our analysis of the Fourier transformed fields it is suitable to introduce a coordinate independent representation. The new base $\{\boldsymbol{e}_{\parallel}, \boldsymbol{e}_{\perp}, \boldsymbol{z}\}$ will then be related to the Fourier variable $\boldsymbol{k}_t$, the tangential part of the wave vector, expressed in the cylindrical coordinates (k_t, ψ), see Figure A.2.

$$\boldsymbol{k}_t = \boldsymbol{x}\,k_x + \boldsymbol{y}\,k_y = \boldsymbol{x}\,k_t\,cos\,\psi + \boldsymbol{y}\,k_t\,sin\,\psi$$

The unit vector $\boldsymbol{e}_{\parallel}$, parallel with the vector $\boldsymbol{k}_t$, becomes

$$\boldsymbol{e}_{\parallel} = \frac{\boldsymbol{k}_t}{k_t} = \boldsymbol{x}\,cos\,\psi + \boldsymbol{y}\,sin\,\psi$$

The unit vector normal to the interface, $\boldsymbol{z}$, and the unit tangential vector, $\boldsymbol{e}_{\parallel}$, forms a plane, i.e. the plane of incidence. The vector normal to this plane is given by, see Figure A.2

$$\boldsymbol{e}_{\perp} = -\boldsymbol{x}\,sin\,\psi + \boldsymbol{y}\,cos\,\psi = \overline{\overline{\mathbf{J}}}\cdot\boldsymbol{e}_{\parallel} = -\boldsymbol{e}_{\parallel}\cdot\overline{\overline{\mathbf{J}}}$$

where

$$\overline{\overline{\mathbf{J}}} = \boldsymbol{e}_y\boldsymbol{e}_x - \boldsymbol{e}_x\boldsymbol{e}_y = \boldsymbol{e}_{\perp}\boldsymbol{e}_{\parallel} - \boldsymbol{e}_{\parallel}\boldsymbol{e}_{\perp}$$

The position vector in the horizontal plane $= \boldsymbol{x}\,x + \boldsymbol{y}\,y$ is preferably represented in cylindrical coordinates

$$\rho = \boldsymbol{x}\,x + \boldsymbol{y}\,y = \boldsymbol{x}\rho\,cos\,\phi + \boldsymbol{y}\rho\,sin\,\phi$$

and has the following relationship to the tangential part of the wave vector

$$\boldsymbol{k}_t\cdot\rho = k_x x + k_y y = k_t\,\rho\,cos(\psi - \phi)$$

The introduction of the coordinate independent representation leads to that the tangential components of the vectors $\boldsymbol{E}(z)$ and $\boldsymbol{H}(z)$, i.e. the *x*-*y*-components, can be represented in the following two ways; in the base $(\boldsymbol{x}, \boldsymbol{y})$ and in the base $(\boldsymbol{e}_{\parallel}, \boldsymbol{e}_{\perp})$:

$$\begin{cases} \boldsymbol{E}_{xy}(z) = \boldsymbol{x}\, E_x(z) + \boldsymbol{y}\, E_y(z) = \boldsymbol{e}_\parallel\, E_\parallel(z) + \boldsymbol{e}_\perp\, E_\perp(z) \\ \boldsymbol{H}_{xy}(z) = \boldsymbol{x}\, H_x(z) + \boldsymbol{y}\, H_y(z) = \boldsymbol{e}_\parallel\, H_\parallel(z) + \boldsymbol{e}_\perp\, H_\perp(z) \end{cases}$$

We have now the tools to proceed with our analysis. The $\overline{\overline{\mathbf{J}}}$ dyadic that appeared in connection with the introduction of the cylindrical coordinate system, has the relationship $\boldsymbol{z} \times \boldsymbol{E}_{xy} = \overline{\overline{\mathbf{J}}} \cdot \boldsymbol{E}_{xy}$ and can thus be used to rewrite Eq. (A.7) and Eq. (A.8)

$$\begin{cases} \dfrac{d}{dz}\boldsymbol{E}_{xy}(z) = i\,\boldsymbol{k}_t\, E_z(z) - \dfrac{i\,\omega\mu}{c_0}\overline{\overline{\mathbf{J}}} \cdot \eta_0 \boldsymbol{H}_{xy}(z) \\ \dfrac{d}{dz}\eta_0 \boldsymbol{H}_{xy}(z) = i\,\boldsymbol{k}_t \eta_0\, H_z(z) + \dfrac{i\,\omega\varepsilon}{c_0}\overline{\overline{\mathbf{J}}} \cdot \boldsymbol{E}_{xy}(z) \end{cases} \tag{A.9}$$

$$\begin{cases} E_z(z) = \dfrac{c_0}{\omega\varepsilon\mu}\mu\, \boldsymbol{k}_t \cdot \overline{\overline{\mathbf{J}}} \cdot \eta_0 \boldsymbol{H}_{xy}(z) \\ \eta_0\, H_z(z) = -\dfrac{c_0}{\omega\varepsilon\mu}\varepsilon\, \boldsymbol{k}_t \cdot \overline{\overline{\mathbf{J}}} \cdot \boldsymbol{E}_{xy}(z) \end{cases} \tag{A.10}$$

We have here four unknowns and four equations. To get a solution we just have to merge the equations together. One way of attaining that is if the equations are restated in a matrix form.

$$\frac{d}{dz}\begin{pmatrix} \boldsymbol{E}_{xy}(z) \\ \eta_0 \boldsymbol{H}_{xy}(z) \end{pmatrix} = i\,\boldsymbol{k}_t \begin{pmatrix} E_z(z) \\ \eta_0\, H_z(z) \end{pmatrix} + \frac{i\,\omega}{c_0}\begin{pmatrix} \overline{\overline{\mathbf{0}}} & -\mu\overline{\overline{\mathbf{J}}} \\ \varepsilon\overline{\overline{\mathbf{J}}} & \overline{\overline{\mathbf{0}}} \end{pmatrix} \cdot \begin{pmatrix} \boldsymbol{E}_{xy}(z) \\ \eta_0 \boldsymbol{H}_{xy}(z) \end{pmatrix} \tag{A.11}$$

$$\begin{pmatrix} E_z(z) \\ \eta_0\, H_z(z) \end{pmatrix} = \frac{c_0}{\omega\varepsilon\mu}\boldsymbol{k}_t \cdot \begin{pmatrix} \overline{\overline{\mathbf{0}}} & \mu\overline{\overline{\mathbf{J}}} \\ -\varepsilon\overline{\overline{\mathbf{J}}} & \overline{\overline{\mathbf{0}}} \end{pmatrix} \cdot \begin{pmatrix} \boldsymbol{E}_{xy}(z) \\ \eta_0 \boldsymbol{H}_{xy}(z) \end{pmatrix} \tag{A.12}$$

By substituting Eq. (A.12) into Eq. (A.11) we obtain

$$\frac{d}{dz}\begin{pmatrix} \boldsymbol{E}_{xy}(z) \\ \eta_0 \boldsymbol{H}_{xy}(z) \end{pmatrix} = i\frac{c_0}{\omega\varepsilon\mu}\begin{pmatrix} \overline{\overline{\mathbf{0}}} & \mu\, \boldsymbol{k}_t\left(\boldsymbol{k}_t \cdot \overline{\overline{\mathbf{J}}}\right) \\ -\varepsilon\, \boldsymbol{k}_t\left(\boldsymbol{k}_t \cdot \overline{\overline{\mathbf{J}}}\right) & \overline{\overline{\mathbf{0}}} \end{pmatrix} \cdot \begin{pmatrix} \boldsymbol{E}_{xy}(z) \\ \eta_0 \boldsymbol{H}_{xy}(z) \end{pmatrix} + \frac{i\,\omega}{c_0}\begin{pmatrix} \overline{\overline{\mathbf{0}}} & -\mu\overline{\overline{\mathbf{J}}} \\ \varepsilon\overline{\overline{\mathbf{J}}} & \overline{\overline{\mathbf{0}}} \end{pmatrix} \cdot \begin{pmatrix} \boldsymbol{E}_{xy}(z) \\ \eta_0 \boldsymbol{H}_{xy}(z) \end{pmatrix}$$

which after some simplifications yields

$$\frac{d}{dz}\begin{pmatrix} \boldsymbol{E}_{xy}(z) \\ \eta_0 \boldsymbol{H}_{xy}(z) \end{pmatrix} = \frac{i\,\omega}{c_0}\begin{pmatrix} \overline{\overline{\mathbf{0}}} & \mu\dfrac{c_0^2}{\omega^2\varepsilon\mu}\boldsymbol{k}_t\left(\boldsymbol{k}_t \cdot \overline{\overline{\mathbf{J}}}\right) - \mu\overline{\overline{\mathbf{J}}} \\ -\varepsilon\dfrac{c_0^2}{\omega^2\varepsilon\mu}\boldsymbol{k}_t\left(\boldsymbol{k}_t \cdot \overline{\overline{\mathbf{J}}}\right) + \varepsilon\overline{\overline{\mathbf{J}}} & \overline{\overline{\mathbf{0}}} \end{pmatrix} \cdot \begin{pmatrix} \boldsymbol{E}_{xy}(z) \\ \eta_0 \boldsymbol{H}_{xy}(z) \end{pmatrix}$$

Since

$$\boldsymbol{k}_t\left(\boldsymbol{k}_t\cdot\overline{\overline{\mathbf{J}}}\right)=k_t\,\boldsymbol{e}_{\|}\left(k_t\,\boldsymbol{e}_{\|}\cdot\left(\boldsymbol{e}_{\perp}\boldsymbol{e}_{\|}-\boldsymbol{e}_{\|}\boldsymbol{e}_{\perp}\right)\right)=-k_t^2\,\boldsymbol{e}_{\|}\boldsymbol{e}_{\perp}$$

$$\tau=\frac{c_0^2k_t^2}{\omega^2\varepsilon\mu}=\frac{k_t^2}{k_0^2\,\varepsilon\mu},\qquad k_0=\frac{\omega}{c_0}$$

we finally achieve a system of first order differential equations

$$\frac{d}{dz}\begin{pmatrix}\boldsymbol{E}_{xy}(z)\\ \eta_0\boldsymbol{H}_{xy}(z)\end{pmatrix}=\frac{i\,\omega}{c_0}\begin{pmatrix}\overline{\overline{\mathbf{W}}}_1 & \overline{\overline{\mathbf{W}}}_2\\ \overline{\overline{\mathbf{W}}}_3 & \overline{\overline{\mathbf{W}}}_4\end{pmatrix}\cdot\begin{pmatrix}\boldsymbol{E}_{xy}(z)\\ \eta_0\boldsymbol{H}_{xy}(z)\end{pmatrix}\tag{A.13}$$

The four dyadics are

$$\begin{cases}\overline{\overline{\mathbf{W}}}_1=\overline{\overline{\mathbf{0}}}\\ \overline{\overline{\mathbf{W}}}_3=\varepsilon(-1+\tau)\boldsymbol{e}_{\|}\boldsymbol{e}_{\perp}+\varepsilon\,\boldsymbol{e}_{\perp}\boldsymbol{e}_{\|}\end{cases}\qquad\begin{cases}\overline{\overline{\mathbf{W}}}_2=\mu(1-\tau)\boldsymbol{e}_{\|}\boldsymbol{e}_{\perp}-\mu\,\boldsymbol{e}_{\perp}\boldsymbol{e}_{\|}\\ \overline{\overline{\mathbf{W}}}_4=\overline{\overline{\mathbf{0}}}\end{cases}$$

with the matrix representation

$$\left[\overline{\overline{\mathbf{W}}}_1\right]=\begin{pmatrix}0&0\\0&0\end{pmatrix}\qquad\left[\overline{\overline{\mathbf{W}}}_2\right]=\mu\begin{pmatrix}0&1-\tau\\-1&0\end{pmatrix}$$

$$\left[\overline{\overline{\mathbf{W}}}_3\right]=\varepsilon\begin{pmatrix}0&-1+\tau\\1&0\end{pmatrix}\qquad\left[\overline{\overline{\mathbf{W}}}_4\right]=\begin{pmatrix}0&0\\0&0\end{pmatrix}$$

The eigenvalues of the coefficient matrix in (A.13) decides which waves that can propagate in the isotropic material. The matrix has the double eigenvalues

$$\begin{cases}\ell_1=\ell_2=(\varepsilon\mu(1-\tau))^{1/2}=k_z/k_0\\ \ell_3=\ell_4=-(\varepsilon\mu(1-\tau))^{1/2}=k_z/k_0\end{cases}$$

The possible modes in the isotropic material are

$$\boldsymbol{E}_{xy}(z,\boldsymbol{k}_t,\omega)=\boldsymbol{E}_{xy}(\boldsymbol{k}_t,\omega)e^{\pm ik_zz}$$

where $\boldsymbol{E}_{xy}(\boldsymbol{k}_t,\omega)$ is an arbitrary vector in the *x*-*y*-plane and the wave constant for propagation in the *z*-direction is k_z — the longitudinal wave constant — defined as

$$k_z=k_0(\varepsilon\mu(1-\tau))^{1/2}=\left(k^2-k_t^2\right)^{1/2}\qquad k=\frac{\omega}{c_0}(\varepsilon\mu)^{1/2}$$

The solution of Eq. (A.13) reads

$$\begin{cases}\boldsymbol{E}_{xy}(z,\boldsymbol{k}_t,\omega)=\boldsymbol{E}_{xy}(\boldsymbol{k}_t,\omega)e^{\pm ik_zz}\\ \boldsymbol{H}_{xy}(z,\boldsymbol{k}_t,\omega)=\boldsymbol{H}_{xy}(\boldsymbol{k}_t,\omega)e^{\pm ik_zz}\end{cases}\tag{A.14}$$

We can also use Eq. (A.13) to express the vector $\boldsymbol{H}_{xy}(\boldsymbol{k}_t,\omega)$ in terms of the vector $\boldsymbol{E}_{xy}(\boldsymbol{k}_t,\omega)$

$$\eta_0 \boldsymbol{H}_{xy}(\boldsymbol{k}_t,\omega) = \pm\frac{\omega}{k_z c_0}\overline{\overline{\mathbf{W}}}_3 \cdot \boldsymbol{E}_{xy}(\boldsymbol{k}_t,\omega) = \pm\frac{\omega}{k_z c_0}\left(\varepsilon(-1+\tau)\boldsymbol{e}_{\|}\boldsymbol{e}_{\perp} + \varepsilon\,\boldsymbol{e}_{\perp}\boldsymbol{e}_{\|}\right)\cdot \boldsymbol{E}_{xy}(\boldsymbol{k}_t,\omega)$$
$$= \pm\frac{c_0}{\mu\omega k_z}\left(k^2\,\boldsymbol{e}_{\perp}\boldsymbol{e}_{\|} - k_z^2\,\boldsymbol{e}_{\|}\boldsymbol{e}_{\perp}\right)\cdot \boldsymbol{E}_{xy}(\boldsymbol{k}_t,\omega)$$

which in short notation gives

$$\begin{cases}\eta_0 \boldsymbol{H}_{xy}(\boldsymbol{k}_t,\omega) = \pm\overline{\overline{\mathbf{Y}}}\cdot \boldsymbol{E}_{xy}(\boldsymbol{k}_t,\omega)\\ \overline{\overline{\mathbf{Y}}} = \dfrac{c_0}{\mu\, k_z\,\omega}\left(k^2\,\boldsymbol{e}_{\perp}\boldsymbol{e}_{\|} - k_z^2\,\boldsymbol{e}_{\|}\boldsymbol{e}_{\perp}\right)\end{cases} \tag{A.15}$$

The sign in front of the dyadic admittance, $\overline{\overline{\mathbf{Y}}}$, + (-) indicates that the wave propagates in the positive (negative) *z*-direction.

A.2 Reflection and transmission at a plane dielectric boundary

Two isotropic materials are separated by a plane partition placed at $z = 0$, see Figure A.1. Region 1, $z < 0$, contains the sources and is characterized by the parameters ε_1 and μ_1 . The corresponding material parameters in region 2 are designated by ε_2 and μ_2 . The materials are not losless but we suppose that the material in region 1 has so small losses that the fields from the sources are able to propagate to the partition. We would now like to derive specific expressions for the reflected and the transmitted field when a plane wave propagates from region 1 to the plane dielectric boundary.
In the analysis it is assumed that the size of the partition is approximately infinite, i.e. no boundary conditions exist. This means that we can assume that it is possible to neglect diffraction effects and internal reflection.

A.2.1 Field solutions

The incident wave (in region 1) is described by a plane wave

$$\begin{cases}\boldsymbol{E}^i(\boldsymbol{r},\omega) = \boldsymbol{E}_0\, e^{i\boldsymbol{k}_1\cdot\boldsymbol{r}}\\ \boldsymbol{E}_0 = \boldsymbol{E}_{0\mathrm{xy}} + \boldsymbol{z}\,E_{0z}\end{cases} \qquad \begin{cases}\boldsymbol{E}_{0\mathrm{xy}} = \boldsymbol{e}_{\|}\,E_{0\|} + \boldsymbol{e}_{\perp}\,E_{0\perp}\\ \boldsymbol{k}_1 = \boldsymbol{k}_t\,k_t + \boldsymbol{z}\,k_{1z}\end{cases} \tag{A.16}$$

The relation between the tangential components of the electric and magnetic field and the incident vertical and horizontal polarized field (see Figure A.1) is

$$\begin{cases}E_{0\|} = E_{i\|}\cos\theta\\ E_{0\perp} = E_{i\perp}\end{cases} \qquad \begin{cases}H_{0\|} = H_{i\|}\cos\theta\\ H_{0\perp} = H_{i\perp}\end{cases} \tag{A.17}$$

Before we proceed with the calculations we transform the incident field, Eq. (A.16), which gives

$$\begin{cases} \boldsymbol{E}^i(z,\boldsymbol{k}_t,\omega) = \boldsymbol{E}^i_{xy}(\boldsymbol{k}_t,\omega)e^{ik_{1z}z} + \boldsymbol{z}\,E^i_z(\boldsymbol{k}_t,\omega)e^{ik_{1z}z} \\ \boldsymbol{E}^i_{xy}(\boldsymbol{k}_t,\omega) = 4\pi^2\,\boldsymbol{E}_{0\mathrm{xy}}\delta(\boldsymbol{k}_t - \boldsymbol{k}'_t) \\ E^i_z(\boldsymbol{k}_t,\omega) = 4\pi^2\,E_{0z}\,\delta(\boldsymbol{k}_t - \boldsymbol{k}'_t) \end{cases} \tag{A.18}$$

We use Eq. (A.15) to get the magnetic field

$$\begin{cases} \eta_0\boldsymbol{H}^i_{xy}(\boldsymbol{k}_t,\omega) = \overline{\overline{\mathbf{Y}}}_1 \cdot \boldsymbol{E}^i_{xy}(\boldsymbol{k}_t,\omega) \\ \overline{\overline{\mathbf{Y}}}_1 = \dfrac{c_0}{\mu_1\,k_{1z}\,\omega}\left(k_1^2\,\boldsymbol{e}_\perp\boldsymbol{e}_\parallel - k_{1z}^2\,\boldsymbol{e}_\parallel\boldsymbol{e}_\perp\right) \end{cases} \tag{A.19}$$

The presence of the partition causes a reflected field $\boldsymbol{E}^r$ and a transmitted field $\boldsymbol{E}^t$. These fields are:

$$\boldsymbol{E}^r(z,\boldsymbol{k}_t,\omega) = \boldsymbol{E}^r_{xy}(\boldsymbol{k}_t,\omega)e^{-ik_{1z}z} + \boldsymbol{z}\,E^r_z(\boldsymbol{k}_t,\omega)e^{-ik_{1z}z} \tag{A.20}$$

$$\boldsymbol{E}^t(z,\boldsymbol{k}_t,\omega) = \boldsymbol{E}^t_{xy}(\boldsymbol{k}_t,\omega)e^{ik_{2z}z} + \boldsymbol{z}\,E^t_z(\boldsymbol{k}_t,\omega)e^{ik_{2z}z} \tag{A.21}$$

The corresponding magnetic fields are give by

$$\begin{cases} \eta_0 H^{\mathrm{r}}_{\mathrm{xy}}(k_{\mathrm{t}},\omega) = -\overline{\overline{\mathbf{Y}}}_1 \cdot E^{\mathrm{r}}_{\mathrm{xy}}(k_{\mathrm{t}},\omega) \\ \overline{\overline{\mathbf{Y}}}_1 = \dfrac{\mathrm{c}_0}{\mu_1\,\mathrm{k}_{1\mathrm{z}}\,\omega}\left(\mathrm{k}_1^2\,e_\perp e_\parallel - \mathrm{k}_{1\mathrm{z}}^2\,e_\parallel e_\perp\right) \end{cases} \tag{A.22}$$

$$\begin{cases} \eta_0 H^{\mathrm{t}}_{\mathrm{xy}}(k_{\mathrm{t}},\omega) = \overline{\overline{\mathbf{Y}}}_2 \cdot E^{\mathrm{t}}_{\mathrm{xy}}(k_{\mathrm{t}},\omega) \\ \overline{\overline{\mathbf{Y}}}_2 = \dfrac{\mathrm{c}_0}{\mu_2\,\mathrm{k}_{2\mathrm{z}}\,\omega}\left(\mathrm{k}_2^2\,e_\perp e_\parallel - \mathrm{k}_{2\mathrm{z}}^2\,e_\parallel e_\perp\right) \end{cases} \tag{A.23}$$

Thus can the total field in the respective region be written as

$$\begin{cases} E_1(k_{\mathrm{t}},\omega) = E^{\mathrm{i}}(k_{\mathrm{t}},\omega) + E^{\mathrm{r}}(k_{\mathrm{t}},\omega) \\ E_2(k_{\mathrm{t}},\omega) = E^{\mathrm{t}}(k_{\mathrm{t}},\omega) \end{cases} \qquad \begin{cases} H_1(k_{\mathrm{t}},\omega) = H^{\mathrm{i}}(k_{\mathrm{t}},\omega) + H^{\mathrm{r}}(k_{\mathrm{t}},\omega) \\ H_2(k_{\mathrm{t}},\omega) = H^{\mathrm{t}}(k_{\mathrm{t}},\omega) \end{cases}$$

Continuity requirements for the tangential components of the electric and magnetic fields across the partition gives the following equation system for the Fourier components of the fields at the partition $z = 0$

$$\begin{cases} E^i_{xy}(k_t,\omega) + E^r_{xy}(k_t,\omega) = E^t_{xy}(k_t,\omega) \\ \overline{\overline{\mathbf{Y}}}_1 \cdot E^i_{xy}(k_t,\omega) - \overline{\overline{\mathbf{Y}}}_1 \cdot E^r_{xy}(k_t,\omega) = \overline{\overline{\mathbf{Y}}}_2 \cdot E^t_{xy}(k_t,\omega) \end{cases}$$

with the solution

$$\begin{cases} \boldsymbol{E}_{xy}^{r}(\boldsymbol{k}_t,\omega) = \overline{\overline{\mathbf{r}}}(k_t,\omega)\cdot \boldsymbol{E}_{xy}^{i}(\boldsymbol{k}_t,\omega) \\ \boldsymbol{E}_{xy}^{t}(\boldsymbol{k}_t,\omega) = \overline{\overline{\mathbf{t}}}(k_t,\omega)\cdot \boldsymbol{E}_{xy}^{i}(\boldsymbol{k}_t,\omega) \end{cases} \tag{A.24}$$

where the reflection and transmission dyadics are given by

$$\begin{cases} \overline{\overline{\mathbf{r}}} = \left(\overline{\overline{\mathbf{Y}}}_1 + \overline{\overline{\mathbf{Y}}}_2\right)^{-1}\cdot\left(\overline{\overline{\mathbf{Y}}}_1 - \overline{\overline{\mathbf{Y}}}_2\right) \\ \overline{\overline{\mathbf{t}}} = \overline{\overline{\mathbf{r}}} + \overline{\overline{\mathbf{I}}} \end{cases} \tag{A.25}$$

The form of the dyadic expressions is

$$\begin{aligned} \overline{\overline{\mathbf{r}}} &= \left(a\,\boldsymbol{e}_\perp\boldsymbol{e}_\parallel + b\,\boldsymbol{e}_\parallel\boldsymbol{e}_\perp\right)^{-1}\cdot\left(c\,\boldsymbol{e}_\perp\boldsymbol{e}_\parallel + d\,\boldsymbol{e}_\parallel\boldsymbol{e}_\perp\right) \\ &= \left(\frac{1}{b}\boldsymbol{e}_\perp\boldsymbol{e}_\parallel + \frac{1}{a}\boldsymbol{e}_\parallel\boldsymbol{e}_\perp\right)\cdot\left(c\,\boldsymbol{e}_\perp\boldsymbol{e}_\parallel + d\,\boldsymbol{e}_\parallel\boldsymbol{e}_\perp\right) = \frac{c}{a}\boldsymbol{e}_\parallel\boldsymbol{e}_\parallel + \frac{d}{b}\boldsymbol{e}_\perp\boldsymbol{e}_\perp \end{aligned} \tag{A.26}$$

which means that they are diagonal in the base $\{\boldsymbol{e}_\parallel, \boldsymbol{e}_\perp\}$. The inverted expression is simplified in the same way as an ordinary matrix (use Cramer s rule). With help of Eq. (A.26) it is easy to understand that Eq. (A.25) can be represented in the form

$$\begin{cases} \overline{\overline{\mathbf{r}}} = r_\parallel\,\boldsymbol{e}_\parallel\boldsymbol{e}_\parallel + r_\perp\,\boldsymbol{e}_\perp\boldsymbol{e}_\perp \\ \overline{\overline{\mathbf{t}}} = t_\parallel\,\boldsymbol{e}_\parallel\boldsymbol{e}_\parallel + t_\perp\,\boldsymbol{e}_\perp\boldsymbol{e}_\perp \end{cases} \tag{A.27}$$

where

$$\begin{cases} r_\parallel = \dfrac{1-p_\parallel}{1+p_\parallel} \\ r_\perp = \dfrac{1-p_\perp}{1+p_\perp} \end{cases} \qquad \begin{cases} t_\parallel = \dfrac{2}{1+p_\parallel} \\ t_\perp = \dfrac{2}{1+p_\perp} \end{cases} \qquad \begin{cases} p_\parallel = \dfrac{\varepsilon_2\,k_{1z}}{\varepsilon_1\,k_{2z}} \\ p_\perp = \dfrac{\mu_1\,k_{2z}}{\mu_2\,k_{1z}} \end{cases}$$

The explicit expressions for the reflection and transmission coefficients[8] are

$$\begin{cases} r_\parallel = \dfrac{\varepsilon_1\,k_{2z} - \varepsilon_2\,k_{1z}}{\varepsilon_1\,k_{2z} + \varepsilon_2\,k_{1z}} \\ r_\perp = -\dfrac{\mu_1\,k_{2z} - \mu_2\,k_{1z}}{\mu_1\,k_{2z} + \mu_2\,k_{1z}} \end{cases} \qquad \begin{cases} t_\parallel = \dfrac{2\varepsilon_1\,k_{2z}}{\varepsilon_1\,k_{2z} + \varepsilon_2\,k_{1z}} \\ t_\perp = \dfrac{2\mu_2\,k_{1z}}{\mu_1\,k_{2z} + \mu_2\,k_{1z}} \end{cases} \tag{A.28}$$

The reflected electric field $\boldsymbol{E}^r(z,\boldsymbol{k}_t,\omega)$ can be calculated if we use Eq. (A.10), Eq. (A.20), Eq. (A.22) and Eq. (A.24)

[8] These are sometimes referred to as Fresnel s equations.

$$\begin{cases} \boldsymbol{E}^r(z,\boldsymbol{k}_t,\omega) = \left\{\boldsymbol{E}_{xy}^r(\boldsymbol{k}_t,\omega) + \boldsymbol{z}\, E_z^r(\boldsymbol{k}_t,\omega)\right\} e^{-ik_{1z}z} \\ \boldsymbol{E}_{xy}^r(\boldsymbol{k}_t,\omega) = \overline{\overline{\mathbf{r}}}(k_t,\omega)\cdot \boldsymbol{E}_{xy}^i(\boldsymbol{k}_t,\omega) \end{cases} \qquad \begin{cases} E_z^r(\boldsymbol{k}_t,\omega) = \dfrac{c_0}{\omega\varepsilon_1}\boldsymbol{k}_t \cdot \overline{\overline{\mathbf{J}}} \cdot \eta_0 \boldsymbol{H}_{xy}^r(\boldsymbol{k}_t,\omega) \\ \eta_0 \boldsymbol{H}_{xy}^r(\boldsymbol{k}_t,\omega) = -\overline{\overline{\mathbf{Y}_1}} \cdot \boldsymbol{E}_{xy}^r(\boldsymbol{k}_t,\omega) \end{cases}$$

which after substitution gives

$$\boldsymbol{E}^r(z,\boldsymbol{k}_t,\omega) = \left\{\overline{\overline{\mathbf{I}}} - \boldsymbol{z}\frac{c_0}{\omega\varepsilon_1}\boldsymbol{k}_t \cdot \overline{\overline{\mathbf{J}}} \cdot \overline{\overline{\mathbf{Y}_1}}\right\} \cdot \overline{\overline{\mathbf{r}}} \cdot \boldsymbol{E}_{xy}^i(\boldsymbol{k}_t,\omega) e^{-ik_{1z}z} \tag{A.29}$$

To obtain a final expression for the reflected wave the inverse transform of Eq. (A.29) is calculated. After some simplifications we get

$$\boldsymbol{E}^r(\boldsymbol{r},\omega) = \left\{\overline{\overline{\mathbf{I}}} + \boldsymbol{z}\frac{1}{k_{1z}}\boldsymbol{k}_t\right\} \cdot \overline{\overline{\mathbf{r}}}(k_t,\omega)\cdot \boldsymbol{E}_0\, e^{i\boldsymbol{k}_t\cdot\rho - ik_{1z}z} \tag{A.30}$$

In a similar way the transmitted field can be calculated and the result is

$$\boldsymbol{E}^t(\boldsymbol{r},\omega) = \left\{\overline{\overline{\mathbf{I}}} - \boldsymbol{z}\frac{1}{k_{2z}}\boldsymbol{k}_t\right\} \cdot \overline{\overline{\mathbf{t}}}(k_t,\omega)\cdot \boldsymbol{E}_0\, e^{i\boldsymbol{k}_2\cdot\boldsymbol{r}} \tag{A.31}$$

The reflected and transmitted fields can also be written in the form

$$\begin{cases} \boldsymbol{E}^r(\boldsymbol{r},\omega) = \left\{E_\parallel^r\, \boldsymbol{e}_\parallel + E_\perp^r\, \boldsymbol{e}_\perp + E_z^r\, \boldsymbol{z}\right\} e^{i\boldsymbol{k}_t\cdot\rho - ik_{1z}z} \\ \boldsymbol{E}^t(\boldsymbol{r},\omega) = \left\{E_\parallel^t\, \boldsymbol{e}_\parallel + E_\perp^t\, \boldsymbol{e}_\perp + E_z^t\, \boldsymbol{z}\right\} e^{i\boldsymbol{k}_2\cdot\boldsymbol{r}} \end{cases} \tag{A.32}$$

where the components are

$$\begin{cases} E_\parallel^r = r_\parallel E_{0\parallel} = r_\parallel E_{i\parallel}\, cos\theta \\ E_\perp^r = r_\perp E_{0\perp} = r_\perp E_{i\perp} \\ E_z^r = \dfrac{k_t}{k_{1z}} r_\parallel E_{0\parallel} = r_\parallel E_{i\parallel}\, sin\theta \end{cases} \qquad \begin{cases} E_\parallel^t = t_\parallel E_{0\parallel} = t_\parallel E_{i\parallel}\, cos\theta \\ E_\perp^t = t_\perp E_{0\perp} = t_\perp E_{i\perp} \\ E_z^t = -\dfrac{k_t}{k_{2z}} t_\parallel E_{0\parallel} = -t_\parallel E_{i\parallel}\, cos\theta\, tan\theta_t \end{cases}$$

A.3 Reflection and transmission at multiple dielectric interfaces

In the case of wave propagation in a homogeneous slab with a finite thickness d, the analysis becomes analogues to the one that was made in section A.1. The geometry is shown in Figure A.3. The area of interest is divided into three isotropic regions. The first partition is placed at $z = 0$ and the second at $z = d$. Region 1, $z < 0$, contains the sources and is characterized by the parameters ε_1 and μ_1. The corresponding material parameters in region 2, $0 < z < d$, and region 3, $z > d$, are denoted by ε_2, μ_2 and ε_3, μ_3. There are no demands that the materials have to be lossless but we suppose, as before, that region 1 has so small losses that the field from the sources can propagate to the partition. We would now like to derive expressions for the reflected and the transmitted fields when the incident wave is a plane wave. It is also interesting to get an analytical expression for the internal fields in region 2. In the analysis of the wave propagation in a slab we have assumed that the cross-section of the slab is infinite, i.e. no boundary conditions exists. If that was not the case we would have to take into consideration that internal reflections not only were caused by the two partitions but also at the other surfaces around region 2 where also transmission would occur. Diffraction effects have also been neglected.

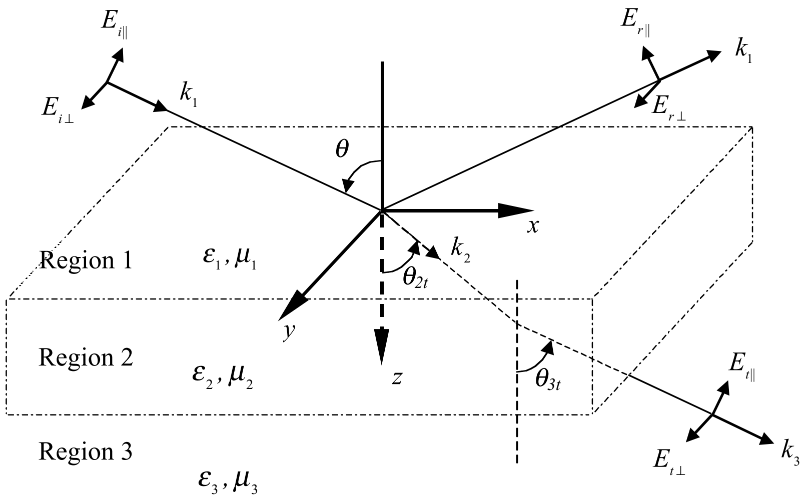

Figure A.3: Geometry for the reflection and transmission at a slab.

A.3.1 Field solutions

The incident wave (in region 1) is represented by a plane wave

$$\begin{cases} \boldsymbol{E}^i(\boldsymbol{r},\omega) = \boldsymbol{E}_0\, e^{i\boldsymbol{k}_1\cdot\boldsymbol{r}} \\ \boldsymbol{E}_0 = \boldsymbol{e}_\| \,E_{0\|} + \boldsymbol{e}_\perp \,E_{0\perp} + \boldsymbol{z}\, E_{0z} \\ \boldsymbol{k}_1 = \boldsymbol{k}_t \,k_t + \boldsymbol{z}\, k_{1z} \end{cases} \tag{A.33}$$

In region 1 the fields are, as before, represented by a sum of an incident and a reflected field. Furthermore the fields are separated into one transversal and one longitudinal part.

$$\begin{cases} \boldsymbol{E}_1(\boldsymbol{r},\omega) = \boldsymbol{E}^i(\boldsymbol{r},\omega) + \boldsymbol{E}^r(\boldsymbol{r},\omega) \\ \boldsymbol{E}^i(\boldsymbol{r},\omega) = \boldsymbol{E}^i_{xy}(\boldsymbol{r},\omega) + \boldsymbol{z}\, E^i_z(\boldsymbol{r},\omega) = \left\{\boldsymbol{E}^i_{xy}(\ ,\omega) + \boldsymbol{z}\, E^i_z(\ ,\omega)\right\} e^{ik_{1z}z} \\ \boldsymbol{E}^r(\boldsymbol{r},\omega) = \boldsymbol{E}^r_{xy}(\boldsymbol{r},\omega) + \boldsymbol{z}\, E^r_z(\boldsymbol{r},\omega) = \left\{\boldsymbol{E}^r_{xy}(\ ,\omega) + \boldsymbol{z}\, E^r_z(\ ,\omega)\right\} e^{-ik_{1z}z} \end{cases} \tag{A.34}$$

In section A.1 it was shown that a way of solving Maxwell s equations (see Eq. (A.1)) was to transform all components — except the z-component. Equation (A.34) is then rewritten as

$$\begin{cases} \boldsymbol{E}_1(z,\boldsymbol{k}_t,\omega) = \boldsymbol{E}^i(z,\boldsymbol{k}_t,\omega) + \boldsymbol{E}^r(z,\boldsymbol{k}_t,\omega) \\ \boldsymbol{E}^i(z,\boldsymbol{k}_t,\omega) = \boldsymbol{E}^i_{xy}(z,\boldsymbol{k}_t,\omega) + \boldsymbol{z}\,E^i_z(z,\boldsymbol{k}_t,\omega) = \left\{\boldsymbol{E}^i_{xy}(\boldsymbol{k}_t,\omega) + \boldsymbol{z}\,E^i_z(\boldsymbol{k}_t,\omega)\right\}e^{ik_{1z}z} \\ \boldsymbol{E}^r(z,\boldsymbol{k}_t,\omega) = \boldsymbol{E}^r_{xy}(z,\boldsymbol{k}_t,\omega) + \boldsymbol{z}\,E^r_z(z,\boldsymbol{k}_t,\omega) = \left\{\boldsymbol{E}^r_{xy}(\boldsymbol{k}_t,\omega) + \boldsymbol{z}\,E^r_z(\boldsymbol{k}_t,\omega)\right\}e^{-ik_{1z}z} \end{cases} \quad \text{(A.35)}$$

The corresponding components of the magnetic field are, see Eq. (A.15)

$$\begin{cases} \eta_0 \boldsymbol{H}^i_{xy}(\boldsymbol{k}_t,\omega) = \overline{\overline{\mathbf{Y}}}_1 \cdot \boldsymbol{E}^i_{xy}(\boldsymbol{k}_t,\omega) \\ \eta_0 \boldsymbol{H}^r_{xy}(\boldsymbol{k}_t,\omega) = -\overline{\overline{\mathbf{Y}}}_1 \cdot \boldsymbol{E}^r_{xy}(\boldsymbol{k}_t,\omega) \end{cases} \quad \text{(A.36)}$$

where the dyadic admittance is

$$\overline{\overline{\mathbf{Y}}}_1 = \frac{c_0}{\mu_1\, k_{1z}\, \omega}\left(k_1^2\, \boldsymbol{e}_\perp \boldsymbol{e}_\parallel - k_{1z}^2\, \boldsymbol{e}_\parallel \boldsymbol{e}_\perp\right)$$

The field in region 2 contains two parts; one part that propagates in the positive *z*-direction and one part that propagates in the negative *z*-direction

$$\begin{cases} \boldsymbol{E}_2(z,\boldsymbol{k}_t,\omega) = \boldsymbol{E}^+(z,\boldsymbol{k}_t,\omega) + \boldsymbol{E}^-(z,\boldsymbol{k}_t,\omega) \\ \boldsymbol{E}^+(z,\boldsymbol{k}_t,\omega) = \boldsymbol{E}^+_{xy}(z,\boldsymbol{k}_t,\omega) + \boldsymbol{z}\,E^+_z(z,\boldsymbol{k}_t,\omega) = \left\{\boldsymbol{E}^+_{xy}(\boldsymbol{k}_t,\omega) + \boldsymbol{z}\,E^+_z(\boldsymbol{k}_t,\omega)\right\}e^{ik_{2z}z} \\ \boldsymbol{E}^-(z,\boldsymbol{k}_t,\omega) = \boldsymbol{E}^-_{xy}(z,\boldsymbol{k}_t,\omega) + \boldsymbol{z}\,E^-_z(z,\boldsymbol{k}_t,\omega) = \left\{\boldsymbol{E}^-_{xy}(\boldsymbol{k}_t,\omega) + \boldsymbol{z}\,E^-_z(\boldsymbol{k}_t,\omega)\right\}e^{-ik_{2z}z} \end{cases} \quad \text{(A.37)}$$

This is caused by the second partition at $z = d$ which causes the reflections (see Figure A.3). The components of the magnetic field are

$$\begin{cases} \eta_0 \boldsymbol{H}^\pm_{xy}(\boldsymbol{k}_t,\omega) = \pm\overline{\overline{\mathbf{Y}}}_2 \cdot \boldsymbol{E}^\pm_{xy}(\boldsymbol{k}_t,\omega) \\ \overline{\overline{\mathbf{Y}}}_2 = \dfrac{c_0}{\mu_2\, k_{2z}\, \omega}\left(k_2^2\, \boldsymbol{e}_\perp \boldsymbol{e}_\parallel - k_{2z}^2\, \boldsymbol{e}_\parallel \boldsymbol{e}_\perp\right) \end{cases} \quad \text{(A.38)}$$

The electric field in region 3 can be described as a transmitted field, $\boldsymbol{E}^t$, that propagates in the positive *z*-direction.

$$\boldsymbol{E}_3(z,\boldsymbol{k}_t,\omega) = \boldsymbol{E}^t(z,\boldsymbol{k}_t,\omega) = \left\{\boldsymbol{E}^t_{xy}(\boldsymbol{k}_t,\omega) + \boldsymbol{z}\,E^t_z(\boldsymbol{k}_t,\omega)\right\}e^{ik_{3z}z} \quad \text{(A.39)}$$

The corresponding components of the magnetic field are

$$\begin{cases} \eta_0 \boldsymbol{H}^t_{xy}(\boldsymbol{k}_t,\omega) = \overline{\overline{\mathbf{Y}}}_3 \cdot \boldsymbol{E}^t_{xy}(\boldsymbol{k}_t,\omega) \\ \overline{\overline{\mathbf{Y}}}_3 = \dfrac{c_0}{\mu_3\, k_{3z}\, \omega}\left(k_3^2\, \boldsymbol{e}_\perp \boldsymbol{e}_\parallel - k_{3z}^2\, \boldsymbol{e}_\parallel \boldsymbol{e}_\perp\right) \end{cases} \quad \text{(A.40)}$$

The continuity of the tangential components of the electric and magnetic fields across the partitions at $z = 0$ and $z = d$ gives the following equation system

$$\begin{cases} \boldsymbol{E}_{xy}^{i} + \boldsymbol{E}_{xy}^{r} = \boldsymbol{E}_{xy}^{+} + \boldsymbol{E}_{xy}^{-} \\ \overline{\overline{\mathbf{Y}}}_1 \cdot \left(\boldsymbol{E}_{xy}^{i} - \boldsymbol{E}_{xy}^{r}\right) = \overline{\overline{\mathbf{Y}}}_2 \cdot \left(\boldsymbol{E}_{xy}^{+} - \boldsymbol{E}_{xy}^{-}\right) \\ \boldsymbol{E}_{xy}^{+} e^{ik_{2z}d} + \boldsymbol{E}_{xy}^{-} e^{-ik_{2z}d} = \boldsymbol{E}_{xy}^{t} e^{ik_{3z}d} \\ \overline{\overline{\mathbf{Y}}}_2 \cdot \left(\boldsymbol{E}_{xy}^{+} e^{ik_{2z}d} + \boldsymbol{E}_{xy}^{-} e^{-ik_{2z}d}\right) = \overline{\overline{\mathbf{Y}}}_3 \cdot \boldsymbol{E}_{xy}^{t} e^{ik_{3z}d} \end{cases}$$

The fields in region 2, $\boldsymbol{E}_{xy}^{\pm}$, are eliminated from the equations which gives the possibility to express the reflected and the transmitted fields in terms of the incident electric field

$$\begin{cases} \boldsymbol{E}_{xy}^{r}(\boldsymbol{k}_t,\omega) = \overline{\overline{\mathbf{r}}}(k_t,\omega)\cdot \boldsymbol{E}_{xy}^{i}(\boldsymbol{k}_t,\omega) \\ \boldsymbol{E}_{xy}^{t}(\boldsymbol{k}_t,\omega) = \overline{\overline{\mathbf{t}}}(k_t,\omega)\cdot \boldsymbol{E}_{xy}^{i}(\boldsymbol{k}_t,\omega) \end{cases} \tag{A.41}$$

The reflection and transmission dyadics are given by

$$\begin{cases} \overline{\overline{\mathbf{r}}} = \left\{\overline{\overline{\mathbf{I}}} + \left(\overline{\overline{\mathbf{a}}}\right)^{-1} \cdot \overline{\overline{\mathbf{r}}}_d \cdot \overline{\overline{\mathbf{a}}} \cdot \overline{\overline{\mathbf{r}}}_0 e^{2ik_{2z}d}\right\}^{-1} \cdot \left\{\overline{\overline{\mathbf{r}}}_0 + \left(\overline{\overline{\mathbf{a}}}\right)^{-1} \cdot \overline{\overline{\mathbf{r}}}_d \cdot \overline{\overline{\mathbf{a}}} e^{2ik_{2z}d}\right\} \\ \overline{\overline{\mathbf{t}}} = \left(\overline{\overline{\mathbf{Y}}}_2 + \overline{\overline{\mathbf{Y}}}_3\right)^{-1} \cdot \left\{\overline{\overline{\mathbf{Y}}}_1 + \overline{\overline{\mathbf{Y}}}_2 - \left(\overline{\overline{\mathbf{Y}}}_1 - \overline{\overline{\mathbf{Y}}}_2\right)\overline{\overline{\mathbf{r}}}\right\} e^{i(k_{2z}-k_{3z})d} \end{cases} \tag{A.42}$$

where

$$\overline{\overline{\mathbf{a}}} = \left(\overline{\overline{\mathbf{Y}}}_2\right)^{-1} \cdot \left(\overline{\overline{\mathbf{Y}}}_1 + \overline{\overline{\mathbf{Y}}}_2\right)$$

and the reflection and transmission dyadics of the separated partitions at $z = 0$ and $z = d$ are given by

$$\begin{cases} \overline{\overline{\mathbf{r}}}_0 = \left(\overline{\overline{\mathbf{Y}}}_1 + \overline{\overline{\mathbf{Y}}}_2\right)^{-1} \cdot \left(\overline{\overline{\mathbf{Y}}}_1 - \overline{\overline{\mathbf{Y}}}_2\right) \\ \overline{\overline{\mathbf{t}}}_0 = \overline{\overline{\mathbf{r}}}_0 + \overline{\overline{\mathbf{I}}} \end{cases} \tag{A.43}$$

and

$$\begin{cases} \overline{\overline{\mathbf{r}}}_d = \left(\overline{\overline{\mathbf{Y}}}_2 + \overline{\overline{\mathbf{Y}}}_3\right)^{-1} \cdot \left(\overline{\overline{\mathbf{Y}}}_2 - \overline{\overline{\mathbf{Y}}}_3\right) \\ \overline{\overline{\mathbf{t}}}_d = \overline{\overline{\mathbf{r}}}_d + \overline{\overline{\mathbf{I}}} \end{cases} \tag{A.44}$$

With the coordinate representations of $\overline{\overline{\mathbf{r}}}_0$ and $\overline{\overline{\mathbf{r}}}_d$ from section A.1 and the coordinate representations of $\overline{\overline{\mathbf{Y}}}_1$ and $\overline{\overline{\mathbf{Y}}}_2$ the reflection and transmission dyadic $\overline{\overline{\mathbf{r}}}$ and $\overline{\overline{\mathbf{t}}}$ in Eq. (A.42) will get the following representation in the $\{\boldsymbol{e}_\parallel, \boldsymbol{e}_\perp\}$ system:

$$\begin{cases} \overline{\overline{\mathbf{r}}} = r_{\|}\, \boldsymbol{e}_{\|}\boldsymbol{e}_{\|} + r_{\perp}\, \boldsymbol{e}_{\perp}\boldsymbol{e}_{\perp} \\ \overline{\overline{\mathbf{t}}} = t_{\|}\, \boldsymbol{e}_{\|}\boldsymbol{e}_{\|} + t_{\perp}\, \boldsymbol{e}_{\perp}\boldsymbol{e}_{\perp} \end{cases} \tag{A.45}$$

where the explicit expressions for $r_{\|}, r_{\perp}, t_{\|}$ and $t_{\perp}$ are given by

$$\begin{cases} r_{\|} = \dfrac{r_{0\|} + r_{d\|} e^{2ik_{2z}d}}{1 + r_{0\|} r_{d\|} e^{2ik_{2z}d}} \\ r_{\perp} = \dfrac{r_{0\perp} + r_{d\perp} e^{2ik_{2z}d}}{1 + r_{0\perp} r_{d\perp} e^{2ik_{2z}d}} \end{cases} \qquad \begin{cases} t_{\|} = \dfrac{(1 + r_{0\|})(1 + r_{d\|}) e^{i(k_{2z} - k_{3z})d}}{1 + r_{0\|} r_{d\|} e^{2ik_{2z}d}} \\ t_{\perp} = \dfrac{(1 + r_{0\perp})(1 + r_{d\perp}) e^{i(k_{2z} - k_{3z})d}}{1 + r_{0\perp} r_{d\perp} e^{2ik_{2z}d}} \end{cases}$$

The reflection coefficients for the respective partition $z = 0, d$ are given by

$$\begin{cases} r_{0\|} = \dfrac{1 - p_{0\|}}{1 + p_{0\|}} \\ r_{0\perp} = \dfrac{1 - p_{0\perp}}{1 + p_{0\perp}} \end{cases} \qquad \begin{cases} r_{d\|} = \dfrac{1 - p_{d\|}}{1 + p_{d\|}} \\ r_{d\perp} = \dfrac{1 - p_{d\perp}}{1 + p_{d\perp}} \end{cases}$$

and

$$\begin{cases} p_{0\|} = \dfrac{\varepsilon_2\, k_{1z}}{\varepsilon_1\, k_{2z}} \\ p_{0\perp} = \dfrac{\mu_1\, k_{2z}}{\mu_2\, k_{1z}} \end{cases} \qquad \begin{cases} p_{d\|} = \dfrac{\varepsilon_3\, k_{2z}}{\varepsilon_2\, k_{3z}} \\ p_{d\perp} = \dfrac{\mu_2\, k_{3z}}{\mu_3\, k_{2z}} \end{cases}$$

We have now the necessary tools to calculate the different fields. We use the same principles as in section A.2 to calculate the reflected electric field, $\boldsymbol{E}^r(z, \boldsymbol{k}_t, \omega)$. After substituting Eq. (A.10), Eq. (A.36) and Eq. (A.41) into Eq. (A.35) we get

$$\boldsymbol{E}^r(z, \boldsymbol{k}_t, \omega) = \left\{ \overline{\overline{\mathbf{I}}} - \boldsymbol{z} \frac{c_0}{\omega \varepsilon_1} \boldsymbol{k}_t \cdot \overline{\overline{\mathbf{J}}} \cdot \overline{\overline{\mathbf{Y}}}_1 \right\} \cdot \overline{\overline{\mathbf{r}}} \cdot \boldsymbol{E}^i_{xy}(\boldsymbol{k}_t, \omega) e^{-ik_{1z}z} \tag{A.46}$$

Eq. (A.46) is identical to the reflected field derived in section A.2, see Eq. (A.29). In the same way as before we calculate the inverse transform of Eq. (A.46) to get the expression for the reflected electric field with the spatial variables as input arguments. After some simplifications we find

$$\boldsymbol{E}^r(\boldsymbol{r}, \omega) = \left\{ \overline{\overline{\mathbf{I}}} + \boldsymbol{z} \frac{1}{k_{1z}} \boldsymbol{k}_t \right\} \cdot \overline{\overline{\mathbf{r}}}(k_t, \omega) \cdot \boldsymbol{E}_0\, e^{i\boldsymbol{k}_t \cdot \rho - ik_{1z}z} \tag{A.47}$$

In a similar way can the transmitted field be calculated and the result is

$$\boldsymbol{E}^t(\boldsymbol{r},\omega)=\left\{\bar{\bar{\mathbf{I}}}-\boldsymbol{z}\frac{1}{k_{3z}}\boldsymbol{k}_t\right\}\cdot\bar{\bar{\mathbf{t}}}(k_t,\omega)\cdot\boldsymbol{E}_0\,e^{i\boldsymbol{k}_3\cdot\boldsymbol{r}} \tag{A.48}$$

It is also possible to derive expressions for the internal fields. These are

$$\begin{cases}\boldsymbol{E}^+(\boldsymbol{r},\omega)=\left\{\bar{\bar{\mathbf{I}}}-\boldsymbol{z}\frac{1}{k_{2z}}\boldsymbol{k}_t\right\}\cdot\boldsymbol{E}_{xy}^+\,e^{ik_{2z}z}e^{i\boldsymbol{k}_t\cdot\rho}\\ \boldsymbol{E}^-(\boldsymbol{r},\omega)=\left\{\bar{\bar{\mathbf{I}}}+\boldsymbol{z}\frac{1}{k_{2z}}\boldsymbol{k}_t\right\}\cdot\boldsymbol{E}_{xy}^-\,e^{-ik_{2z}z}e^{i\boldsymbol{k}_t\cdot\rho}\end{cases} \tag{A.49}$$

The transversal vectorial amplitudes are defined as

$$\begin{cases}\boldsymbol{E}_{xy}^+=E_{\parallel}^+\,\boldsymbol{e}_{\parallel}+E_{\perp}^+\,\boldsymbol{e}_{\perp}=\left(e_{\parallel}^+\,\boldsymbol{e}_{\parallel}\boldsymbol{e}_{\parallel}+e_{\perp}^+\,\boldsymbol{e}_{\perp}\boldsymbol{e}_{\perp}\right)\cdot\boldsymbol{E}_0\\ \boldsymbol{E}_{xy}^-=E_{\parallel}^-\,\boldsymbol{e}_{\parallel}+E_{\perp}^-\,\boldsymbol{e}_{\perp}=\left(e_{\parallel}^-\,\boldsymbol{e}_{\parallel}\boldsymbol{e}_{\parallel}+e_{\perp}^-\,\boldsymbol{e}_{\perp}\boldsymbol{e}_{\perp}\right)\cdot\boldsymbol{E}_0\end{cases}$$

where the different coefficients are

$$\begin{cases}e_{\parallel}^+=\dfrac{t_{0\parallel}}{1+r_{0\parallel}r_{d\parallel}e^{2ik_{2z}d}}\\ e_{\perp}^+=\dfrac{t_{0\perp}}{1+r_{0\perp}r_{d\perp}e^{2ik_{2z}d}}\end{cases}\qquad\begin{cases}e_{\parallel}^-=\dfrac{t_{0\parallel}r_{d\parallel}e^{2ik_{2z}d}}{1+r_{0\parallel}r_{d\parallel}e^{2ik_{2z}d}}\\ e_{\perp}^-=\dfrac{t_{0\perp}r_{d\perp}e^{2ik_{2z}d}}{1+r_{0\perp}r_{d\perp}e^{2ik_{2z}d}}\end{cases}$$

The reflected and transmitted fields can also be written in the form

$$\begin{cases}\boldsymbol{E}^r(\boldsymbol{r},\omega)=\left\{E_{\parallel}^r\,\boldsymbol{e}_{\parallel}+E_{\perp}^r\,\boldsymbol{e}_{\perp}+E_z^r\,\boldsymbol{z}\right\}e^{i\boldsymbol{k}_t\cdot\rho-ik_{1z}z}\\ \boldsymbol{E}^t(\boldsymbol{r},\omega)=\left\{E_{\parallel}^t\,\boldsymbol{e}_{\parallel}+E_{\perp}^t\,\boldsymbol{e}_{\perp}+E_z^t\,\boldsymbol{z}\right\}e^{i\boldsymbol{k}_3\cdot\boldsymbol{r}}\end{cases} \tag{A.50}$$

where the components are

$$\begin{cases}E_{\parallel}^r=r_{\parallel}E_{0\parallel}=r_{\parallel}E_{i\parallel}\,cos\theta\\ E_{\perp}^r=r_{\perp}E_{0\perp}=r_{\perp}E_{i\perp}\\ E_z^r=\dfrac{k_t}{k_{1z}}r_{\parallel}E_{0\parallel}=r_{\parallel}E_{i\parallel}\,sin\theta\end{cases}\qquad\begin{cases}E_{\parallel}^t=t_{\parallel}E_{0\parallel}=t_{\parallel}E_{i\parallel}\,cos\theta\\ E_{\perp}^t=t_{\perp}E_{0\perp}=t_{\perp}E_{i\perp}\\ E_z^t=-\dfrac{k_t}{k_{3z}}t_{\parallel}E_{0\parallel}=-t_{\parallel}E_{i\parallel}\,cos\theta\,tan\theta_{3t}\end{cases}$$

Since

$$\begin{cases}E_{r\parallel}=E_{\parallel}^r\,\dfrac{1}{cos\theta}\\ E_{r\perp}=E_{\perp}^r\end{cases}\qquad\begin{cases}E_{t\parallel}=E_{\parallel}^t\,\dfrac{1}{cos\theta_{3t}}\\ E_{t\perp}=E_{\perp}^t\end{cases}$$

we get

$$\begin{cases} E_{r\|} = r_{\|} E_{i\|} \\ E_{r\perp} = r_{\perp} E_{i\perp} \end{cases} \qquad \begin{cases} E_{t\|} = t_{\|} E_{i\|} \dfrac{cos\theta}{cos\theta_{3t}} \\ E_{t\perp} = t_{\perp} E_{i\perp} \end{cases} \tag{A.51}$$

To calculate the angle of transmission, θ_{3t} , we use the relation

$$k_1 \, sin\theta = k_3 \, sin\theta_{3t} \tag{A.52}$$

which is Snell s law of refraction.

Appendix B

Scattered electric field from a body with arbitrary volume

B.1 Scattered field

In this section we will analyze how electromagnetic waves can be generated and represented. The analysis is restricted to time harmonic fields that propagate in homogeneous medium. To derive the scattered electric field that arises when an external field induces currents in a dielectric body, we use Maxwell s field equations as a starting point. These are

$$\begin{cases} \nabla \times \boldsymbol{E} = i\omega \boldsymbol{B} \\ \nabla \times \boldsymbol{H} = \boldsymbol{J} - i\omega \boldsymbol{D} \end{cases}$$

An additional limitation is that the material is isotropic, i.e. the constitutive relations are

$$\begin{cases} \boldsymbol{D} = \varepsilon_0 \varepsilon \boldsymbol{E} \\ \boldsymbol{B} = \mu_0 \mu \boldsymbol{H} \end{cases}$$

If these equations are combined we get

$$\begin{aligned} \nabla \times (\nabla \times \boldsymbol{E}) &= i\omega\mu_0\mu \nabla \times \boldsymbol{H} \\ &= i\omega\mu_0\mu(\boldsymbol{J} - i\omega\boldsymbol{D}) = i\omega\mu_0\mu\boldsymbol{J} + \omega^2\varepsilon_0\mu_0\varepsilon\mu\boldsymbol{E} \end{aligned}$$

which gives

$$\begin{cases} \nabla \times (\nabla \times \boldsymbol{E}) - k^2\, \boldsymbol{E} = i\omega\mu_0\mu\boldsymbol{J} \\ k = k' + ik'' = \dfrac{\omega}{c_0}(\varepsilon\mu)^{1/2} \end{cases} \tag{B.1}$$

Eq. (B.1) is a differential equation for the electric field with given sources ***J***. Since this quantities are vectorial Eq. (B.1) becomes a system of three dependent equations. It is now desirable to rewrite this equation in such a way that the cross connection is eliminated. One way of doing that is to use the fact that since the divergence of the magnetic flux density is zero

$$\nabla \cdot \boldsymbol{B} = 0$$

a vector potential ***A*** defined as

$$\boldsymbol{B} = \nabla \times \boldsymbol{A}$$

must exist. Since $\nabla \times \boldsymbol{E} = i\omega\boldsymbol{B}$ we get

$$\nabla \times \boldsymbol{E} = i\omega \nabla \times \boldsymbol{A}$$

which becomes

$$\nabla \times (\boldsymbol{E} - i\omega\boldsymbol{A}) = \boldsymbol{0}$$

The fact that the curl of the electric field and the vector potential is zero guaranties the existence of a scalar potential, ϕ. We find

$$\boldsymbol{E} - i\omega\boldsymbol{A} = -\nabla\phi$$

from which we receive

$$\boldsymbol{E} = i\omega\boldsymbol{A} - \nabla\phi \qquad \text{(B.2)}$$

The magnetic flux density and the electric field can thus be calculated from the vector potential $\boldsymbol{A}$ and the scalar potential ϕ. These potentials are not unambiguously defined. If a Gauge transformation is used

$$\begin{cases} \boldsymbol{A}' = \boldsymbol{A} + \nabla\psi \\ \phi' = \phi + i\omega\psi \end{cases}$$

where ψ is an arbitrary (differentiable) function, the magnetic flux density and the electric field will be unaffected because of

$$\nabla \times \boldsymbol{A}' = \nabla \times \boldsymbol{A} + \nabla \times \nabla\psi = \nabla \times \boldsymbol{A}$$
$$i\omega\boldsymbol{A}' - \nabla\phi' = i\omega\boldsymbol{A} + i\omega\nabla\psi - \nabla\phi - i\omega\nabla\psi = i\omega\boldsymbol{A} - \nabla\phi$$

Consequently we obtain the same physical fields $\boldsymbol{E}$ and $\boldsymbol{B}$ independently of which potential we use. This property of the vector potential makes it possible, for us, to find a simplified differential equation for $\boldsymbol{A}$ than the one stated for $\boldsymbol{E}$, Eq. (B.1). We therefor use an condition that $\boldsymbol{A}$ and ϕ both must fulfil. The most common is the Lorenz condition (or Lorenz gauge)

$$\nabla \cdot \boldsymbol{A} = \frac{ik^2}{\omega}\phi \qquad \text{(B.3)}$$

It is always possible to choose $\boldsymbol{A}$ and ϕ so that Eq. (B.3) will be fulfilled.
Suppose that we have a vector potential $\boldsymbol{A}_0$ and a scalar potential ϕ_0 that satisfy

$$\begin{cases} \boldsymbol{B} = \nabla \times \boldsymbol{A}_0 \\ \boldsymbol{E} = i\omega\boldsymbol{A}_0 - \nabla\phi_0 \end{cases}$$

but does not fulfil the Lorenz condition. We can now define a new vector potential $\boldsymbol{A}$ and a new scalar potential ϕ

$$\begin{cases} \boldsymbol{A} = \boldsymbol{A}_0 - \nabla\psi \\ \phi = \phi_0 - i\omega\psi \end{cases}$$

where the function ψ is an arbitrary solution to the inhomogeneous Helmholtz equation

$$\nabla^2\psi + k^2\psi = \nabla\cdot\boldsymbol{A}_0 - \frac{ik^2}{\omega}\phi_0$$

Observe that the right part of this equation is known and differs from zero, since $\boldsymbol{A}_0$ and ϕ_0 not satisfies (B.3). The physical fields $\boldsymbol{E}$ and $\boldsymbol{B}$ are not affected by the change of the potentials since the change of the potentials is a Gauge transformation. The new potentials $\boldsymbol{A}$ and ϕ will however fulfil the Lorenz condition. The partial differential equation that $\boldsymbol{A}$ fulfils becomes especially simple if we demand that the Lorenz condition should be valid. Substitution of Eq. (B.2) into Eq. (B.1) yields

$$\nabla\times\left[\nabla\times\left(i\,\omega\boldsymbol{A} - \nabla\phi\right)\right] - k^2\left[i\,\omega\boldsymbol{A} - \nabla\phi\right] = i\,\omega\mu_0\mu\boldsymbol{J}$$

Use the fact that $\nabla\times\left(\nabla\times\phi\right) = \boldsymbol{0}$ and insert the Lorenz condition

$$\nabla\times\left(\nabla\times\boldsymbol{A}\right) - k^2\,\boldsymbol{A} - \nabla\left(\nabla\cdot\boldsymbol{A}\right) = \mu_0\mu\boldsymbol{J}$$

Furthermore is $\nabla^2\boldsymbol{A} = \nabla\left(\nabla\cdot\boldsymbol{A}\right) - \nabla\times\left(\nabla\times\boldsymbol{A}\right)$ which leads to that the differential equation of the vector potential finally can be written as

$$\nabla^2\boldsymbol{A} + k^2\,\boldsymbol{A} = -\mu_0\mu\boldsymbol{J} \qquad \text{(B.4)}$$

A common way to solve Eq. (B.4) is to find the solution of a canonical problem where the source is special. Suppose that we know the solution to the equation

$$\nabla^2\,g\left(k,\boldsymbol{r},\boldsymbol{r}'\right) + k^2 g\left(k,\boldsymbol{r},\boldsymbol{r}'\right) = -\delta\left(\boldsymbol{r} - \boldsymbol{r}'\right) \qquad \text{(B.5)}$$

where differentiation is evaluated with the variable $\boldsymbol{r}$ as a differential variable. The function $g\left(k,\boldsymbol{r},\boldsymbol{r}'\right)$ is called the Green function of the problem. The solution to Eq. (B.4) becomes

$$\boldsymbol{A}\left(\boldsymbol{r}\right) = \mu_0\mu\iiint_V g\left(k,\boldsymbol{r},\boldsymbol{r}'\right)\boldsymbol{J}\left(\boldsymbol{r}'\right)dv' \qquad \text{(B.6)}$$

where integration is done over the parts where $\boldsymbol{J} \neq \boldsymbol{0}$. It is left now to solve the canonical problem Eq. (B.5). Since we in this case have spherical symmetry (the source has the same properties in all directions) we can suppose that $g\left(k,\boldsymbol{r},\boldsymbol{r}'\right)$ is only dependent of the distance $R = \left|\boldsymbol{r} - \boldsymbol{r}'\right|$. One way to handle the problem is to first solve Eq. (B.5) when the source is placed at the origin of the coordinate system. In that case the equation can be restated as

$$\nabla^2\,g\left(k,r\right) + k^2 g\left(k,r\right) = -\delta\left(\boldsymbol{r}\right) \qquad \text{(B.7)}$$

where $r = \left|\boldsymbol{r}\right|$. For $r \neq 0$ we find

$$\nabla^2\,g\left(k,r\right) + k^2 g\left(k,r\right) = 0$$

which for spherical symmetry becomes

$$\frac{1}{r}\frac{d^2}{dr^2}\big(rg(k,r)\big)+k^2g(k,r)=0$$

or

$$\frac{d^2}{dr^2}\big(rg(k,r)\big)+k^2rg(k,r)=0$$

The formal solution is

$$rg(k,r)=A\,e^{ikr}+B\,e^{-ikr}$$

or

$$g(k,r)=A\frac{e^{ikr}}{r}+B\frac{e^{-ikr}}{r}$$

The solution consists of two parts, one inward-oriented and one outward-oriented travelling spherical wave. The wave constant equals $k=k_0\sqrt{\varepsilon\mu}$ for $r\in V$, i.e. for all points inside the scattering body, and $k=k_0$ in the surrounding medium. Since the unity charge in the origin corresponds to an outward-oriented spherical wave we find that the constant *B* = 0. The other constant *A* can be determined if we integrate Eq. (B.7) over a sphere with radius *ε*.

$$\iiint_{r\le\varepsilon}\nabla^2\,g(k,r)dv+k^2\iiint_{r\le\varepsilon}g(k,r)dv=-\iiint_{r\le\varepsilon}\delta(\boldsymbol{r})dv=-1$$

We find that

$$\iiint_{r\le\varepsilon}g(k,r)dv=4\pi\,A\int_0^{\varepsilon}\frac{e^{ikr}}{r}r^2\,dr=4\pi\,A\int_0^{\varepsilon}e^{ikr}r\,dr\;\rightarrow\;0$$

when $\varepsilon\rightarrow 0$. And since

$$\begin{aligned}\iiint_{r\le\varepsilon}\nabla^2\,g(k,r)dv&=\iiint_{r\le\varepsilon}\nabla\cdot\nabla\,g(k,r)dv=\iint_{r=\varepsilon}\boldsymbol{n}\cdot\nabla\,g(k,r)dS\\&=\iint_{r=\varepsilon}\frac{dg(k,r)}{dr}dS=4\pi\varepsilon^2\left.\frac{dg(k,r)}{dr}\right|_{r=\varepsilon}\\&=4\pi\varepsilon^2\,A\,e^{ik\,\varepsilon}\left\{\frac{ik}{\varepsilon}-\frac{1}{\varepsilon^2}\right\}\rightarrow -4\pi\,A\end{aligned}$$

when $\varepsilon\rightarrow 0$ (we have here used the divergence theorem) we get $-4\pi\,A=-1$ and $g(k,r)=e^{ikr}/4\pi\,r$. Moving back the source point to the position $\boldsymbol{r}'$ gives

$$g(k,|\boldsymbol{r}-\boldsymbol{r}'|)=\frac{e^{ik|\boldsymbol{r}-\boldsymbol{r}'|}}{4\pi|\boldsymbol{r}-\boldsymbol{r}'|} \tag{B.8}$$

If Eq. (B.8) is substituted into Eq. (B.6) we find a solution of the vector potential $\boldsymbol{A}$. This is

$$\boldsymbol{A}(\boldsymbol{r})=\mu_0\mu\iiint_V\frac{e^{ik|\boldsymbol{r}-\boldsymbol{r}'|}}{4\pi|\boldsymbol{r}-\boldsymbol{r}'|}\boldsymbol{J}(\boldsymbol{r}')dv' \tag{B.9}$$

Making use of Eq. (B.2) and Eq. (B.3) we find an expression for the electric field. It becomes

$$\begin{aligned}\boldsymbol{E}(\boldsymbol{r})&=i\omega\left[\boldsymbol{A}(\boldsymbol{r})+\frac{1}{k^2}\nabla(\nabla\cdot\boldsymbol{A}(\boldsymbol{r}))\right]\\&=i\omega\mu_0\mu\left[\overline{\overline{\mathbf{I}}}+\frac{1}{k^2}\nabla\nabla\right]\cdot\iiint_V\frac{e^{ik|\boldsymbol{r}-\boldsymbol{r}'|}}{4\pi|\boldsymbol{r}-\boldsymbol{r}'|}\boldsymbol{J}(\boldsymbol{r}')dv',\quad \boldsymbol{r}\notin V\end{aligned} \tag{B.10}$$

where $\overline{\overline{\mathbf{I}}}$ is the unit dyadic. This integral implies that the scattered field $\boldsymbol{E}$ (or $\boldsymbol{E}_s$) is given by that in the medium induced current density (or $\boldsymbol{J}_s$) that has been generated by the incident electric field $\boldsymbol{E}_i$. To get an expression for the scattered field in terms of the incident electric field we use Eq. (B.1) as a starting point. The expression is valid even when the permittivity function ε varies in the space. If we suppose that no other currents than the ones that have been induced (by that to the scattering body incident field $\boldsymbol{E}_i$) exist in the volume of the scattering body (V_s) we can restate Eq. (B.1) as

$$\nabla\times(\nabla\times\boldsymbol{E}(\boldsymbol{r},\omega))-\omega^2\varepsilon_0\mu_0\varepsilon(\boldsymbol{r},\omega)\boldsymbol{E}(\boldsymbol{r},\omega)=\mathbf{0}$$

We have here assumed that the medium is nonmagnetic, i.e. $\mu=1$. The next step is to rewrite the permittivity as

$$\varepsilon(\boldsymbol{r},\omega)=1+\chi_e(\boldsymbol{r},\omega)$$

The susceptibility function χ_e (see section 2) indicates the discrepancy from free space. We will use the indication $\boldsymbol{J}_s$ for the induced current density in V_s. The magnitude of these currents, that arises from that ε varies in space, can be obtained if the equation for the electric field, stated above, is used

$$\nabla\times(\nabla\times\boldsymbol{E}(\boldsymbol{r},\omega))-k_0^2\,\boldsymbol{E}(\boldsymbol{r},\omega)=k_0^2\,\chi_e(\boldsymbol{r},\omega)\boldsymbol{E}(\boldsymbol{r},\omega) \tag{B.11}$$

Here is $k_0^2=\omega^2\varepsilon_0\mu_0$ the wave constant for a wave in vacuum (the surrounding medium) and not the wave constant for the medium in the scattering object. From the right side of Eq. (B.11) and Eq. (B.1) we can identify the magnitude of the induced current density expressed in the total electric field

$$i\omega\mu_0\boldsymbol{J}_s=k_0^2\,\chi_e\boldsymbol{E}$$

or

$$\boldsymbol{J}_s = -i\omega\varepsilon_0\chi_e\boldsymbol{E} \tag{B.12}$$

The scattered electric field can finally be written if we substitute Eq. (B.12) into Eq. (B.10) which yields

$$\boldsymbol{E}_s(\boldsymbol{r}) = \left[k^2\,\overline{\overline{\mathbf{I}}} + \nabla\nabla\right]\iiint_{V_s}\frac{e^{ik|\boldsymbol{r}-\boldsymbol{r}'|}}{4\pi|\boldsymbol{r}-\boldsymbol{r}'|}\chi_e(\boldsymbol{r}')\boldsymbol{E}(\boldsymbol{r}')dv', \qquad \boldsymbol{r}\notin V_s \tag{B.13}$$

where $\boldsymbol{E} = \boldsymbol{E}_{ind}$ (the electric field in the integral corresponds to that in the scattering body induced electric field). Sometimes it can be useful to represent Eq. (B.13) in the form

$$\boldsymbol{E}_s(\boldsymbol{r}) = k^2\iiint_{V_s}\chi_e(\boldsymbol{r}')\overline{\overline{\mathbf{G}}}\cdot\boldsymbol{E}(\boldsymbol{r}')dv' \tag{B.14}$$

We have here introduced the dyadic Green function

$$\overline{\overline{\mathbf{G}}} = \left[\overline{\overline{\mathbf{I}}} + \frac{1}{k^2}\nabla\nabla\right]\frac{e^{ik|\boldsymbol{r}-\boldsymbol{r}'|}}{4\pi|\boldsymbol{r}-\boldsymbol{r}'|} \tag{B.15}$$

and the unit dyadic described by

$$\overline{\overline{\mathbf{I}}} = \boldsymbol{xx} + \boldsymbol{yy} + \boldsymbol{zz}$$

B.2 Far field

To be able to calculate the field large distances from the scattering object, i.e. in the far zone, some criterion must be fulfilled. These criterions are based on the conception of large distance that is related to the size of the scattering object and to the wavelength $\lambda = 2\pi/k$. If r is the distance from the origin in the volume V_s to the point of observation, we can define large distance as

$$\begin{cases} r >> d \\ r >> kd^2 \\ r >> \lambda \end{cases} \tag{B.16}$$

where the maximum extension of the scattering object d is given by

$$d = \max_{r'\in V_s}|\boldsymbol{r}'|$$

We use Eq. (B.10) where we have supposed that the — by the incident field — induced current density is $\boldsymbol{J}_s$ and the scattered field is $\boldsymbol{E}_s$. The distance $|\boldsymbol{r}-\boldsymbol{r}'|$ between the source point $\boldsymbol{r}'$ and the observation point $\boldsymbol{r}$ can be written as a dot product

$$|\boldsymbol{r}-\boldsymbol{r}'| = \sqrt{(\boldsymbol{r}-\boldsymbol{r}')\cdot(\boldsymbol{r}-\boldsymbol{r}')} = \sqrt{r^2+r'^2-2\boldsymbol{r}\cdot\boldsymbol{r}'}$$

Thereafter the unit vector $\boldsymbol{r} = \boldsymbol{r}/r$ is introduced. The unit vector is pointing in the direction from the origin of coordinates to the observation point. The distance $|\boldsymbol{r}-\boldsymbol{r}'|$ can, with help of $\sqrt{1+x} = 1+x/2+\ldots$, be approximated with the major contribution of

$$\begin{aligned}|\boldsymbol{r}-\boldsymbol{r}'| &= r\sqrt{1+\left(\frac{r'}{r}\right)^2 - 2\boldsymbol{r}\cdot\frac{\boldsymbol{r}'}{r}} = r\left\{1+\frac{1}{2}\left[\left(\frac{r'}{r}\right)^2 - 2\boldsymbol{r}\cdot\frac{\boldsymbol{r}'}{r}\right]+\ldots\right\} \\ &= r-\boldsymbol{r}\cdot\boldsymbol{r}' + O\left(d^2/r\right)\end{aligned} \tag{B.17}$$

when $r \to \infty$. The Green function $g(k,|\boldsymbol{r}-\boldsymbol{r}'|) = e^{ik|\boldsymbol{r}-\boldsymbol{r}'|}/4\pi|\boldsymbol{r}-\boldsymbol{r}'|$ can now be written as

$$\begin{aligned}\frac{e^{ik|\boldsymbol{r}-\boldsymbol{r}'|}}{4\pi|\boldsymbol{r}-\boldsymbol{r}'|} &= \frac{1}{4\pi\, r(1+O(d/r))}\exp\left\{k\left(r-\boldsymbol{r}\cdot\boldsymbol{r}'+O\left(d^2/r\right)\right)\right\} \\ &= \frac{e^{ikr}}{4\pi\, r}e^{-ik\,\boldsymbol{r}\cdot\boldsymbol{r}'}\left(1+O\left(kd^2/r\right)\right)\left(1+O(d/r)\right)\end{aligned}$$

The dominating contribution to the scattered electric field in Eq. (B.10) becomes

$$\boldsymbol{E}_s(\boldsymbol{r}) = i\,\omega\mu_0\mu\left[\overline{\overline{\mathbf{I}}}+\frac{1}{k^2}\nabla\nabla\right]\cdot\frac{e^{ikr}}{4\pi\, r}\iiint_{V_s} e^{-ik\,\boldsymbol{r}\cdot\boldsymbol{r}'}\,\boldsymbol{J}_s(\boldsymbol{r}')dv', \quad \boldsymbol{r}\notin V_s$$

It is now suitable to introduce the vector field defined by

$$\boldsymbol{K}(\boldsymbol{r}) = \frac{ik^2\eta_0\eta}{4\pi}\iiint_{V_s} e^{-ik\,\boldsymbol{r}\cdot\boldsymbol{r}'}\,\boldsymbol{J}_s(\boldsymbol{r}')dv'$$

where $\eta = \sqrt{\mu/\varepsilon}$ is the relative wave impedance of the medium and η_0 is the wave impedance of vacuum. Observe that the field $\boldsymbol{K}$ is only a function of the direction, $\boldsymbol{r}$, to the observation point and not by the distance r. The electric field can now be written as

$$\boldsymbol{E}_s(\boldsymbol{r}) = \left[\overline{\overline{\mathbf{I}}}+\frac{1}{k^2}\nabla\nabla\right]\cdot\left(\frac{e^{ikr}}{kr}\boldsymbol{K}(\boldsymbol{r})\right) \tag{B.18}$$

Making use of the calculation rules of vector analysis we find

$$\nabla\cdot\left[\frac{e^{ikr}}{kr}\boldsymbol{K}(\boldsymbol{r})\right] = \frac{e^{ikr}}{kr}\nabla\cdot\boldsymbol{K}(\boldsymbol{r}) + \boldsymbol{K}(\boldsymbol{r})\cdot\nabla\left(\frac{e^{ikr}}{kr}\right)$$

Since $\boldsymbol{K}(\boldsymbol{r})$ is only a function of the direction $\boldsymbol{r}$, which is given by the spherical angles θ and ϕ, and not by the distance r, we get

$$\begin{cases} \nabla \cdot \boldsymbol{K}(\boldsymbol{r}) = \dfrac{1}{r\sin\theta}\dfrac{\partial}{\partial\theta}(\sin\theta\, K_\theta) + \dfrac{1}{r\sin\theta}\dfrac{\partial}{\partial\phi}(K_\phi) \\ K_\theta = \theta \cdot \boldsymbol{K}(\boldsymbol{r}) \qquad K_\phi = \phi \cdot \boldsymbol{K}(\boldsymbol{r}) \end{cases}$$

where $\nabla \cdot \boldsymbol{K}(\boldsymbol{r})$ is vanishing as $1/r$. We find

$$\begin{aligned} \frac{1}{k}\nabla \cdot \left[\frac{e^{ikr}}{kr}\boldsymbol{K}(\boldsymbol{r})\right] &= \frac{1}{k}\boldsymbol{K}(\boldsymbol{r})\cdot \nabla\left(\frac{e^{ikr}}{kr}\right)\left(1 + O\left((kr)^{-1}\right)\right) \\ &= i\,\boldsymbol{r}\cdot \boldsymbol{K}(\boldsymbol{r})\frac{e^{ikr}}{kr}\left(1 + O\left((kr)^{-1}\right)\right) \end{aligned}$$

and in a similar way we get

$$\begin{aligned} \frac{1}{k^2}\nabla\left\{\nabla \cdot \left[\frac{e^{ikr}}{kr}\boldsymbol{K}(\boldsymbol{r})\right]\right\} &= \nabla\left\{\frac{i}{k}\boldsymbol{r}\cdot \boldsymbol{K}(\boldsymbol{r})\frac{e^{ikr}}{kr}\left(1 + O\left((kr)^{-1}\right)\right)\right\} \\ &= -\boldsymbol{r}(\boldsymbol{r}\cdot \boldsymbol{K}(\boldsymbol{r}))\frac{e^{ikr}}{kr}\left(1 + O\left((kr)^{-1}\right)\right) \end{aligned}$$

Approximation of Eq. (B.18) generates an expression for the scattered electric field in the far zone. The dominating contribution of the electric field is

$$\begin{cases} \boldsymbol{E}_s(\boldsymbol{r}) = [\boldsymbol{K}(\boldsymbol{r}) - \boldsymbol{r}\,K_r(\boldsymbol{r})]\dfrac{e^{ikr}}{kr} \\ K_r = \boldsymbol{r}\cdot \boldsymbol{K}(\boldsymbol{r}) \end{cases} \tag{B.19}$$

We can here use the reversed BAC-CAB rule ($\boldsymbol{b}(\boldsymbol{a}\cdot\boldsymbol{c}) - \boldsymbol{c}(\boldsymbol{a}\cdot\boldsymbol{b}) = \boldsymbol{a}\times(\boldsymbol{b}\times\boldsymbol{c})$) to rewrite Eq. (B.19) which yields

$$\boldsymbol{E}_s(\boldsymbol{r}) = \boldsymbol{r}\times(\boldsymbol{K}(\boldsymbol{r})\times\boldsymbol{r})\frac{e^{ikr}}{kr}$$

Observe that we now have used all three conditions that were postulated in the criterion for the far zone (B.16). Finally we get an expression for the scattered electric field

$$\boldsymbol{E}_s(\boldsymbol{r}) = \frac{e^{ikr}}{kr}\boldsymbol{F}(\boldsymbol{r}) \tag{B.20}$$

where $\boldsymbol{F}(\boldsymbol{r})$ is the far field amplitude of the wave

$$\boldsymbol{F}(\boldsymbol{r}) = \boldsymbol{r}\times(\boldsymbol{K}(\boldsymbol{r})\times\boldsymbol{r}) = \frac{ik^2\eta_0\eta}{4\pi}\boldsymbol{r}\times\left(\iiint_{V_s} e^{-ik\,\boldsymbol{r}\cdot\boldsymbol{r}'}\,\boldsymbol{J}_s(\boldsymbol{r}')dv'\times\boldsymbol{r}\right) \tag{B.21}$$

The parameters k and η correspond to the medium that surrounds the scattering body.
In the end of the former section we expressed the scattered electric field in terms of the dyadic Green function. We are now interested in a corresponding expression to Eq (B.15) valid in the far zone. To obtain this we expand Eq (B.19)

$$\boldsymbol{E}_s(\boldsymbol{r}) = \left[\overline{\overline{\mathbf{I}}} - \boldsymbol{rr}\right]\boldsymbol{K}(\boldsymbol{r})\frac{e^{ikr}}{kr} = \left[\overline{\overline{\mathbf{I}}} - \boldsymbol{rr}\right]\frac{e^{ikr}}{kr}\cdot\frac{ik^2\eta_0\eta}{4\pi}\left(\iiint_{V_s} e^{-ik\,\boldsymbol{r}\cdot\boldsymbol{r}'}\,\boldsymbol{J}_s(\boldsymbol{r}')dv'\right)$$

$$= i\,\omega\mu_0\mu\left[\overline{\overline{\mathbf{I}}} - \boldsymbol{rr}\right]\iiint_{V_s}\frac{e^{ikr}}{4\pi\,r}e^{-ik\,\boldsymbol{r}\cdot\boldsymbol{r}'}\,\boldsymbol{J}_s(\boldsymbol{r}')dv'$$

Since neither $\overline{\overline{\mathbf{I}}}$ nor $\boldsymbol{rr}$ contain integration variables we can move this terms into the integral. We get

$$\boldsymbol{E}_s(\boldsymbol{r}) = i\,\omega\mu_0\mu\iiint_{V_s}\left[\overline{\overline{\mathbf{I}}} - \boldsymbol{rr}\right]\frac{e^{ik(r-\boldsymbol{r}\cdot\boldsymbol{r}')}}{4\pi\,r}\boldsymbol{J}_s(\boldsymbol{r}')dv' \tag{B.22}$$

If we assume that the medium is nonmagnetic, i.e. $\mu = 1$, and use the Eq. (B.12)

$$\boldsymbol{J}_s = -i\,\omega\varepsilon_0\chi_e\boldsymbol{E}$$

we find

$$\boldsymbol{E}_s(\boldsymbol{r}) = \omega^2\varepsilon_0\mu_0\iiint_{V_s}\left[\overline{\overline{\mathbf{I}}} - \boldsymbol{rr}\right]\frac{e^{ik(r-\boldsymbol{r}\cdot\boldsymbol{r}')}}{4\pi\,r}\chi_e\boldsymbol{E}(\boldsymbol{r}')dv'$$

which can be simplified to

$$\boldsymbol{E}_s(\boldsymbol{r}) = k_0^2\,\chi_e\iiint_{V_s}\left[\overline{\overline{\mathbf{I}}} - \boldsymbol{rr}\right]\frac{e^{ik(r-\boldsymbol{r}\cdot\boldsymbol{r}')}}{4\pi\,r}\boldsymbol{E}(\boldsymbol{r}')dv' \tag{B.23}$$

Here will the electric field in the integral, in Eq. (B.23), correspond to that in the scattering body induced electric field, i.e. $\boldsymbol{E} = \boldsymbol{E}_{ind}$. If we compare Eq (B.22) to Eq (B.10) and Eq (B.15) we find that the expression for the dyadic Green function in the far zone is given by

$$\overline{\overline{\mathbf{G}}}(\boldsymbol{r},\boldsymbol{r}') = \left[\overline{\overline{\mathbf{I}}} - \boldsymbol{rr}\right]\frac{e^{ik(r-\boldsymbol{r}\cdot\boldsymbol{r}')}}{4\pi\,r} \tag{B.24}$$

This means that Eq (B.23) can be restated as

$$\boldsymbol{E}_s(\boldsymbol{r}) = k_0^2\,\chi_e\iiint_{V_s}\overline{\overline{\mathbf{G}}}(\boldsymbol{r},\boldsymbol{r}')\cdot\boldsymbol{E}(\boldsymbol{r}')dv' \tag{B.25}$$

To calculate the power density of the scattered field we first use Eq. (2.29)

$$\boldsymbol{H}(\boldsymbol{r}) = \frac{1}{ik\eta_0\eta}\nabla\times\boldsymbol{E}(\boldsymbol{r}) \tag{B.26}$$

to calculate the magnetic field. Insertion of Eq. (B.20) into Eq. (B.26) yields

$$\boldsymbol{H}_s(\boldsymbol{r}) = \frac{1}{ik\eta_0\eta}\nabla\times\left\{\frac{e^{ikr}}{kr}\boldsymbol{F}(\boldsymbol{r})\right\} = \frac{1}{\eta_0\eta}\frac{e^{ikr}}{kr}\boldsymbol{r}\times\boldsymbol{F}(\boldsymbol{r}) \tag{B.27}$$

We have here used the fact that components that vanish faster than $1/kr$ are negligible. If we now use Eq. (2.33)

$$\langle\boldsymbol{S}(\boldsymbol{r},t)\rangle = \frac{1}{2}\mathrm{Re}\{\boldsymbol{E}_s(\boldsymbol{r},\omega)\times\boldsymbol{H}_s^*(\boldsymbol{r},\omega)\} \tag{B.28}$$

and insert Eq. (B.20) and Eq. (B.27) we get

$$\begin{aligned}
\langle\boldsymbol{S}(\boldsymbol{r},t)\rangle &= \frac{1}{2}\mathrm{Re}\left\{\frac{e^{ikr}}{kr}\boldsymbol{F}(\boldsymbol{r})\times\left(\frac{1}{\eta_0\eta}\frac{e^{ikr}}{kr}\boldsymbol{r}\times\boldsymbol{F}(\boldsymbol{r})\right)^*\right\} \\
&= \frac{1}{2}\mathrm{Re}\left\{\frac{e^{ikr}}{kr}\left(\frac{1}{\eta_0\eta}\frac{e^{ikr}}{kr}\right)^*\boldsymbol{F}(\boldsymbol{r})\times\left(\boldsymbol{r}\times\boldsymbol{F}^*(\boldsymbol{r})\right)\right\} \\
&= \frac{1}{2}\mathrm{Re}\left\{\frac{1}{k^2\eta_0\eta^* r^2}\boldsymbol{F}(\boldsymbol{r})\times\left(\boldsymbol{r}\times\boldsymbol{F}^*(\boldsymbol{r})\right)\right\}
\end{aligned} \tag{B.29}$$

With use of the BAC-CAB rule and the case of wave propagating in air, i.e.$\eta^* = \eta$, we find

$$\langle\boldsymbol{S}(\boldsymbol{r},t)\rangle = \frac{\boldsymbol{r}}{2\eta_0\eta\, k^2 r^2}|\boldsymbol{F}(\boldsymbol{r})|^2 \tag{B.30}$$

which describes the time-average power density for a propagating time harmonic electromagnetic wave.

Appendix C

The T-matrix method

The T-matrix method is a method for calculating the electromagnetic scattering by spherical and nonspherical particles. Although the method is applicable to arbitrarily shaped particles it has been applied almost exclusively to axisymmetric particles, i.e. bodies-of-revolution. The T-matrix method (or the transition matrix method) is based on a method where the different fields are expanded into an infinitely number of propagating modes. This is done when the Helmholtz vector equation Eq. (2.18) is solved for finite bodies. Thus the incident, internal and scattered fields are represented by this mode expansion where the respective mode is represented by a spherical vector wave function. Thereafter — with help of the boundary conditions — the Fourier coefficients of the modes can be calculated and it is possible to achieve expressions for the internal and scattered fields expressed in terms of the coefficients of the incident field. The coefficients of the scattered field are related to the coefficients of the incident field through the infinite dimensional T-matrix. The T-matrix method should be used preferably in the resonance region where the scattering body is of the same size as the wavelength. Since some parts of the theory behind this method are very complex and complicated to explain, our effort will be put on the parts that are fundamental in the theory. This means that we will not, in this appendix, penetrate deep into the parts that concerns solution methods of advanced differential equations and simplifications of surface integrals in the case of spheroidal surfaces.
For the more interested reader there are several books (for example [14] and [15]) where the theory behind the T-matrix method is elucidated and described in a more complete way.

C.1 General formulations

The mode expansion is a direct consequence when the Helmholtz vector equation is solved for a finite body. The differential equation is

$$\nabla^2 \boldsymbol{F}(\boldsymbol{r}) + k^2 \boldsymbol{F}(\boldsymbol{r}) = 0 \tag{C.1}$$

where the notation $\boldsymbol{F}$ stands for the electric, $\boldsymbol{E}$, or the magnetic, $\boldsymbol{H}$, field. In spherical coordinates Eq. (C.1) becomes

$$\left(\frac{1}{r^2}\frac{\partial}{\partial r}\left(r^2\frac{\partial}{\partial r}\right)+\frac{1}{r^2 \sin\theta}\frac{\partial}{\partial\theta}\left(\sin\theta\frac{\partial}{\partial\theta}\right)+\frac{1}{r^2 \sin^2\theta}\frac{\partial^2}{\partial\phi^2}+k^2\right)\boldsymbol{F}(\boldsymbol{r})=\boldsymbol{0} \tag{C.2}$$

To solve this equation we use the method of separation of variables

$$\boldsymbol{F}(\boldsymbol{r}) = f(r)\boldsymbol{A}(\boldsymbol{r})$$

After insertion in Eq. (C.2) we get

$$\left(\frac{d}{dr}\left(r^2\frac{d}{dr}\right)-\xi+k^2r^2\right)f(r)=0 \tag{C.3}$$

and

$$\left(\frac{1}{sin\theta}\frac{\partial}{\partial\theta}\left(sin\theta\frac{\partial}{\partial\theta}\right)+\frac{1}{sin^2\theta}\frac{\partial^2}{\partial\phi^2}+k^2\right)\boldsymbol{A}(\boldsymbol{r})=-\xi\boldsymbol{A}(\boldsymbol{r}) \tag{C.4}$$

where ξ is an arbitrary constant. We identify Eq. (C.3) as Bessel s differential equation in spherical coordinates

$$\left(\frac{d}{dz}\left(z^2\frac{d}{dz}\right)-n(n+1)+k^2z^2\right)f(z)=0 \tag{C.5}$$

from which we observe that the constant ξ equals $n(n+1)$. A solution to Eq (C.5) is the spherical Bessel functions $j_n(kz)$. They are defined as

$$j_n(z)=2^n z^n\sum_{k=0}^{\infty}\frac{(-1)^k(k+n)!}{k!(2k+2n+1)!}z^{2k} \tag{C.6}$$

where n is a positive integer and z can be a complex number. This solution is real for real arguments and finite at $z=0$. Furthermore is Eq. (C.6) even for even n and odd for odd n. That is

$$j_n(-z)=(-1)^n j_n(z) \tag{C.7}$$

Another linearly independent solution to Eq. (C.5) is the spherical Neumann functions $n_n(kz)$. They are defined as

$$n_n(z)=\frac{(-1)^{n+1}}{2^n z^{n+1}}\sum_{k=0}^{\infty}\frac{(-1)^k(k-n)!}{k!(2k-2n)!}z^{2k} \tag{C.8}$$

This solution is also real for real arguments but gets singular at $z=0$. In some wave problems it is convenient to define linear combinations of the Bessel and Neumann functions

$$\begin{cases}h_n^{(1)}(z)=j_n(z)+in_n(z)\\h_n^{(2)}(z)=j_n(z)-in_n(z)\end{cases} \tag{C.9}$$

These two functions are called the spherical Hankel functions of the first and second kind, respectively, and forms thus further solutions to Eq. (C.5).
The technique of how to solve Eq. (C.4) is very comprehensive and thus will we not get into it here. If we define the constant ξ as $\xi=l(l+1)$, where l is a positive integer, Eq. (C.4) becomes

$$\left(\frac{1}{sin\theta}\frac{\partial}{\partial\theta}\left(sin\theta\frac{\partial}{\partial\theta}\right)+\frac{1}{sin^2\theta}\frac{\partial^2}{\partial\phi^2}+k^2\right)\boldsymbol{A}(\boldsymbol{r})=-l(l+1)\boldsymbol{A}(\boldsymbol{r}) \tag{C.10}$$

One solution to this equation is

$$\boldsymbol{A}_{\sigma ml}(\boldsymbol{r}) = \frac{1}{\sqrt{l(l+1)}} \nabla Y_{\sigma ml}(\boldsymbol{r}) \times \boldsymbol{r} \tag{C.11}$$

Here is $l = 0, 1, 2, ...,$ and $m = 0, 1, ..., l$. The quantity σ indicates if the function is even (e) or odd (o). The spherical surface functions $Y_{\sigma ml}(\boldsymbol{r})$ are defined as

$$Y_{\sigma ml}(\boldsymbol{r}) = Y_{\sigma ml}(\theta, \phi) = \sqrt{\frac{\varepsilon_m}{2\pi}} \sqrt{\frac{2l+1}{2} \frac{(l-m)!}{(l+m)!}} P_l^m(\cos\theta) \begin{Bmatrix} \cos m\phi \\ \sin m\phi \end{Bmatrix} \tag{C.12}$$

where

$$\varepsilon_m = 2 - \delta_{m0} = \begin{cases} 1, & m = 0 \\ 2, & m > 0 \end{cases}$$

In Eq. (C.12) we find the associated Legendre functions P_l^m. They are defined as

$$P_l^m(x) = \left(1 - x^2\right)^{m/2} \frac{d^m}{dx^m} P_l(x) \tag{C.13}$$

where $P_l(x)$ are the Legendre polynomials

$$P_l(x) = \sum_{k=0}^{l/2} (-1)^k \frac{(2l - 2k)!}{2^l\, k!\,(l-k)!\,(l-2k)!} x^{l-2k} \tag{C.14}$$

A solution to Eq. (C.2) is thus

$$\boldsymbol{F}_{\sigma ml}(k\boldsymbol{r}) = f_l(kr) \boldsymbol{A}_{\sigma ml}(\boldsymbol{r}) \tag{C.15}$$

where $f_l(kr) = f_{\sigma ml}(r)$ is a linear combination of the spherical Bessel functions $j_l(kr)$ and the spherical Hankel functions $h_l(kr)$ and $\boldsymbol{A}_{\sigma ml}(\boldsymbol{r})$ is the spherical vector surface functions defined by Eq. (C.11). The base function Eq. (C.15) is a suitable candidate to the spherical vector waves that forms the solution to Eq. (C.2) but it is not the only one. A new base function can be constructed if we take the curl of Eq. (C.15), i.e.

$$\nabla \times f_l(kr) \boldsymbol{A}_{\sigma ml}(\boldsymbol{r}) \tag{C.16}$$

Another possible candidate that satisfies Helmholtz vector equation is

$$\nabla\left(f_l(kr) Y_{\sigma ml}(\boldsymbol{r})\right) \tag{C.17}$$

since $f_l(kr) Y_{\sigma ml}(\boldsymbol{r})$ is a solution to the Helmholtz equation in the case of scalar quantities.

We have now the necessary tools to define the spherical vector waves, which will work as a set of basis functions. Every solution to Helmholtz equation can in this way be expressed by these basis functions. The outward going spherical vector waves are defined by

$$\begin{cases} \boldsymbol{u}_{1\sigma ml}(k\boldsymbol{r}) = h_l^{(1)}(kr)\boldsymbol{A}_{\sigma ml}(\boldsymbol{r}) \\ \boldsymbol{u}_{2\sigma ml}(k\boldsymbol{r}) = \dfrac{1}{k}\nabla\times\left(h_l^{(1)}(kr)\boldsymbol{A}_{\sigma ml}(\boldsymbol{r})\right) \\ \boldsymbol{u}_{3\sigma ml}(k\boldsymbol{r}) = \dfrac{1}{k}\nabla\left(h_l^{(1)}(kr)Y_{\sigma ml}(\boldsymbol{r})\right) \end{cases} \tag{C.18}$$

and the regular spherical vector waves by

$$\begin{cases} \boldsymbol{v}_{1\sigma ml}(k\boldsymbol{r}) = j_l(kr)\boldsymbol{A}_{\sigma ml}(\boldsymbol{r}) \\ \boldsymbol{v}_{2\sigma ml}(k\boldsymbol{r}) = \dfrac{1}{k}\nabla\times\left(j_l(kr)\boldsymbol{A}_{\sigma ml}(\boldsymbol{r})\right) \\ \boldsymbol{v}_{3\sigma ml}(k\boldsymbol{r}) = \dfrac{1}{k}\nabla\left(j_l(kr)Y_{\sigma ml}(\boldsymbol{r})\right) \end{cases} \tag{C.19}$$

The first two equations in every set — i.e $\boldsymbol{u}_{1\sigma ml}$, $\boldsymbol{u}_{2\sigma ml}$, $\boldsymbol{v}_{1\sigma ml}$ and $\boldsymbol{v}_{2\sigma ml}$ — are divergence free ($\nabla\cdot\boldsymbol{v}=0$) but the two remaining are not. In this way will the electromagnetic field in source free regions is represented by the first two basis functions in each set while electromagnetic fields in regions with sources are represented by $\boldsymbol{u}_{3\sigma ml}$ and $\boldsymbol{v}_{3\sigma ml}$. In Eq. (C.18) and Eq. (C.19) we have used the functions $\boldsymbol{A}_{\sigma ml}(\boldsymbol{r})$ to define the basis functions. In order to simplify these equations we use the fact that $\boldsymbol{A}_{\sigma ml}(\boldsymbol{r})$ is just one of three types of spherical vector surface functions. These are defined by

$$\begin{cases} \boldsymbol{A}_{1\sigma ml}(\boldsymbol{r}) = \boldsymbol{A}_{\sigma ml}(\boldsymbol{r}) = \dfrac{1}{\sqrt{l(l+1)}}\nabla Y_{\sigma ml}(\boldsymbol{r})\times\boldsymbol{r} \\ \boldsymbol{A}_{2\sigma ml}(\boldsymbol{r}) = \dfrac{1}{\sqrt{l(l+1)}}r\nabla Y_{\sigma ml}(\boldsymbol{r}) \\ \boldsymbol{A}_{3\sigma ml}(\boldsymbol{r}) = \boldsymbol{r}\,Y_{\sigma ml}(\boldsymbol{r}) \end{cases} \tag{C.20}$$

The base functions can now be restated and we find

$$\begin{cases} \boldsymbol{v}_{1\sigma ml}(k\boldsymbol{r}) = j_l(kr)\boldsymbol{A}_{1\sigma ml}(\boldsymbol{r}) \\ \boldsymbol{v}_{2\sigma ml}(k\boldsymbol{r}) = \dfrac{(krj_l(kr))'}{kr}\boldsymbol{A}_{2\sigma ml}(\boldsymbol{r}) + \sqrt{l(l+1)}\dfrac{j_l(kr)}{kr}\boldsymbol{A}_{3\sigma ml}(\boldsymbol{r}) \\ \boldsymbol{v}_{3\sigma ml}(k\boldsymbol{r}) = j_l'(kr)\boldsymbol{A}_{3\sigma ml}(\boldsymbol{r}) + \sqrt{l(l+1)}\dfrac{j_l(kr)}{kr}\boldsymbol{A}_{2\sigma ml}(\boldsymbol{r}) \end{cases} \tag{C.21}$$

and

$$\begin{cases} \boldsymbol{u}_{1\sigma ml}(k\boldsymbol{r}) = h_l^{(1)}(kr)\boldsymbol{A}_{1\sigma ml}(\boldsymbol{r}) \\ \boldsymbol{u}_{2\sigma ml}(k\boldsymbol{r}) = \dfrac{\left(krh_l^{(1)}(kr)\right)'}{kr}\boldsymbol{A}_{2\sigma ml}(\boldsymbol{r}) + \sqrt{l(l+1)}\dfrac{h_l^{(1)}(kr)}{kr}\boldsymbol{A}_{3\sigma ml}(\boldsymbol{r}) \\ \boldsymbol{u}_{3\sigma ml}(k\boldsymbol{r}) = h_l^{(1)\prime}(kr)\boldsymbol{A}_{3\sigma ml}(\boldsymbol{r}) + \sqrt{l(l+1)}\dfrac{h_l^{(1)}(kr)}{kr}\boldsymbol{A}_{2\sigma ml}(\boldsymbol{r}) \end{cases} \tag{C.22}$$

The general solution to Helmholtz vector equation Eq. (C.2) can now be written in terms of these base functions. The result is

$$\boldsymbol{F}(\boldsymbol{r}) = \sum_{l=0}^{\infty}\sum_{m=0}^{l}\sum_{\sigma=\mathrm{e,o}}\sum_{\tau=1}^{3}\left(c_{\tau\sigma ml}\,\boldsymbol{v}_{\tau\sigma ml}(k\boldsymbol{r}) + d_{\tau\sigma ml}\,\boldsymbol{u}_{\tau\sigma ml}(k\boldsymbol{r})\right) \tag{C.23}$$

where the index τ represents the three different base functions and thus takes the values $\tau = 1, 2, 3$ and the index σ represents the parity (odd or even). We can now use this result to express the electric and magnetic field. A general mode expansion of the total electric field in a region on the outside of a sphere that surrounds a scattering body in a source free region is represented by

$$\boldsymbol{E}(\boldsymbol{r},\omega) = \sum_{l=0}^{\infty}\sum_{m=0}^{l}\sum_{\sigma=\mathrm{e,o}}\sum_{\tau=1}^{2}\left(a_{\tau\sigma ml}\,\boldsymbol{v}_{\tau\sigma ml}(k\boldsymbol{r}) + f_{\tau\sigma ml}\,\boldsymbol{u}_{\tau\sigma ml}(k\boldsymbol{r})\right) \tag{C.24}$$

The corresponding mode expansion of the total magnetic field becomes

$$\boldsymbol{H}(\boldsymbol{r},\omega) = \frac{1}{i\eta_0\eta}\sum_{l=0}^{\infty}\sum_{m=0}^{l}\sum_{\sigma=\mathrm{e,o}}\sum_{\tau=1}^{2}\left(a_{\tau\sigma ml}\,\boldsymbol{v}_{\tau\sigma ml}(k\boldsymbol{r}) + f_{\tau\sigma ml}\,\boldsymbol{u}_{\tau\sigma ml}(k\boldsymbol{r})\right) \tag{C.25}$$

We have here introduced the dual index to τ that is defined by $\overline{1} = 2$ and $\overline{2} = 1$. The expansion coefficients $a_{\tau\sigma ml}$ represent that to the scattered body incident field while the expansion coefficients $f_{\tau\sigma ml}$ represents the scattered field.

C.2 Plane wave

If the incident field is a plane wave it can be represented by the regular spherical vector waves $\boldsymbol{v}_{\tau\sigma ml}(k\boldsymbol{r})$. The electric field becomes

$$\boldsymbol{E}_i(\boldsymbol{r},\omega) = \boldsymbol{E}_0\, e^{ik\boldsymbol{k}_i\cdot\boldsymbol{r}} = \sum_{l=1}^{\infty}\sum_{m=0}^{l}\sum_{\sigma=\mathrm{e,o}}\sum_{\tau=1}^{2} a_{\tau\sigma ml}\,\boldsymbol{v}_{\tau\sigma ml}(k\boldsymbol{r}) \tag{C.26}$$

Since only $\tau = 1,2$ is included the *l*-index starts on $l = 1$ ($l = 0$ gives no contribution). The expansion coefficients becomes

$$\begin{cases} a_{1\sigma ml} = 4\pi(i)^l\,\boldsymbol{E}_0\cdot\boldsymbol{A}_{1\sigma ml}(\boldsymbol{k}_i) \\ a_{2\sigma ml} = -4\pi(i)^{l+1}\,\boldsymbol{E}_0\cdot\boldsymbol{A}_{2\sigma ml}(\boldsymbol{k}_i) \end{cases} \tag{C.27}$$

If the incident wave is propagating in the direction of the z-axis, i.e. $\boldsymbol{k}_i = \boldsymbol{z}$, we find

$$\begin{cases} a_{1\sigma ml} = i^l \delta_{m1} \sqrt{2\pi(2l+1)} \boldsymbol{E}_0 \cdot (\delta_{\sigma o} \boldsymbol{x} - \delta_{\sigma e} \boldsymbol{y}) \\ a_{2\sigma ml} = -i^{l+1} \delta_{m1} \sqrt{2\pi(2l+1)} \boldsymbol{E}_0 \cdot (\delta_{\sigma e} \boldsymbol{x} + \delta_{\sigma o} \boldsymbol{y}) \end{cases} \tag{C.28}$$

C.3 Far field

The scattered electric field, outside a sphere that surrounds a scattering body, is represented by an outward traveling spherical vector wave, i.e.

$$\boldsymbol{E}_s(\boldsymbol{r},\omega) = \sum_{l=1}^{\infty} \sum_{m=0}^{l} \sum_{\sigma=\mathrm{e,o}} \sum_{\tau=1}^{2} f_{\tau\sigma ml}\, \boldsymbol{u}_{\tau\sigma ml}(k\boldsymbol{r}) \tag{C.29}$$

Observe that we in this case start with $l = 1$ since only the modes $\tau = 1, 2$ are included. The corresponding magnetic field is

$$\boldsymbol{H}_s(\boldsymbol{r},\omega) = \frac{1}{i\eta_0\eta} \sum_{l=1}^{\infty} \sum_{m=0}^{l} \sum_{\sigma=\mathrm{e,o}} \sum_{\tau=1}^{2} f_{\tau\sigma ml}\, \boldsymbol{u}_{\tau\sigma ml}(k\boldsymbol{r}) \tag{C.30}$$

On a large distance from the scattering body ($kr >> 1$) the spherical Hankel functions, $h_l^{(1)}(kr)$, can be approximated by

$$\begin{cases} h_l^{(1)}(z) = \dfrac{i^{-l-1}}{z} e^{iz} + O(z^{-2}) \\ h_l^{(1)\prime}(z) = \dfrac{i^{-l}}{z} e^{iz} + O(z^{-2}) \end{cases} \tag{C.31}$$

This leads to that the outward traveling spherical vector waves can be approximated by

$$\boldsymbol{u}_{\tau\sigma ml}(k\boldsymbol{r}) = i^{-l-2+\tau} \frac{e^{ikr}}{kr} \boldsymbol{A}_{\tau\sigma ml}(\boldsymbol{r}) + o\left((kr)^{-1}\right) \quad \tau = 1, 2 \tag{C.32}$$

The fields in the far zone can now be restated as

$$\begin{cases} \boldsymbol{E}_s(\boldsymbol{r},\omega) = \dfrac{e^{ikr}}{kr} \displaystyle\sum_{l=1}^{\infty} \sum_{m=0}^{l} \sum_{\sigma=\mathrm{e,o}} \sum_{\tau=1}^{2} i^{-l-2+\tau} f_{\tau\sigma ml}\, \boldsymbol{A}_{\tau\sigma ml}(\boldsymbol{r}) + o\left((kr)^{-1}\right) \\ \boldsymbol{H}_s(\boldsymbol{r},\omega) = \dfrac{1}{\eta_0\eta} \dfrac{e^{ikr}}{kr} \displaystyle\sum_{l=1}^{\infty} \sum_{m=0}^{l} \sum_{\sigma=\mathrm{e,o}} \sum_{\tau=1}^{2} i^{-l-\tau} f_{\tau\sigma ml}\, \boldsymbol{A}_{\bar{\tau}\sigma ml}(\boldsymbol{r}) + o\left((kr)^{-1}\right) \end{cases} \tag{C.33}$$

If we use the relationship between the spherical vector surface functions

$$\begin{cases} \boldsymbol{A}_{1\sigma ml}(\boldsymbol{r}) = \boldsymbol{A}_{2\sigma ml}(\boldsymbol{r}) \times \boldsymbol{r} \\ \boldsymbol{A}_{2\sigma ml}(\boldsymbol{r}) = \boldsymbol{r} \times \boldsymbol{A}_{1\sigma ml}(\boldsymbol{r}) \end{cases} \tag{C.34}$$

we get

$$\begin{cases} \boldsymbol{r} \times \boldsymbol{E}_s(\boldsymbol{r},\omega) = \dfrac{e^{ikr}}{kr} \displaystyle\sum_{l=1}^{\infty} \sum_{m=0}^{l} \sum_{\sigma=\mathrm{e,o}} \sum_{\tau=1}^{2} i^{-l-\tau} f_{\tau\sigma ml} \boldsymbol{A}_{\bar{\tau}\sigma ml}(\boldsymbol{r}) + o\left((kr)^{-1}\right) \\ \boldsymbol{r} \times \boldsymbol{H}_s(\boldsymbol{r},\omega) = -\dfrac{1}{\eta_0 \eta} \dfrac{e^{ikr}}{kr} \displaystyle\sum_{l=1}^{\infty} \sum_{m=0}^{l} \sum_{\sigma=\mathrm{e,o}} \sum_{\tau=1}^{2} i^{-l-2+\tau} f_{\tau\sigma ml} \boldsymbol{A}_{\tau\sigma ml}(\boldsymbol{r}) + o\left((kr)^{-1}\right) \end{cases} \tag{C.35}$$

From these expressions we find that the radiation conditions defined by

$$\begin{cases} (\boldsymbol{r} \times \boldsymbol{E}_s(\boldsymbol{r})) - \eta_0 \eta \boldsymbol{H}_s(\boldsymbol{r}) = o\left((kr)^{-1}\right) \\ \eta_0 \eta (\boldsymbol{r} \times \boldsymbol{H}_s(\boldsymbol{r})) + \boldsymbol{E}_s(\boldsymbol{r}) = o\left((kr)^{-1}\right) \end{cases} \quad \text{when } r \to \infty \tag{C.36}$$

is fulfilled which affirm the validity of the expression for the fields in the far zone, Eq. (C.33). From appendix B we get

$$\boldsymbol{E}_s(\boldsymbol{r}) = \frac{e^{ikr}}{kr} \boldsymbol{F}(\boldsymbol{r}) \tag{C.37}$$

which is the general expression for the far field. If we compare it with Eq. (C.33) we find that the far field amplitude can be written as

$$\boldsymbol{F}(\boldsymbol{r}) = \sum_{l=1}^{\infty} \sum_{m=0}^{l} \sum_{\sigma=\mathrm{e,o}} \sum_{\tau=1}^{2} i^{-l-2+\tau} f_{\tau\sigma ml} \boldsymbol{A}_{\tau\sigma ml}(\boldsymbol{r}) \tag{C.38}$$

The total scattered cross section can now be calculated if the expression for the far field amplitude is inserted into Eq. (5.26). We find

$$\sigma_s(\boldsymbol{k}_i) = \frac{1}{k^2 |\boldsymbol{E}_0|^2} \iint \sum_{l=1}^{\infty} \sum_{m=0}^{l} \sum_{\sigma=\mathrm{e,o}} \sum_{\tau=1}^{2} i^{-l-2+\tau} f_{\tau\sigma ml} \boldsymbol{A}_{\tau\sigma ml}(\boldsymbol{k}_i) d\,\Omega \tag{C.39}$$

Since the orthogonal[9] nature of the spherical vector surface functions Eq. (C.39) can be simplified which results in

$$\sigma_s(\boldsymbol{k}_i) = \frac{1}{k^2 |\boldsymbol{E}_0|^2} \sum_{l=1}^{\infty} \sum_{m=0}^{l} \sum_{\sigma=\mathrm{e,o}} \sum_{\tau=1}^{2} |f_{\tau\sigma ml}|^2 \tag{C.40}$$

With help of the optical theorem, Eq. (5.33), we get an expression for the total cross section

[9] The spherical vector surface functions are orthogonal when the integration is done over a whole sphere, i.e. $0 < \phi < 2\pi$ and $0 < \theta < \pi$.

$$\begin{aligned}\sigma_t(\boldsymbol{k}_i) &= \frac{4\pi}{k^2}\operatorname{Im}\left\{\frac{\boldsymbol{E}_0^*}{|\boldsymbol{E}_0|^2}\cdot \boldsymbol{F}(\boldsymbol{k}_i)\right\} \\ &= \frac{4\pi}{k^2}\operatorname{Im}\left\{\frac{\boldsymbol{E}_0^*}{|\boldsymbol{E}_0|^2}\cdot \sum_{l=1}^{\infty}\sum_{m=0}^{l}\sum_{\sigma=\mathrm{e,o}}\sum_{\tau=1}^{2} \boldsymbol{i}^{-l-2+\tau} f_{\tau\sigma ml}\, \boldsymbol{A}_{\tau\sigma ml}(\boldsymbol{k}_i)\right\}\end{aligned} \tag{C.41}$$

and the total absorption cross section

$$\sigma_a(\boldsymbol{k}_i) = \sigma_t(\boldsymbol{k}_i) - \sigma_s(\boldsymbol{k}_i)$$

C.4 Scattering from a dielectric oblate spheroid

We will here analyze the scattering from a dielectric body that has the form of an oblate spheroid

$$\left(\frac{x}{b}\right)^2 + \left(\frac{y}{b}\right)^2 + \left(\frac{z}{a}\right)^2 = 1 \tag{C.42}$$

The spheroidal particle has the dimensions of $2a$ along the symmetry axis (z-axis) and $2b$ across the equatorial plane (the x-y-plane) where the center of the spheroidal is placed at the origin of the coordinate system. The incident electric field is represented by a plane wave and propagates along the z-axis, in the positive direction. The electric field vector of the incident wave is polarized parallel to the x-y-plane and the field is expanded as

$$\boldsymbol{E}_i(\boldsymbol{r},\omega) = \boldsymbol{E}_0\, e^{ik\,\boldsymbol{k}_i\cdot\boldsymbol{r}} = \sum_{l=1}^{\infty}\sum_{m=0}^{l}\sum_{\sigma=\mathrm{e,o}}\sum_{\tau=1}^{2} a_{\tau\sigma ml}\, \boldsymbol{v}_{\tau\sigma ml}(k\,\boldsymbol{r}) \tag{C.43}$$

where the expansion coefficients are

$$\begin{cases} a_{1\sigma ml} = i^l\, \delta_{m1}\sqrt{2\pi(2l+1)}\boldsymbol{E}_0\cdot(\delta_{\sigma\mathrm{o}}\boldsymbol{x} - \delta_{\sigma\mathrm{e}}\boldsymbol{y}) \\ a_{2\sigma ml} = -i^{l+1}\, \delta_{m1}\sqrt{2\pi(2l+1)}\boldsymbol{E}_0\cdot(\delta_{\sigma\mathrm{e}}\boldsymbol{x} + \delta_{\sigma\mathrm{o}}\boldsymbol{y}) \end{cases} \tag{C.44}$$

The scattered field is expanded as

$$\boldsymbol{E}_s(\boldsymbol{r},\omega) = \sum_{l=1}^{\infty}\sum_{m=0}^{l}\sum_{\sigma=\mathrm{e,o}}\sum_{\tau=1}^{2} f_{\tau\sigma ml}\, \boldsymbol{u}_{\tau\sigma ml}(k\,\boldsymbol{r}) \tag{C.45}$$

and the total electric field outside the spheroid becomes thus

$$\boldsymbol{E}(\boldsymbol{r},\omega) = \sum_{l=1}^{\infty}\sum_{m=0}^{l}\sum_{\sigma=\mathrm{e,o}}\sum_{\tau=1}^{2} \left(a_{\tau\sigma ml}\, \boldsymbol{v}_{\tau\sigma ml}(k\,\boldsymbol{r}) + f_{\tau\sigma ml}\, \boldsymbol{u}_{\tau\sigma ml}(k\,\boldsymbol{r})\right) \tag{C.46}$$

The corresponding magnetic field is

$$i\eta_0\eta \boldsymbol{H}(\boldsymbol{r},\omega)=\sum_{l=1}^{\infty}\sum_{m=0}^{l}\sum_{\sigma=\mathrm{e,o}}\sum_{\tau=1}^{2}\left(a_{\tau\sigma ml}\,\boldsymbol{v}_{\bar{\tau}\sigma ml}(k\boldsymbol{r})+f_{\tau\sigma ml}\,\boldsymbol{u}_{\bar{\tau}\sigma ml}(k\boldsymbol{r})\right) \tag{C.47}$$

where $\bar{\tau}$ is the dual index to τ that was introduced before.
The total electric field inside the spheroid is expanded in terms of the regular spherical vector waves since they are finite at $z=0$. We find

$$\boldsymbol{E}_1(\boldsymbol{r},\omega)=\sum_{l=1}^{\infty}\sum_{m=0}^{l}\sum_{\sigma=\mathrm{e,o}}\sum_{\tau=1}^{2}\alpha_{\tau\sigma ml}\boldsymbol{v}_{\tau\sigma ml}(k_1\boldsymbol{r}) \tag{C.48}$$

where $k=\omega\sqrt{\varepsilon_1\mu_1}/c_0$ and represents the wave number inside the scattering body. The corresponding magnetic field inside the spheroid is

$$i\eta_0\eta_1\boldsymbol{H}_1(\boldsymbol{r},\omega)=\sum_{l=1}^{\infty}\sum_{m=0}^{l}\sum_{\sigma=\mathrm{e,o}}\sum_{\tau=1}^{2}\alpha_{\tau\sigma ml}\boldsymbol{v}_{\tau\sigma ml}(k_1\boldsymbol{r}) \tag{C.49}$$

where the wave impedance is denoted by $\eta_1=\sqrt{\mu_1/\varepsilon_1}$. The next step is to find a way to express the expansion coefficients of the scattered field, $f_{\tau\sigma ml}$, in terms of the expansion coefficients of the incident field, $a_{\tau\sigma ml}$. This can be achieved if we use the continuity requirements for the tangential components of the electric and magnetic fields across an arbitrary partition. We find

$$\begin{cases}\boldsymbol{n}\times\boldsymbol{E}_1(\boldsymbol{r},\omega)=\boldsymbol{n}\times\boldsymbol{E}(\boldsymbol{r},\omega)\\ \boldsymbol{n}\times\boldsymbol{H}_1(\boldsymbol{r},\omega)=\boldsymbol{n}\times\boldsymbol{H}(\boldsymbol{r},\omega)\end{cases},\qquad \boldsymbol{r}\in\Gamma \tag{C.50}$$

where $\boldsymbol{n}$ is the outward directed normal of the surface and Γ is the surface boundary of the spheroid. These expressions should be used together with the surface integral representation for the electric and magnetic fields. For the electric field the representation is defined by

$$\begin{aligned}&-i\frac{\eta_0\eta_1}{k_1}\nabla\times\left\{\nabla\times\iint_S g(k_1,|\boldsymbol{r}-\boldsymbol{r}'|)(\boldsymbol{n}(\boldsymbol{r}')\times\boldsymbol{H}_1(\boldsymbol{r}'))dS'\right\}\\ &\qquad-\nabla\times\iint_S g(k_1,|\boldsymbol{r}-\boldsymbol{r}'|)(\boldsymbol{n}(\boldsymbol{r}')\times\boldsymbol{E}_1(\boldsymbol{r}'))dS'=\begin{cases}\boldsymbol{E}_1(\boldsymbol{r}), & \boldsymbol{r}\text{ inside } S\\ \boldsymbol{0}, & \boldsymbol{r}\text{ outside } S\end{cases}\end{aligned} \tag{C.51}$$

and for the magnetic field by

$$\begin{aligned}&i\frac{1}{k_1\,\eta_0\eta_1}\nabla\times\left\{\nabla\times\iint_S g(k_1,|\boldsymbol{r}-\boldsymbol{r}'|)(\boldsymbol{n}(\boldsymbol{r}')\times\boldsymbol{E}_1(\boldsymbol{r}'))dS'\right\}\\ &\qquad-\nabla\times\iint_S g(k_1,|\boldsymbol{r}-\boldsymbol{r}'|)(\boldsymbol{n}(\boldsymbol{r}')\times\boldsymbol{H}_1(\boldsymbol{r}'))dS'=\begin{cases}\boldsymbol{H}_1(\boldsymbol{r}), & \boldsymbol{r}\text{ inside } S\\ \boldsymbol{0}, & \boldsymbol{r}\text{ outside } S\end{cases}\end{aligned} \tag{C.52}$$

Here is η_1 the intrinsic wave impedance of the medium and k_1 the wave constant for the internal field in the scattering body. The Green function is denoted by $g(k,|\boldsymbol{r}-\boldsymbol{r}'|)$ and was discussed in appendix B. Since the symmetry of the scattering body is spheroidal it is not a simple task to simplify these expressions even with help of the continuity requirements. In the case of spherical symmetry the different spherical vector surface functions are orthogonal, which leads to that the sums disappears. This is not the case with oblate spheroids. The reason is that the radius no longer is constant for different angles, which means that the Bessel and Hankel functions will take different values during the integration and thus must all modes be included in the calculations. Eq. (C.52) must consequently be solved numerically. From the calculations we finally get

$$f_{\tau\sigma\, ml} = \sum_{l'=1}^{\infty} \sum_{m'=0}^{l'} \sum_{\sigma'=\mathrm{e,o}} \sum_{\tau'=1}^{2} T_{\tau\sigma\, ml,\tau'\sigma'\, m'l'}\, a_{\tau'\sigma'\, m'l'} \tag{C.53}$$

where the infinite dimensional matrix $T_{\tau\sigma\, ml,\tau'\sigma'\, m'l'}$ is called the transition matrix. Eq. (C.53) is valid in cases when the medium parameters (μ, ε) of the scattering body are linear.

Appendix D

Calculation of two integrals

We will in this appendix calculate the integrals that appear in section 5.2.3. In this section is the short wave approximation discussed and the two integrals appears when the induced field in the far field expression is approximated by the internal field inside a slab. The integrals are

$$
\begin{aligned}
I_1 &= \iiint_{V_s} e^{-ik_0 \boldsymbol{r}\cdot\boldsymbol{r}'} e^{ik_{2z}z'} e^{i\boldsymbol{k}_t\cdot\rho'}\, dv' \\
I_2 &= \iiint_{V_s} e^{-ik_0 \boldsymbol{r}\cdot\boldsymbol{r}'} e^{-ik_{2z}z'} e^{i\boldsymbol{k}_t\cdot\rho'}\, dv'
\end{aligned}
\tag{D.1}
$$

We will start to solve the first integral. The results from these calculations can thereafter be used in the calculation of the second integral since the differences between the two integrals are minor.

Since the dielectric disc has the form of a thin cylinder, a natural choice will be to introduce cylindrical coordinates. The first integral becomes

$$
I_1 = \int_{-d/2}^{d/2} \int_0^{2\pi} \int_0^{a} e^{-ik_0 \boldsymbol{r}\cdot\boldsymbol{r}' + ik_{2z}z' + i\boldsymbol{k}_t\cdot\rho'}\, \rho' d\rho' d\phi' dz' \tag{D.2}
$$

where $\boldsymbol{r}$ is the direction to the observation point, k_{2z} the longitudinal wave constant inside the disc and $\boldsymbol{k}_t$ the transversal wave vector. Furthermore is d the thickness and a the radius of the disc. The exponent is simplified in the following way

$$
\begin{aligned}
-ik_0 \boldsymbol{r}\cdot\boldsymbol{r}' + ik_{2z}z' + i\boldsymbol{k}_t\cdot\rho' &= -ik_0 \boldsymbol{r}\cdot\boldsymbol{r}' + i\boldsymbol{k}_2\cdot\boldsymbol{r}' \\
&= -ik_0 \boldsymbol{r}\cdot\boldsymbol{r}' + ik_0\sqrt{\varepsilon}\boldsymbol{k}_2\cdot\boldsymbol{r}' = ik_0 \boldsymbol{q}\cdot\boldsymbol{r}'
\end{aligned}
\tag{D.3}
$$

where $\boldsymbol{q} = \sqrt{\varepsilon}\boldsymbol{k}_2 - \boldsymbol{r}$. Since the two vectors $\boldsymbol{r}$ and $\boldsymbol{k}_2$ preferably are expressed in spherical coordinates

$$
\begin{cases}
\boldsymbol{r} = \boldsymbol{x}\cos\phi\sin\theta + \boldsymbol{y}\sin\phi\sin\theta + \boldsymbol{z}\cos\theta \\
\boldsymbol{k}_2 = \boldsymbol{x}\cos\psi\sin\gamma + \boldsymbol{y}\sin\psi\sin\gamma + \boldsymbol{z}\cos\gamma
\end{cases}
\tag{D.4}
$$

the new vector becomes

$$
\boldsymbol{q} = q\{\boldsymbol{x}\cos\alpha\sin\beta + \boldsymbol{y}\sin\alpha\sin\beta + \boldsymbol{z}\cos\beta\} \tag{D.5}
$$

where the two angles α and β are given by

$$
\tan\alpha = \frac{\sqrt{\varepsilon}\sin\psi\sin\gamma - \sin\phi\sin\theta}{\sqrt{\varepsilon}\cos\psi\sin\gamma - \cos\phi\sin\theta} \tag{D.6}
$$

and

$$\cos\beta = \frac{1}{q}\left[\sqrt{\varepsilon}\cos\gamma - \cos\theta\right] \tag{D.7}$$

The angle γ is calculated with help of Snell s law of refraction, i.e.

$$\sin\delta = \sqrt{\varepsilon}\sin\gamma \tag{D.8}$$

where δ is the angle of incidence (see Figure 5.2). The wave vector of the incident wave is given by

$$\boldsymbol{k}_1 = k_0\{\boldsymbol{x}\cos\psi\sin\delta + \boldsymbol{y}\sin\psi\sin\delta + \boldsymbol{z}\cos\delta\} \tag{D.9}$$

Since the tangential part of the wave vector is continuous across the interface, the azimuth angle ψ is used to describe the direction of the tangential part of the wave vector in region 1 ($\boldsymbol{k}_1$) and region 2 ($\boldsymbol{k}_2$). The angle is defined in Figure A.2. Due to the cylindrical symmetry the integration variable $\boldsymbol{r}'$ becomes

$$\boldsymbol{r}' = \boldsymbol{x}\rho'\cos\phi' + \boldsymbol{y}\rho'\sin\phi' + \boldsymbol{z}z' \tag{D.10}$$

The dot product of $\boldsymbol{q}$ and $\boldsymbol{r}'$ can now be calculated and we get

$$\begin{aligned}\boldsymbol{q}\cdot\boldsymbol{r}' &= q\,\rho'\cos\alpha\sin\beta\cos\phi' \\ &\quad + q\,\rho'\sin\alpha\sin\beta\sin\phi' + qz'\cos\beta \\ &= q\,\rho'\sin\beta\{\cos\alpha\cos\phi' + \sin\alpha\sin\phi'\} + qz'\cos\beta \\ &= q\,\rho'\sin\beta\cos(\phi'-\alpha) + qz'\cos\beta\end{aligned}$$

Insertion of this result into Eq. (D.3) leads to that the integral I_1 can be written as

$$\begin{aligned}I_1 &= \int_{-d/2}^{d/2}\int_0^{2\pi}\int_0^a e^{-ik_0q\,\rho'\sin\beta\cos(\phi'-\alpha)}e^{-ik_0qz'\cos\beta}\,\rho'\,d\rho'\,d\phi'\,dz' \\ &= \int_0^a \rho'\int_0^{2\pi} e^{-ik_0q\,\rho'\sin\beta\cos(\phi'-\alpha)}\,d\phi'\,d\rho'\int_{-d/2}^{-d/2} e^{-ik_0qz'\cos\beta}\,dz'\end{aligned} \tag{D.11}$$

The last integral in Eq. (D.11) is a standard problem and the solution is

$$\int_{-d/2}^{-d/2} e^{-ik_0qz'\cos\beta}\,dz' = \frac{2}{k_0q\cos\beta}\sin\left(k_0q\cos\beta\frac{d}{2}\right) \tag{D.12}$$

The second integral can be simplified in the following way

$$\int_0^{2\pi} e^{-ik_0q\,\rho'\sin\beta\cos(\phi'-\alpha)}\,d\phi' = \int_{-\alpha}^{2\pi-\alpha} e^{-iz\cos\phi'}\,d\phi' = \int_0^{2\pi} e^{-iz\cos\phi'}\,d\phi' \tag{D.13}$$

where $z = k_0 q\, \rho' \sin\beta$. If we compare this result to the integral representation of the Bessel function of zeroth order

$$J_0(z) = \frac{1}{2\pi}\int_0^{2\pi} e^{-iz\cos t}\, dt$$

we find

$$\int_0^{2\pi} e^{-ik_0 q\, \rho' \sin\beta \cos(\phi'-\alpha)}\, d\phi' = 2\pi\, J_0(k_0 q\, \rho' \sin\beta) \qquad \text{(D.14)}$$

The first and second integral in Eq. (D.11) can be restated as

$$\int_0^a \rho' \int_0^{2\pi} e^{-ik_0 q\, \rho' \sin\beta \cos(\phi'-\alpha)}\, d\phi'\, d\rho' = 2\pi \int_0^a \rho'\, J_0(k_0 q\, \rho' \sin\beta)\, d\rho' \qquad \text{(D.15)}$$

To simplify this expression further we use the relation

$$\frac{d}{dz}\left(zJ_1(z)\right) = zJ_0(z)$$

which leads to

$$\begin{aligned}\int_0^a \rho' J_0(b\rho')\, d\rho' &= \frac{1}{b^2}\int_0^{a/b} zJ_0(z)\, dz \\ &= \frac{1}{b^2}\int_0^{a/b} \frac{d}{dz}\left(zJ_1(z)\right) dz = \frac{1}{b^2}\left\{\frac{a}{b}J_1\left(\frac{a}{b}\right) - 0\right\} = \frac{a}{b^3}J_1\left(\frac{a}{b}\right)\end{aligned}$$

and the integral in Eq. (D.15) becomes

$$\int_0^a \rho' \int_0^{2\pi} e^{-ik_0 q\, \rho' \sin\beta \cos(\phi'-\alpha)}\, d\phi'\, d\rho' = \frac{2\pi\, a}{(k_0 q \sin\beta)^3} J_1\left(\frac{a}{k_0 q \sin\beta}\right) \qquad \text{(D.16)}$$

The different integrals, in Eq. (D.11), are now solved. If we insert these results, i.e. Eq. (D.12) and Eq. (D.16), into Eq. (D.11) we finally get the solution

$$I_1 = \frac{4\pi\, a}{(k_0 q)^4 \sin^3\beta \cos\beta} \sin\left(k_0 q \cos\beta\, \frac{d}{2}\right) J_1\left(\frac{a}{k_0 q \sin\beta}\right) \qquad \text{(D.17)}$$

The technique of solving the other integral, I_2 , is straightforward and the result is

$$I_2 = \frac{4\pi a}{(k_0 p)^4 \sin^3\varphi \cos\varphi} \sin\left(k_0 p \cos\varphi \frac{d}{2}\right) J_1\left(\frac{a}{k_0 p \sin\varphi}\right) \tag{D.18}$$

We have here introduced p and φ that are defined as

$$\begin{aligned} p &= |\boldsymbol{p}| \\ \boldsymbol{p} &= \sqrt{\varepsilon}\left(\boldsymbol{k}_t \sin\gamma - \boldsymbol{z}\cos\gamma\right) - \boldsymbol{r} \\ \cos\varphi &= -\frac{1}{p}\left[\sqrt{\varepsilon}\cos\gamma + \cos\theta\right] \end{aligned} \tag{D.19}$$

where the spherical coordinates representation for the vector $\boldsymbol{p}$ is

$$\boldsymbol{p} = p\left\{\boldsymbol{x}\cos\xi \sin\varphi + \boldsymbol{y}\sin\xi \sin\varphi + \boldsymbol{z}\cos\varphi\right\} \tag{D.20}$$

And finally will the relation

$$\tan\xi = \frac{\sqrt{\varepsilon}\sin\psi \sin\gamma - \sin\phi \sin\theta}{\sqrt{\varepsilon}\cos\psi \sin\gamma - \cos\phi \sin\theta} \tag{D.21}$$

give the polar angle ξ. If we compare this expression to Eq. (D.6) we find that the two expression are identical which means that $\xi = \alpha$.